LAMINAR FLAME SPEED AND STRETCH SENSITIVITY OF HYDROCARBON FUELS AT HIGH PREHEAT PRESSURE AND VITIATION

A Dissertation
Presented to
The Academic Faculty

By

Yash N. Kochar

In Partial Fulfillment
Of the Requirements for the Degree
Doctor of Philosophy in the
School of Aerospace Engineering

Georgia Institute of Technology

August 2014

LAMINAR FLAME SPEED AND STRETCH SENSITIVITY OF HYDROCARBON FUELS AT HIGH PREHEAT AND PRESSURE

Approved by:

Dr. Jerry M. Seitzman, Advisor
School of Aerospace Engineering
Georgia Institute of Technology

Dr. Timothy C. Lieuwen
School of Aerospace Engineering
Georgia Institute of Technology

Dr. Jechiel I. Jagoda
School of Aerospace Engineering
Georgia Institute of Technology

Dr. Wenting Sun
School of Aerospace Engineering
Georgia Institute of Technology

Dr. Frederick Dryer
Department of Mechanical and Aerospace Engineering
Princeton University

Dr. Gilles Bourque
Combustion Research and Technology
Rolls-Royce, Canada

Date approved: May 15, 2014

To my wife Komal, family and friends

And

In the loving memory of my cousin Nishant and uncle Avinash

ACKNOWLEDGEMENTS

First and foremost I would like to thank my advisor Dr. Jerry Seitzman for providing me the opportunity to work in a great environment. He was very understanding and helpful through the course of my graduate studies. His guidance and support made it possible for me to complete this thesis. I am extremely grateful for his insightful questions and comments during the innumerable hours he spent on discussions. His approach to solving problems and dedication to helping students will always be a source of inspiration to me. I would also like to express my sincere thanks to Dr. Tim Lieuwen who acted as a co-advisor for this research work. His comments and feedbacks were helpful in pushing me towards new direction in research. He too was very patient and accommodating throughout my course of research work. I am also grateful to my undergraduate advisor Dr. S. R. Charkravarthy who got me interested in combustion research and provided valuable guidance on doing research.

I am thankful to my committee members, Dr. Jeff Jagoda, Dr. Wenting Sun, Dr. Fred Dryer and Dr. Gilles Bourque, along with Dr. Sang Hee Won, for taking the time and effort to critically review the thesis and provide valuable feedback on improving this document. I am also grateful to Dr. Jagoda for the help and support with my graduate studies. I would like to acknowledge the financial support from Rolls-Royce, Canada and Combustion Science & Engineering, Inc. which made this work possible and express my thanks, for the valuable feedback and guidance on the research work, to Dr. Henry Curran, Dr. Ponnuthurai Gokulakrishnan, Dr. Michael Klassen and Dr. Casey Fuller.

A number of fellow students helped me with my studies and research work and without them it would have taken much more time and effort to learn the tricks of the trade. I would like to express my special thanks to Thao Tran who taught me not only about research but also much about American culture during my early years at Tech, and Jayaprakash Natarajan whose guidance and mentoring was very helpful in getting me up and running on flame speed project. My research work would have taken even longer to complete if not for the hard work of fellow graduate students, Danny Bloomer and Sampath Adusumilli and undergraduate students, Sarah Vaden, Matthew Clay, Basil Soofi, Nicholas Ciaccio, and Jorge, who helped me a lot in my research work. I am grateful to them for providing me the opportunity to mentor them. Sarah and Matthew's enthusiasm and motivation towards their work was always appreciated. I am also thankful to Jacqueline O'Connor for helping me setup the PIV system. I am grateful to Andrew Marshall and Prabhakar Venkateswaran and their team of undergrads for the help during various phases experiment planning and lab room organization.

I am grateful to the lab research engineers, John Holthaus and Shane Getchell for ensuring a safe and smooth working environment. Bobby Noble was very helpful in making sure I had the resources needed for the experiments and Sasha Bibik was a great help when it came to troubleshooting the lab equipments. I was fortunate to have them around during my research work. I am also thankful to the staff members of School of Aerospace engineering, machine shop personnel, esp. Scott Elliott, and library staff members, Kathy Tomajko and others, for their help in timely resolving many issues during my graduate studies.

Working at the Ben Zinn Combustion Laboratory was a great experience and it would not have been possible without the dynamic group of students, staff and faculty members. Special thanks to Anne, Alberto Amato, Arun Radhakrishnan, Mohan Bobba, Brandon Sforzo, Chiluwata Lungu, Chris Foley, David Scarborough, Eugene Lubarsky, Ianko Chetrev, Jackie Crawford, John Cutright, Karthik Periagaram, Julia Lundrigan, Krishna Chaitanya, Kyung Hak Choo, Muruganandam Thiruchengode, Nishant Jain, Preetham, Preksha D'Souza, Priya Gopalakrishnan, Qingguo Zhang, Rajesh Rajaram, Ravi Kiran Bompelly, Sai Kumar Thumuluru, Santosh Hemchandra, Santosh Shanbhogue, Shashvat Prakash, Shimon Shani, Shreekrishna, Suraj Nair, Venkat Narra, Venkata Nori, Vishal Acharya, Yogish Gopala and may others, for making the work experience supportive, enjoyable and stress-free. They knowingly and unknowingly taught me a lot of useful things about research and life in general and I will always be indebted to them.

I am also thankful to my friends outside the lab who helped me take my mind of research and supported me in times of need. Special thanks to Akash, Arun S., Arun R., Deepak, Deepthi, Kapil, Kiruthika, Nagesh, Nandita, Neelakantan, Nischint, Prasad, Ramanan, Sandeep, Saptharishi, Shubha, Smita, Smitha, Sravani, Tapo and others who made my stay in Atlanta a memorable experience. Special thanks to Arun, Nischint, Karthik, Sandeep, Santosh and Yogish for being such a great roommates.

I owe my deepest gratitude to my wife Komal who kept pushing me and has been patient, caring and affectionate while dealing with my idiosyncrasies. Without her help I would have had a difficult time finishing this thesis. I am also thankful to my family for their support and patience.

This thesis is a culmination of years of effort and I could not have reached here without the help, guidance and motivation from others in times of need. I will always be beholden to the people who made it possible for me to be here.

TABLE OF CONTENTS

LIST OF TABLES

LIST OF FIGURES

LIST OF SYMBOLS

A	Flame area
A_b	Reaction-zone (burned) area
B_c	Frequency factor
ΔcH	Heat of combustion
D	Burner diameter
	Diameter of tubing
E_a	Overall activation energy
Ka	Karlovitz number
L	Separation distance between the nozzle exit and the stagnation plane
	Length of tubing
	Characteristic PIV window dimension
Le	Lewis number
Ma	Markstein number
Q	Heat release
$\dot{Q}$	Volumetric flowrate
R, R_u	Universal gas constant
R^2	Coefficient of determination
Re	Reynolds number
S	(Laminar) Flame speed
St	Stokes number
T	Temperature
$\tilde{T}_a$	Modified activation temperature
ΔT	Difference in product and reactant temperature
ΔT_{ad}	Decrease in adiabatic flame temperature from undiluted to diluted case
U	Nozzle exit velocity
U	Local flow velocity

Ze	Zeldovich number

Lowercase

c	Molar heat capacity
d	Diameter
e	Base of natural logarithm (2.71828…)
h	Flame height
l	Markstein length
m	Exponent for scaling temperature
m'	Effective exponent for scaling fractional change in flame temperature
$\dot{m}$	Mass flowrate
n	Number of moles of product, including diluent, from one mole of fuel
p	Pressure
r	Radius of spherical flame front
s	Laminar flame speed
u	Uncertainty
x	Mole fraction
y	Mass fraction

Greek

α	Half cone angle of Bunsen flame
	Strain rate imposed on stagnation flame
	Energy fraction
γ	Curvature
δ	Flame thickness
κ	Strain rate
λ	Thermal conductivity
ρ	Density
ϕ	Equivalence ratio

Subscripts

L	Laminar
T	Temperature profile
	Turbulent
ad	Adiabatic
b	Burned (downstream of reaction zone)
f	Fluid
	Flame
i	Index for gases in a mixture
m	Mixture
max	Maximum value
p	Constant pressure
	Particle
r	Room conditions
u	Unburned (upstream of preheat zone)

Superscripts

0	Unstretched (1-D) values
	Undiluted case

LIST OF ABBREVIATIONS

CCD	Charge-Coupled Device
CNG	Compressed Natural Gas
HC	Hydrocarbon
ICCD	Intensified Charge-Coupled Device
ISI	Inlet Spray Inter-cooling
LDV	Laser Doppler Velocimetry
LNG	Liquefied Natural Gas
NG	Natural Gas
PIV	Particle Image Velocimetry
PLIF	Planar Laser Induced Fluorescence
PTV	Particle Tracking Velocimetry
ROI	Region Of Interest
RQL	Rich-burn/Quick-quench/Lean-burn
slpm	Flowrate in liter per minute at standard room condition (1 atm and 298 K)
TC	Thermocouple
UHC	Unburned Hydrocarbon
UV	Ultraviolet

SUMMARY

This thesis investigates the laminar flame speed of C_1–C_3 alkanes and their binary mixtures at conditions of interest in gas turbines. Natural gas is a primary fuel for power generation. It is primarily composed of methane but can contain significant proportions of higher hydrocarbons (typically C_2–C_4 alkanes). Gas turbine combustors operate at high preheat temperature and pressure. Furthermore, steam injection, product recirculation and fuel-staging can lead to significant levels of vitiation. Understanding the combustion characteristics of such systems is important, and many chemical kinetics mechanisms have been developed to assist in this. However the development of these mechanisms is limited, in part, due to lack of experimental results for validation. One such parameter is laminar flame speed, which has been found useful not only for validating the mechanisms but also for developing empirical scaling laws for practical combustion systems.

This thesis addresses the lack of laminar flame speed data of C_1–C_3 alkanes at high preheat and significant oxidizer dilution. To this effect, unstretched and stretched flame speeds were measured for pure propane and methane/ethane and methane/propane mixtures (with 60–80 vol% CH_4) at a range of preheat temperatures (300–650 K), pressures (1–10 atm), equivalence ratios (0.6–1.8) and oxidizer dilution (15–21 vol% O_2). Three diluents viz. N_2 (0–28%), CO_2 (0–10%) and H_2O (0–30%) were tested. The unstretched flame speed measurements were performed using a modified Bunsen flame technique based on reaction zone area from chemiluminescence imaging, whereas the strain sensitivity measurements were performed using a bluff-body stabilized stagnation

flame with high resolution PIV. Over 400 measurements are reported over a wide range of conditions along with comparisons to predictions from leading chemical mechanisms. These measurements are used to: (i) discern the uncertainties associated with the measurements, (ii) understand the effect of fuel mixture and vitiation on flame speed, and (iii) validate the performance of the leading chemical kinetics mechanisms.

Extensive testing shows the unstretched flame speed measurements from the modified Bunsen technique are generally within ±10% of other stretched corrected results while the mechanism predictions are within ±20% of the measured flame speeds. Vitiation studies for propane/methane/air flames at high preheat show the reduction in flame speed results primarily from the thermal effect of the diluent; the direct chemical influence is roughly 30% for CO_2, 10% for H_2O and <1% for N_2. The relative change in flame speed from the undiluted mixture is well correlated with the fractional change in the adiabatic flame temperature over a range of equivalence ratios, dilution levels and fuel mixtures. These correlations can be useful for combustor design. Significant difference in the measured and predicted flame speeds were observed at certain conditions, highlighting possible avenues for improvements in the chemical kinetics mechanisms. Systematic errors were also identified in the Bunsen flame measurements at specific conditions, such as for rich flames with dilution, indicating a need for better understanding of the technique at these conditions. The flame speeds measured using Bunsen flame technique do not show any clear correlation with the flame height or the strain sensitivity of the reactant mixture. Previously proposed mixing rules for estimating flame speed of fuel mixtures from pure fuel values are shown to be reasonably accurate (within 5%) for range of pressure, reactant temperature and dilution conditions.

CHAPTER 1

INTRODUCTION

This thesis investigates laminar flame speed of C_1–C_3 alkane fuels over a range of conditions of interest in gas turbine applications. The motivation for the current work and its context in relation to previous work done in the field is presented in this chapter.

1.1 Motivation

Gas turbines operate over a wide range of conditions including pressure, temperature and reactant (e.g., fuel, oxidizer and diluent) composition. Turbines used for power generation are subjected to strict economic and environmental constraints which limit their emissions, specific fuel consumption and power load. Variations in the operating conditions of the gas turbine can have significant effect on its component life and combustor performance, as they can alter the flowfield and the spatial distribution of heat release. These in turn affect the combustor characteristics such as flashback, lift-off, blowout, combustor cooling and dynamic stability [1, 2]. These variations can also affect the emission characteristics of the combustor due to incomplete combustion or poor mixing leading to increased NOx, CO, unburned hydrocarbon (UHC) and soot production. Clearly, accounting for the relationship between combustor performance and operating conditions during the gas turbine design phase can lead to significant improvements and cost savings. Since there is a lack of sufficient experimental fundamental combustion data over the wide range of operating conditions of gas turbines,

predictions from chemical kinetics mechanisms are often used. However while these predictions are useful, they still need to be validated at appropriate conditions.

Recently, we have seen a rise in natural gas as a major source for electrical power generation. Natural gas is used as fuel for power generation primarily through land based gas turbines. In the USA alone, the power generation from natural gas is expected to increase significantly in the next few decades [3] . This has renewed the interest in better understanding the combustion chemistry of natural gas, which is a mixture of methane, higher hydrocarbons and small fractions of nitrogen, carbon dioxide and hydrogen sulfide. The increased availability of natural gas world-wide, as compressed natural gas (CNG) and liquefied natural gas (LNG), and from unconventional sources like coal-bed methane have led to higher variability in the composition of natural gas supplied to end-users. While natural gas primarily consists of methane (75–98% by vol.), depending on its source, it can contain significant proportion of higher alkanes (0–15%) such as ethane and propane. Table 1.1 shows typical variation in the composition of natural gas at extraction site and after treatment.

Table 1.1. Variability in natural gas composition (percent mole fraction).

Content	**U.S.A. (treated)** [5]	**World (pre-treatment)** [4]
Methane	75–98	42–85
Ethane	0.5–13	0.1–9
Propane	0–3 (24[a])	0–5
Higher-hydrocarbons[b]	0–0.4	0–25
Non-hydrocarbons[c]	Trace	4–20

[a] The higher value is due to addition of propane during peak shaving processes.
[b] Higher hydrocarbons mainly consist of C_4–C_9 alkanes.
[c] Non-hydrocarbons primarily refers to (but not limited to) nitrogen, carbon dioxide, hydrogen sulfide, sulfur, helium and mercury.

Furthermore practices wherein reserve fuels such as LNG or propane are used, to meet the increased power demand during peak shaving , increase the fuel variability significantly [5]. Naturally fuel flexibility has been an important concern in design of modern land-based gas turbines, especially those which rely on lean premixed combustion to meet emissions restrictions.

While a number of studies have examined the combustion characteristics of each of the alkanes individually, few studies have investigated mixture of alkanes, especially at operating conditions close to those found in gas turbines. Although it is not practical to measure combustion characteristics of all different possible compositions of natural gas, it is worthwhile to investigate a range of compositions in order to improve mixing rules previously developed for fuel mixtures and to validate the performance of chemical kinetics mechanisms.

Apart from fuel composition, oxidizer composition can also alter the combustion characteristics. Vitiated air refers to air with significantly lower oxygen percentage than standard air. It is often encountered in gas turbines applications, due to implementation of techniques such as exhaust gas recirculation, inter-turbine combustion, and fuel staging, to help reduce emissions and improve efficiency and performance [1]. Vitiated air from combustion processes contains increased level of N_2, CO_2, H_2O, CO, NOx and unburned hydrocarbons. The O_2 mole fraction in vitiated air can be as low as 12%. Table 1.2 lists typical conditions encountered by the reactant mixture at the inlet of gas turbine combustors and afterburners/augmentors. Furthermore, gas turbines for power generation sometimes employ water mist (inlet spray inter-cooling (ISI)) to cool the air flow to the compressor, which is useful for power augmentation and power retention on hot days [6].

This can lead to an oxidizer with significant proportion of H_2O and reduced O_2 mole fraction even before combustion.

Table 1.2. Typical inlet conditions in gas turbine combustors and afterburners. [7]

Inlet conditions	Main combustor	Augmentor
Temperature (°C)	350–650	650–1050
Pressure (atm)	10–30	0.5–6
Oxygen (% vol.)	21	12–17

Gas turbines operate at elevated pressures [1]; as a result the temperature of the reactant at combustor inlet is also increased. Furthermore combustors based on concepts like staged combustion or rich-burn/quick-quench/lean-burn (RQL), to meet emissions requirements, also encounter an increase in reactant temperature. Increased pressure and temperature have a significant effect on the combustion characteristics of a fuel/air mixture and influence every aspect of combustor design. It is apparent that their effect must be accounted for in the design phase.

With such multiple factors viz. reactant composition, pressure and temperature, it gets increasingly complex to account for various combustion characteristics that may be affected. Traditionally, studies have focused on measuring properties such as ignition and extinction characteristics, flammability limits, laminar and turbulent flame speeds and emissions, as a way to quantify the combustion process and use the results to improve chemical kinetics mechanisms [8]. With respect to laminar flame speed, an extensive database exists, but over a limited range of conditions. Laminar flame speed has proved to be useful in gas turbine design in terms of improving the understanding and developing empirical models for turbulent flame speed, flame propagation through heterogeneous fuel–air mixtures, ignition energy requirements, and other conditions of interest in gas turbines [1]. It serves as a global parameter accounting for the reactivity, diffusivity and

exothermicity of the fuel–air mixture and physical conditions at which combustion occurs [9]. The comprehensive nature of laminar flame speed and its sensitivity, in accounting for combustion processes, have encouraged its use as a measure for validating chemical kinetics mechanism. Also while the definition of laminar flame speed is straightforward, measuring it accurately has proved to be difficult. Various techniques have been developed to measure laminar flame speed. The following section provides a brief overview of a few techniques used for measuring laminar flame speed and discusses the results reported for low-order (C_1–C_3) alkanes.

1.2 Literature review

Essentially, flame speed is the speed at which a flame propagates into a reactant mixture. In reference to laminar flames, terms such as flame speed, burning velocity, propagation velocity and deflagration velocity are often used interchangeably. The laminar flame speed is generally used to refer to an unstrained (uniform flow), unstretched (planar) and adiabatic flame propagation [10]. Flame speeds affected by strain, stretch and the non-adiabatic nature of the flow are referred to by appropriate adjectives. Since it is experimentally difficult to simultaneously satisfy all the criteria for generating an appropriate flame for flame speed measurement, various techniques have been developed for establishing a stationary or propagating flame front and observing it.

Laminar flame speed of hydrocarbon fuels has been studied since the early 20th century [11, 12]. However the early measurements did not account for effect of stretch on the flame speed due to the motion of the flame surface and its shape. Also different observation techniques resulted in measurement of velocities in different region of the flame front. As a result, a significant differences (as high as 50%) from currently

accepted values were observed in the measured flame speeds [13–16]. More recent measurements have tried to account for systematic errors introduced due to stretch effects, variations in pressure and heat loss to the burner, thereby reducing the spread in the measured flame speeds. This section first provides a brief overview of some of the recent measurements of laminar flame speed of C_1–C_3 alkanes at different pressures, temperatures and fuel/air compositions. A discussion of different flame speed measurement techniques follows.

1.2.1 Flame speed measurements of pure fuels

Since methane is the first member of alkane family, its chemistry is relevant for studying combustion chemistry of higher hydrocarbons. Consequently, laminar flame speeds of methane–air mixtures have been reported by various groups over a wide range of conditions [17–20]. Instead of reviewing all the measurements reported, the following discussion highlights some of the results from studies that have extended the range of conditions. Rozenchan et al. [21] measured the flame speed for methane–air and methane–oxygen–helium mixtures up to 60 atm at room temperature. They used schlieren imaging to observe the evolution of an outwardly propagating spherical flame from which the burned flame speed was calculated. The flame speed was corrected for stretch effects using linear regression and then converted to unburned unstretched flame speed by correcting for the density ratio across the flame. They observed that at high pressure (20 atm and above) the thermo-diffusive and hydrodynamic instabilities become predominant, which results in increasingly wrinkled flames. The instabilities were suppressed by using a highly diffusive species such as helium as the diluent and increasing the inert diluent in the oxidizer. Their comparison with predictions from the

GRI 3.0 mechanism [22] shows a reasonable agreement for lower pressures but significant differences are observed for pressures over 20 atm, where the mechanism was observed to over-predict the measurements over the range of equivalence ratio (ϕ = 0.8–1.4). The differences are more acute at rich conditions ($\phi > 1.1$). The overall reaction order (n)[d] for methane–air mixtures calculated from the measurements varied non-monotonically from 1.3 at atmospheric pressure to a low of 1.02 at 5 atm before increasing to 1.05 at 10 atm and 1.18 at 20 atm for a fuel lean (ϕ = 0.8) mixture, and were 1.35, 0.80, 1.07 and 1.68 at 1, 5, 10 and 20 atm respectively for a rich (ϕ = 1.2) mixture.

Dong et al. [23] measured laminar flame speed of methane–air and ethane–hydrogen–air mixtures, with nitrogen and helium dilution, at room conditions. They also investigated the effect of varying composition at constant flame temperature. Particle image velocimetry (PIV) was used to characterize the flowfield of a flame transitioning from a positively stretched stagnation flame to a negatively stretched Bunsen flame. The local flow velocity measured at the zero stretch rate condition was used to determine the unstretched laminar flame speed. Their comparisons of flame speed for methane mixtures with predictions from GRI 3.0 showed that the mechanism over-predicts the flame speed at lower flame temperatures by up to 20%. Interestingly the differences were lower for rich mixtures. Significant differences were also observed between the measured and predicted flame speeds of mixtures with ethane. However this could be due to the fact that the GRI mechanism is designed to model natural gas mixtures primarily consisting of methane.

[d] The overall reaction order was calculated from $n = 2 + 2(\partial \ln s_u^0)/(\partial \ln p)$, where s_u^0 is the unburned and unstretched flame speed of the mixture and p is the pressure.

Laminar flame speed measurements for methane–air mixtures with argon, nitrogen and carbon dioxide dilution were reported by Zhu et al. [24]. They performed the velocity measurements using Laser Doppler Velocimetry (LDV) on counter-flow twin flames, with linear regression to correct for stretch effects. Flame speed measurements were reported for reactants at room temperature over a pressure range of 0.25–2 atm. The adiabatic flame temperature of the flame was varied from 1550–2250 K by adjusting the level of the diluent gases and equivalence ratio of the mixture. They observed that flame speed for methane–air mixtures at a fixed adiabatic flame temperature has a local minimum close to stoichiometric conditions and shows a local maximum at a slightly rich ($\phi \sim 1.2$) condition. The comparison of the measurements with predictions from their C_1 and C_2 mechanisms shows a good agreement over most of conditions considered. However at rich equivalence ratios, the C_2 mechanism over-predicted the flame speed value (by 10–20%) especially for the argon dilution.

A recent study by Ogami et al. [25] used a flame stabilized over a slot burner to measure laminar flame speed for methane–air–helium mixtures with preheat temperature up to 600 K, pressures of 1–10 atm and equivalence ratios of 0.8–1.2. Helium was added to the mixture to suppress the instabilities in the flame front. Particle Tracking Velocimetry (PTV) was used to determine the velocity field, and Planar Laser-Induced Fluorescence (PLIF) of the OH-radicals was used to determine the flame front location and angle. The flame speed was then calculated from the component of interpolated velocity normal to the flame front. Although the local stretch rate was calculated from the velocity field and flame front position, no correction was made to the flame velocity as the calculated stretch rate (in terms of Karlovitz number) was close to zero ($O(10^{-3})$).

Their results indicate that the predictions from GRI 3.0 show good agreement with the measurements for low pressure, but at high pressure over-predict the flame speed at room temperature and under-predict the flame speed at higher preheat temperature over the range of equivalence ratios. Recent studies have also reported flame speed measurements of methane with steam dilution at atmospheric pressure using various techniques [26–28]. These studies have shown reasonable agreement (within 10%) with prediction from GRI 3.0 over range of dilution levels.

1.2.1.1 Higher alkanes

In relation to higher alkanes, Jomass et al. [29] measured flame speed of C_2–C_3 hydrocarbons at room temperature and 1–5 atm. The flame speed measurements were performed by observing the evolution of an outwardly propagating spherical flame front using schlieren imaging. The unstretched flame speed was calculated by extrapolating to zero stretch and correcting for the density ratio across the flame. Their results indicate that the predictions from the tested chemical kinetics mechanism (C_1–C_3 mechanism [30]) over-predicted the flame speed for both ethane and propane especially at high pressure and fuel-rich conditions. Konnov et al. [31] measured laminar flame speed of ethane–oxygen mixtures, with nitrogen and argon dilution, at room temperature and pressure. The oxygen mole fraction in the oxidizer was varied from 15–21%. The measurements were performed on a non-stretched flat flame using the heat flux method. Their results show a good agreement with the prediction from their detailed chemical kinetics mechanism for small hydrocarbons.

Zhao et al. [32] reported flame speeds of propane–air mixtures with nitrogen dilution (up to 40% of total reactant volume) at high preheat conditions (up to 650 K) and

atmospheric pressure. They measured the strained flame speed of a flame stabilized in a bluff-body stagnation flow using PIV. The unstrained flame speed was determined from linear extrapolation to zero strain rate. Their measurements show that the flame speed, for a rich ($\phi = 1.1$) mixture, decreases linearly with increase in nitrogen dilution level. The measurements were also compared with predictions from the C_1–C_3 mechanism [30]. Here radiative heat losses were accounted for by implementing an optically thin radiation submodel (for H_2O, CO_2, CO and CH_4). The radiative heat losses resulted in a negligible (less than 0.1 cm/s) difference in predicted flame speed. The comparison shows that at high preheat temperatures the mechanism tends to under-predict the flame speed for rich ($\phi > 1.1$) and sufficiently lean ($\phi < 0.7$) mixtures.

1.2.2 Flame speed measurements of fuel mixtures

Many studies have reported laminar flame speeds for natural gas (NG) with methane as the primary constituent (> 90%). Measurements have also been reported for mixtures of hydrocarbons and hydrogen [33, 34]. However relatively few measurements have been reported for natural gas-type mixtures with high levels (> 20%) of secondary hydrocarbons. Kishore et al. [35] measured flame speeds for a methane–ethane (75:25 by volume) mixture at 307 K and atmospheric pressure using the heat flux method. They also reported flame speeds for methane with nitrogen and carbon dioxide dilution (up to 40% vol. of fuel). They observed that the addition of ethane significantly influences the flame speed of rich mixtures, whereas lean mixtures showed small change from the flame speed of pure methane.

In a study, parallel to work reported in this thesis, Bourque et al. [36] reported stretch-corrected laminar flame speed measurements of natural gas–air mixtures, with

low methane (up to 62.5% vol. of fuel) and significant proportion of higher alkanes (C_2–nC_5). The measurements were performed at room temperature and atmospheric pressure using schlieren imaging to track the evolution of an outward propagating spherical flame. A comparison of the measurements with those for pure methane shows that effect of higher alkanes is more noticeable at rich and significantly lean ($\phi \sim 0.7$) conditions. Also flame speed predictions from their natural gas mechanism [37] tended to slightly (~10%) over-predict for lean mixtures and under-predict for rich-mixtures. A comparison of measurements for stoichiometric natural gas-type mixtures (with 62.5% methane) at high pressure showed that flame speeds predicted by the mechanism are lower by almost 25%.

1.2.2.1 Mixing rules

Laminar flame speed is affect by number factors, such as heat release and specific heat capacity (hence the flame temperature), activation energy and diffusivity of reacting species, which scale differently for different fuels. Furthermore these factors can influence each other and can alter the flame structure significantly. Due to the difficulty in separating the coupling between these different factors, it is challenging to determine the flame speed of a fuel mixture from the flame speeds of the individual fuel components. Simple linear mixing rules based on fuel composition (such as mole or mass fraction) are not expected to be sufficiently accurate. Nonetheless attempts have been made to develop mixing rules for fuel mixture based on the properties of the constituents. Hirasawa et al. [38] proposed a mixing rule for binary fuel mixtures (of ethylene, n-butane and toulene) based on a mixing rule developed for flame temperature. They observed a good agreement between the measured and predicted flame speed over a wide range of equivalence ratios at atmospheric pressure and hence suggested that “the kinetic

coupling between the components of the [hydrocarbon] fuel blend, if any, is of minimal importance to the flame speed". Ji et al. [39] showed that this mixing rule, based on the adiabatic flame temperature, also gives good predictions for higher hydrocarbon fuels.

Sileghem et al. [40] observed that a linear mixing rule based on reciprocal of flame speed and energy fraction instead or mole fraction of the fuel, predicted the flame speed of gasoline–alcohol blends reasonably well even at high pressure and temperature. They also reported that these rules did not work well for hydrogen–methane blends, where they expect the kinetic coupling to be an important factor affecting the flame speed of the mixture. Yu et al. [33] reported a linear correlation between the relative amount of hydrogen addition[e] and flame speed of methane and propane with small quantities of hydrogen addition. Similar linear correlations have been reported for other hydrocarbon fuels with hydrogen addition [41, 42]. Further discussion on different mixing rules is covered in Section 2.2.

1.2.3 Flame speed measurement techniques

Numerous techniques have been developed to measure laminar flame speed. Of the different approaches used, the Bunsen flame, spherical flame, counter-flow or bluff-body stagnation flame and flat flame configurations have received considerable attention. The flame speed so measured often needs to be corrected, for example to account for the influence of stretch and heat transfer. This section presents a general discussion of these techniques. A detailed discussion of the modified Bunsen flame technique and stagnation flame technique is presented in subsequent chapters.

[e]The relative amount of hydrogen is quantified by R_H, which is the ratio of amount of hydrogen and the air required to oxidize it totally to the amount of hydrocarbon fuel and the air available for its oxidation.

1.2.3.1 Flat flame burner configuration

The flat flame configuration [43, 44, 45] provides a simple flame front to analyze and is considered to be theoretically most accurate [10]. It consists of a flat flame stabilized, over a porous plug or multiple small jets, by adjusting the flowrate and/or the heat flux to the burner. Figure 1.1 shows a simplified schematic of such a burner. The separation between the burner and the flame is of the order of flame thickness (~100 μm–1 mm). The flame speed is measured by measuring the volumetric flowrate of the reactant mixture and the flame area. In the presence of heat flux, the flame speed is corrected by extrapolation to zero heat flux. Measurements from this technique are generally limited to low pressures and low flame speed mixtures. At high pressure, there is a higher heat transfer to the burner because the flame is positioned close to the burner; also there is an increased propensity of the flow to turn turbulent.

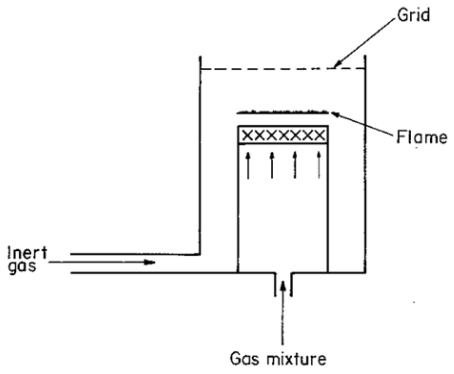

Figure 1.1. Schematic of a flat flame stabilized on a burner. [10]

1.2.3.2 Spherical flame configuration

Spherically propagating flames [9] also provide a simple flame configuration and are relatively more accessible for high pressure measurements. The most commonly used configuration has an outwardly propagating flame. The flame front evolution is determined either by measuring the pressure history in the chamber [46] or by tracking

the location of the flame front [21]. The latter approach has gained traction due to its better accuracy and reliability. For tracking the flame front motion, schlieren or shadowgraph imaging is commonly used. Figure 1.2 shows a typical evolution of a spherical flame. The stretch rate, which affects the measured flame speed, is calculated from the rate of change of the flame radius by $S_L = (2/r_f)(\mathrm{d}r_f/\mathrm{d}t)$, where r_f is the radius of the flame front at time t. The measured flame speed is then extrapolated to zero stretch rate to determine the unstretched flame speed, which is then corrected for density change across the flame to determine unburned flame speed [9]. Models have been developed to address linear and non-linear extrapolation to zero stretch rate [47, 48].

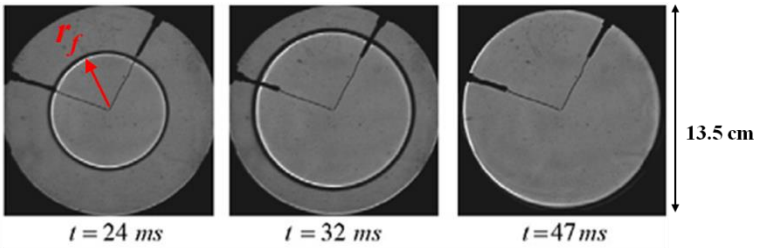

Figure 1.2. Evolution of an outward propagating spherical flame visualized using shadowgraph imaging. Adapted from [49].

Since the pressure and temperature in the combustion chamber are changing while the flame is evolving, this limits the accuracy of the technique for measurements at large flame radii (small stretch rates). This problem has been addressed to some extent by the dual-chamber design [50]. In addition, recent measurements by Lowry et al. [51] show that by using a large pressure vessel, it is possible to maintain the pressure and temperature constant over the duration of flame speed measurement so that no significant flame acceleration is observed. However the primary limitation of this technique is the difficulty in measuring flame speed at relatively high reactant temperature. At high temperatures, the auto-ignition time of the reactant is reduced and can be comparable to

the residence time required to ensure no motion of the reactants in the combustion chamber. In addition, it can be difficult to ensure a uniform temperature distribution in the vessel due to heat losses to the chamber walls.

1.2.3.3 Stagnation flame configuration

One way to address the residence time issue for high temperature reactants is by using flowing systems. By adjusting the flowrate of the reactants and length of heating section, it is possible to control the time reactants spend at high temperature before the flame front. For such measurements, the stagnation flame configuration [52], which provides a relatively simple flame configuration to model, is often used. This technique measures the strained flame speed of a stationary flame stabilized in a stagnating jet, which can then be extrapolated to zero strain if a sufficient number of flowrates are used [9]. The flame speed and strain rate are determined by measuring the axial velocity along the central streamline (Figure 1.3b) using techniques such as LDV [24], PTV [25] or PIV [32]. The minimum velocity location is conventionally used as the reference location for the flame speed and the local strain rate upstream of this location is considered the reference strain imposed on the flame.

The stagnation plane is achieved either by impinging two axisymmetric jets (counter flow or opposed flow flame) or by impinging the jet on a bluff-body (bluff-body stagnation flame). For the counter flow flame, the two jets do not have to have the same composition, although it is preferred as it provides an adiabatic stagnation plane. This configuration, sometimes referred to as the twin flame configuration, is not readily extensible to high pressure due to the complexity of the setup at high pressure resulting from requirements of cooling of the nozzle in the product zone, the size of the pressure

chamber and high fuel consumption. On the other hand, in the bluff-body stagnation flame approach, one of the nozzles is replaced by a stagnation plug. Not only does this allow for a simpler setup and lower reactant flowrate requirements but also the flames so obtained are steadier (as the stagnation plane is fixed). The primary drawback is this approach is that the stagnation plane is no longer adiabatic, which prevents accurate measurements close to extinction strain rates.

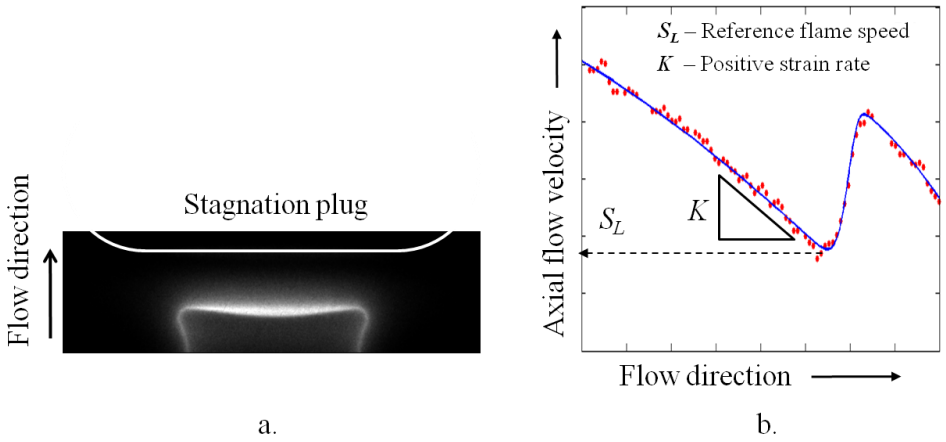

Figure 1.3. (a) Chemiluminescence image of a stagnation flame and (b) reference flame speed and strain rate calculated from axial velocity profile along the central streamline.

1.2.3.4 Bunsen flame configuration

Another configuration that is of interest for high temperature measurements is the Bunsen flame configuration. Similar to the stagnation flame configuration, the Bunsen flame configuration can allow for easy adjustment to residence time. Experimentally it is one of the simplest techniques to implement and one of the earliest methods used. Two approaches are commonly used for determining the flame speed from a Bunsen flame configuration viz. (i) flame angle and (ii) flame area. The flame angle method determines the flame speed in the linear portion of the Bunsen flame shape from, $S_L = U \sin \alpha$, where U is either the nozzle exit velocity [9] or the local flow velocity [46] and α is the half cone angle of the flame. On the other hand, the flame area method defines an average

flame speed over the full flame surface from, $S_L = \dot{Q}/A$, where $\dot{Q}$ is the volumetric flowrate at the exit of burner nozzle and A is the area of the flame surface. The geometry of the Bunsen flame poses a problem in accurately defining the flame surface location for velocity or area measurements. Different definitions of flame surface based on schlieren [10], shadowgraph [53] or chemiluminescence [57] imaging have been reported. Figure 1.4 shows the effect of imaging technique on the definition of the flame surface. Due to the differences in flame surface definition, there has been variability in the measurements reported.

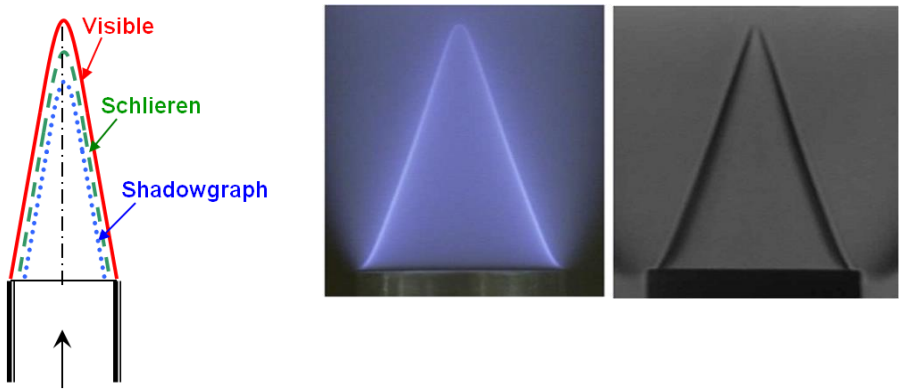

Figure 1.4. Flame edge location in a Bunsen flame determined using different visualization techniques. The schematic on the left shows the relative positions of the different edges (not to scale). Adapted from [10, 55]. The center figure a chemiluminescence image of a Bunsen flame with the corresponding schlieren image on the right. Adapted from [54].

Furthermore, a Bunsen flame is affected by varying strain and curvature effects along the flame surface and heat transfer to the burner [10]. These effects are not easy to correct for, which limits the accuracy of the measurements. As such various approaches have been used to minimize the influence of these effects on the final flame speed measurement. Natarajan [55] suggested that a modified Bunsen flame area technique that relies on the reaction-zone area of the flame for determining the flame speed, provides a good estimate of the unstretched and unburned flame speed. Another approach to reduce the stretch effect due to the flame curvature is by using a 2-D slot burner. This approach

is known to provide a better estimate of the flame speed when only the planar region of the flame is used as in the flame angle method [56, 57]. However slot burners are expensive to scale to high pressure measurements due to the high flowrate requirements.

1.2.4 Summary

The literature review shows that there is significant lack of flame speed data at conditions relevant in gas turbine applications. Until recently, most of the flame speed measurements for C_1–C_3 alkanes were limited to either atmospheric pressure or room temperature. Furthermore there is also a lack of measurements for blends of alkanes relevant to changes in natural gas composition. To address this different mixing rules have been proposed for determining flame speed of fuel blends from the properties of pure components. However these mixing rules need to be verified for alkane fuel blends under relevant conditions. Measurements are also scarce for oxidizer compositions with low oxygen content (< 21%) especially with steam and carbon dioxide dilution.

The comparisons of the measurements reported with prediction from chemical kinetics mechanism show a need for improvements in the mechanism. The mechanisms are observed to over-predict flame speed values for mixtures with low adiabatic flame temperature. They also over-predict the flame speed for lean alkane blends while under-predicting the flame speed for rich blends. Furthermore these mechanisms need to be validated at high temperature conditions similar to those observed in gas turbines.

1.3 Present work

The primary goal of this thesis is develop a database of unstretched and stretched laminar flame speed measurements at high temperatures relevant to gas turbines. These

measurements are used to understand the effect of fuel composition through binary mixtures of methane with ethane and propane. Furthermore, the effect of diluents (N_2, CO_2 and H_2O) on the flame speed of pure and binary fuel mixtures is also studied for different oxygen concentrations. To this effect, the measurements are performed at preheat temperatures of 300–650 K and 1–10 atm pressures over a wide range equivalence ratios (0.6–1.8). The O_2 mole fraction in the oxidizer is varied from 15–21% by adding diluents viz. N_2 (0–28%), CO_2 (0–10%) and H_2O (0–30%) to standard air. The measurements reported are for pure fuels and binary fuel mixtures with 60–80% methane.

These flame speed measurements are performed using the modified Bunsen flame technique (for unstretched flame speed) and the bluff-body stagnation flame technique (for strained flame speed). A secondary goal of the thesis is to understand the performance of the modified Bunsen flame technique for measuring flame speed of hydrocarbon fuels. As such the technique is validated over a wide range of conditions by comparing the measurements to the stretch corrected flame speed measurements reported in the literature and the predictions from different leading chemical kinetics mechanisms. The systematic uncertainties in both the measurement approaches are discussed in detail to identify different sources of error and their effect on the flame speed measurements and to develop a better understanding of expected uncertainties and differences. Based on the analysis, a high resolution PIV technique was tested and implemented to reduce the uncertainty in stagnation flame approach measurements. The unstretched flame speed measurements from the Bunsen and the stagnation flame approach are compared with each other at few conditions of interest.

The final objective of this work is to use the measurements to verify the performance of leading chemical kinetics mechanisms over range of conditions and to identify possible regions of improvements. The predictions from chemical kinetics mechanisms are then used to understand the effect of different diluents and to compare the performance of different mixing rules for estimating flame speed of fuel mixtures over range of conditions.

1.3.1 Thesis outline

This thesis is organized as follows. Chapter 2 provides a detailed overview of modified Bunsen flame and stagnation flame techniques used for flame speed measurement. It also provides a discussion on different mixing rules proposed for estimating flame speed of fuel mixtures from individual components. Chapter 3 provides a detailed description of the experimental setups and numerical simulation approaches along with details on data reduction. It also discusses various sources of uncertainty in measurements and modeling.

Chapter 4–6 present flame speed measurement and simulation results. Chapter 4 presents the validation tests of the current measurement approaches over a range of conditions and discusses the expected accuracy of the current techniques and kinetic mechanisms. Chapter 5 describes the effect of diluents on flame speed for pure fuels at high temperature. Chapter 6 presents flame speed measurements for binary fuel mixtures and discusses the performance of different mixing rules in predicting the flame speed of a mixture. The thesis concludes with a summary of current measurements and modeling work along with recommendations for future work, which are presented in Chapter 7.

CHAPTER 2

LAMINAR FLAME SPEED

This chapter provides a detailed background on the two laminar flame speed measurement techniques employed in this thesis, viz. the modified Bunsen flame and stagnation flame techniques. The latter portion of the chapter also reviews various mixing rules that have been proposed for estimating flame speeds of fuel mixtures based on the properties of the pure fuels.

2.1 Flame speed measurement techniques

A brief overview of the primary techniques used for flame speed measurement was presented earlier in Section 1.2.3. This part of the thesis discusses in detail the rationale behind the Bunsen and stagnation flame approaches. One of the motivations behind employing these approaches is the goal of making measurements at high preheat. These techniques are based on flowing reactants, and hence it is possible to reduce the residence time of the reactant mixture at high temperature compared to quiescent approaches like the spherically expanding flame method. The reduced residence time prevents chemical degradation of the reactants before they reach the flame. Furthermore these two techniques are also relatively simple to extend to high pressure.

2.1.1 Modified Bunsen flame technique

The modified Bunsen flame approach is used to determine the unstretched flame speed of a mixture by measuring the reaction zone area of an axisymmetric Bunsen

flame. Natarajan et al. [58] showed that this technique performs well for *lean to stoichiometric* syngas (H_2/CO) mixtures over a considerable range of pressures, temperatures and dilution. Since the current work intends to extend the implementation of this technique for measuring flame speed of hydrocarbon fuels, it is useful to revisit the theory behind the implementation of this technique.

When determining the laminar flame speed, it is necessary to account for the effect of movement of the flame edge (normal to itself) and the strain and curvature of the flame surface. A stationary axisymmetric Bunsen flame removes the concern in discerning the difference between flame propagation speed and flame displacement speed, but it does experience both strain and curvature effects. Sun et al. [59] performed a generalized integral analysis to describe the unsteady propagation of a curved flame in a strained flowfield. Their analysis, of a quasi-one-dimensional system, showed that for a weakly curved stationary flame with a thin reaction zone in the small perturbation limit, the burned flame speed, i.e., the velocity of the product gases leaving the flame, is linearly affected by the strain, whereas the unburned flame speed is linearly affected by both the strain and curvature of the flame. Their analysis shows that the relationship describing the sensitivity of flame speed (S_L) to curvature and strain, i.e., stretch, effects can be expressed as,

$$\frac{S_{L,u}}{S^0_{L,u}} = 1 + \frac{Ze}{2}\left(\frac{1}{Le} - 1\right)\frac{\alpha^0 \delta^0_T}{S^0_{L,u}}\kappa + \gamma\delta^0_T \qquad 2.1$$

$$\frac{S_{L,b}}{S^0_{L,b}} = 1 + \left[\frac{Ze}{2}\left(\frac{1}{Le} - 1\right) - \frac{1}{Le}\right]\frac{\alpha^0 \delta^0_T}{S^0_{L,u}}\kappa \qquad 2.2$$

where the subscripts u and b refer to the unburned (upstream of the preheat zone) and burned (downstream of the reaction sheet) flame zones. The superscript 0 is used to

denote one-dimensional (unstretched) values. δ_T^0 is the flame thickness based on the temperature (T) profile and is the same as the thickness of the preheat zone. $\gamma = \nabla_t \cdot \boldsymbol{n}$ is the curvature of the flame and $\kappa = \nabla_t \cdot (u_t/u)$ is the strain rate. Le is the mixture Lewis number, $Ze = E_a(T_b^0 - T_u)/[R_u(T_b^0)^2]$ is the Zeldovich number, E_a is the one-step overall activation energy and R_u is the universal gas constant. The effect of thermal expansion is captured by the factor $\alpha^0 = 1 + \ln[\sigma^0 + (1-\sigma^0)e^{-1}]$ where $\sigma^0 = T_u/T_b^0 = \rho_b^0/\rho_u$, i.e., the density ratio between the 1-d flame's products and the stretched flame's reactants.

Since the burned flame speed is only affected by the strain, the reaction zone based flame speed measured from an axisymmetric Bunsen flame should be independent of (or only weakly sensitive to) the curvature of the flame. Furthermore Choi et al. [57] showed that for an axisymmetric methane–air flame, the effect of strain on the speed of the reaction zone (as determined by C_2^* chemiluminescence) is marginal in the linear portion of the flame (i.e., where the flame angle is nearly constant) as compared to the curved region close to the tip. However near the tip, the strong curvature effect can not be ignored when determining the overall stretch rate in this portion of the flame. Choi et al. also reported that the flame speed along the linear portion of the reaction-zone front is similar for different locations within the reaction-zone, with $S_{L,b} \approx S_{L,b}^0$, over range of stretch rate. Based on these analyses Natarajan et al. [58] suggested that it is possible to determine unstretched flame speed of a mixture using the Bunsen flame approach.

When measuring flame speed using the area of a Bunsen flame, it should be noted that the resulting flame speed is an area-weighted average over the flame edge. However, the conical geometry of the flame suggests that for tall flames, the contribution to the

total flame area is primarily from the linear and shoulder (i.e., the flame base) regions and the contribution of the curved region, near the tip, is small in comparison. Thus, for flames stabilized at high flowrates, with large flame height (h) to burner diameter (D) ratio, the effect of flame stretch from the tip is small. This suggests that the flame speed determined from the reaction-zone based area of a Bunsen flame is a good estimate of the unstretched one-dimensional burned flame speed i.e. $S_{L,b} \approx S_{L,b}^0$. Furthermore from the continuity equation, it follows that mass flowrate through the flame is $\dot{m} = \rho_b S_{L,b} A_b$, where subscript b represents the burned (reaction) zone, ρ is the density and A is the area of the flame front. For a one-dimensional flow, continuity dictates that $\rho_u S_{L,u}^0 = \rho_b S_{L,b}^0$. From these relations it follows,

$$S_{L,u}^0 = \frac{\rho_b S_{L,b}^0}{\rho_u} \approx \frac{\rho_b S_{L,b}}{\rho_u} = \frac{\dot{m}}{\rho_u A_b} = \frac{\dot{Q}_u}{A_b} \qquad 2.3$$

where $\dot{Q}_u$ is the volumetric flowrate of the unburned reactant mixture. Thus the Bunsen flame method can be used to measure unstretched one-dimensional unburned flame speed from the volumetric flowrate of the reactants exiting the tube and the reaction-zone based flame area.

2.1.2 Stagnation flame technique

The stagnation flame technique measures flame speed by determining the flow velocity approaching a 1-D flat flame established in a stagnating flow. The flame speed so measured is affected by strain rate imposed on the flame and needs to be extrapolated to zero strain to determine unstretched flame speed.

Two common methods are used to produce the stagnation flame: a twin flame approach where two reactants jets are arranged to create an opposed flow [60, 33]; and a

stagnation body approach where one reactant jet is directed at a solid body [61, 32]. For this study the stagnation region is created by impinging the reactant jet on a metal plug as shown in Figure 2.1.

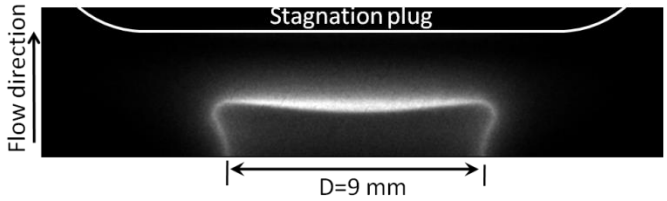

Figure 2.1. Chemiluminescence image of an axisymmetric stagnation flame. The separation between the flame and the stagnation plug varies depending on the flowrate of the reactants.

The single jet-stagnation bluff body approach, compared to the twin-flame configuration, results in a more stable flame, reduces the complexity of the setup and results in a lower required reactant flowrate. However the non-adiabatic nature of the stagnation plane can introduce a systematic error in the determination of $S_{L,u}^{0}$, an adiabatic flame speed. This issue can be addressed to some extent by reducing the heat transfer rate to the bluff body by: (i) using a ceramic plug, (ii) letting the stagnation plug get heated close to the product temperature, which requires a nearly adiabatic plug, and/or (iii) by having the flame located at a sufficient distance from the plug.

Egolfopoulos et al. [61] showed that by ensuring that the flame is at least a few flame thicknesses away from the wall, it is possible to neglect the effect of heat loss to the wall on the flame propagation. The heat loss in such cases is primarily from the products and not the flame front, which is essentially adiabatic. The non-adiabatic nature of the stagnation plane would still be a concern at strain rates closer to values that can produce flame extinction. However, since this study focuses on measuring the flame speed at low strain rate, the non-adiabatic nature of the stagnation plug is not a primary concern.

In the stagnation flame configuration, the axial flow velocity in the stagnation flow decreases from the nozzle exit to the stagnation plane (see Figure 2.2). In the presence of a flame, the velocity reaches a local minimum upstream of the preheat zone and then rises sharply across the flame due to the thermal expansion. After the heat release region, the velocity decreases again as one approaches the stagnation plane. Since the axial velocity changes continuously along the central streamline, different locations have been proposed as a reference for measuring the flame speed [62]. These include the point of 1% temperature rise or the minimum velocity location for cold edge of the flame and the maximum velocity location or the downstream edge of the preheat zone (defined based on the maximum temperature rise) for the hot edge of the flame. Of these, the 1% temperature rise based location is expected to be theoretically more appropriate [62] but results in an increased experimental uncertainty due to the difficulty in experimentally measuring the temperature profile. As such velocity based reference locations are often preferred.

The minimum velocity point is conventionally referenced as the flame speed upstream of the preheat zone, i.e., the unburned flame speed, whereas the maximum velocity point is approximated as the reference flame speed downstream of the reaction zone [9]. The strain rate imposed on the flow is specified by the negative velocity gradient just upstream of the minimum velocity (see Figure 2.2). It has been shown that the flame structure defined by these values is relatively insensitive to the outer flowfield conditions [63]. Varying the jet velocity, for a fixed separation between the nozzle and bluff-body, changes the strain rate imposed on the flame. Increasing the jet velocity increases the strain rate and pushes the flame closer to the bluff-body. While direct

measurement of the local strain rate from the velocity profile should be used in this approach, the imposed strain rate can roughly be estimated from: $\alpha \approx 2U/L$, where U is the mean flow velocity at burner nozzle exit and L is the separation between the nozzle exit and the stagnation plane. This is useful for planning the flowrate requirements for the experiments.

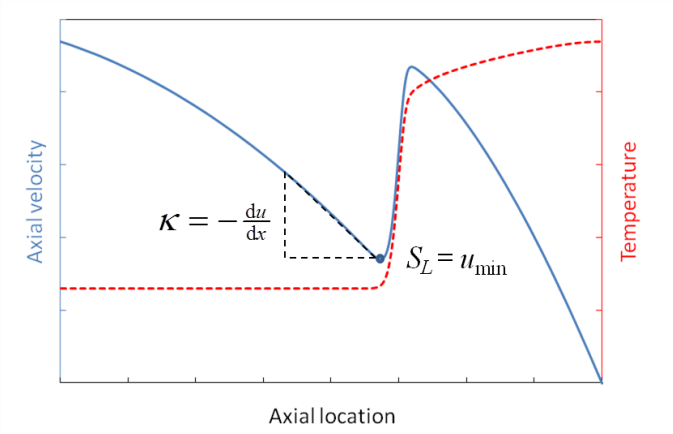

Figure 2.2. Axial velocity and temperature profile in stagnation flow with a flame. The minimum velocity is used as a reference flame speed and the local strain rate upstream of this location is the strain rate imposed on the flame.

The flame speed measured with the stagnation flame technique, S_u, is affected by the stretch effect, κ, due to the non-uniform flowfield approaching the flame, i.e., the streamlines are not normal to the flame. This stretch effect can be corrected by appropriate extrapolation to zero strain (and therefore to zero stretch). Typically a simple linear extrapolation, $S_u = S_u^0 - l\,\kappa$, is sufficient to correct for the non-zero strain rate, especially when the measurements are limited to low strain rates and low Karlovitz number[f] [18]. The unstretched flame speed is then given by S_u^0, and the strain sensitivity of the flame speed is given by the Markstein length, l. Studies based on higher-order

[f] Karlovitz number, $\mathrm{Ka} = \kappa\delta/S_u^0$, is the ratio of characteristic residence time in flame zone to that in the hydrodynamic zone. δ is the characteristic flame thickness. A low Karlovitz number represents a thinner flame and hence smaller influence of separation distance on stagnation flame.

analysis [62, 64] have reported using nonlinear extrapolation for better accuracy in determining the unstretched flame speed due to its slight nonlinear variation at small strain rates. This inaccuracy can be minimized by increasing the distance between the nozzle and stagnation plane so that the flame can be approximated as a surface [9, 18].

2.2 Flame speed mixing rules

One of the goals of this thesis is to examine flame speeds for binary fuel mixtures under high preheat and with dilution. However for combustor design, it is impractical to measure or run simulations to predict flame speeds for all possible fuel mixtures. Therefore different mixing rules have been proposed to estimate the flame speed of a mixture based on the flame speeds of its individual fuel components. This section presents some of the mixing rules derived based on:

1. mole fraction weighting;
2. mass fraction weighting;
3. energy fraction weighting; and
4. adiabatic flame temperature weighting.

2.2.1 Mole and mass fraction based rules

In terms of mole and mass fraction weighting, the mixing rules are similar and are either: (a) a linear combination of the flame speed, or (b) a linear combination of the reciprocal of the flame speed [65]. These rules can be expressed as follows,

$$S_{L,m} = \sum_i x_i S_{L,i} \tag{2.4a}$$

$$\frac{1}{S_{L,m}} = \sum_i \frac{x_i}{S_{L,i}} \tag{2.4b}$$

$$S_{L,m} = \sum_i y_i S_{L,i} \quad \text{2.5a}$$

$$\frac{1}{S_{L,m}} = \sum_i \frac{y_i}{S_{L,i}} \quad \text{2.5b}$$

where, $S_{L,m}$ is the flame speed of the fuel mixture. x_i, y_i and $S_{L,i}$ are respectively the mole fraction, mass fraction and flame speed of the i^{th} component of the fuel mixture. Di Sarli [65] et al. studied the mole fraction based mixing rule for methane/hydrogen mixtures. They reported that the linear combination of flame speed (2.4a) always resulted in a flame speed estimate well above the actual flame speed of the mixture (sometimes more than 100% difference). They attributed this difference to the strong non-linear effects in chemical kinetics that provided greater influence to the more slowly reacting methane. They also reported that the linear combination of reciprocal of flame speed (2.4b) results in a better estimate (±20%) of flame speed for lean and stoichiometric methane/hydrogen mixtures over a wide range of hydrogen content (10–95% mole fraction), pressure (1–10 atm) and reactant temperature (300–400 K).

Sileghem et al. [40] studied the mole and mass fraction weighted mixing rules (2.4a, 2.4b and 2.5a) for blends of hydrocarbons and ethanol. They observed that the mole (2.4a) and mass (2.5a) fraction weighted mixing rules predicted higher (~4%) flame speeds than the actual values, with the mass fraction based weighting performing better. They also reported that the mole fraction based mixing rule based on reciprocal of flame speed (2.5b) resulted in higher differences and are not good enough for ethanol and n-heptane mixtures.

2.2.2 Energy and temperature based rules

Sileghem et al. [40] also proposed and investigated the performance of energy fraction weighted mixing rule, expressed as,

$$S_{L,m} = \sum_i \alpha_i S_{L,i} \tag{2.6a}$$

$$\frac{1}{S_{L,m}} = \sum_i \frac{\alpha_i}{S_{L,i}} \tag{2.6b}$$

where, $\alpha_i = \Delta cH_i^0 x_i \,/\, \sum_i \Delta cH_i^0 x_i$ is the energy fraction and ΔcH_i is the heat of combustion of the i^{th} fuel component. Their calculations showed that the energy fraction based mixing rule (2.6a) and adiabatic flame temperature based rule (see following) produced very similar results and are usually better than the mole and mass fraction based rules. They also reported that the energy fraction based mixing rule using reciprocal of flame speed (2.6b) resulted in good estimate of the flame speed of the mixture.

The adiabatic flame temperature based mixing rule was proposed by Hirasawa et al. [38]. They noticed that adiabatic flame temperature is the primary factor affecting the flame speed of binary mixtures of ethylene, n-butane and toluene, and that the effect of kinetic coupling of the fuel species is negligible. From this they developed an empirical mixing rule as follows. First, the heat release (Q_i) from one mole of fuel is related to the adiabatic flame temperature $\left(T_{\text{ad},i}\right)$ through,

$$T_{\text{ad},i} - T_{u,i} = \Delta T_i = \frac{Q_i}{n_i c_{p,i}} \tag{2.7}$$

where n_i is the number of moles in the product (including diluents), $c_{p,i}$ is the molar specific heat of the products and $T_{u,i}$ is the temperature of the reactants. Assuming the same relation is valid for fuel mixture, the heat release for the mixture is $Q_m = \sum_i x_i Q_i$

and the number of moles of the product is $n_m = \sum_i x_i n_i$, then the adiabatic flame temperature of the fuel mixture can be expressed as,

$$\mathrm{T_{ad,m}} - \mathrm{T_u} = \Delta T_m = \sum_i \frac{x_i n_i \Delta T_i}{n_m} \tag{2.8}$$

Next the flame speed can be related to the adiabatic flame temperature through [66],

$$\ln S_{L,i} = -\frac{\tilde{T}_{a,i}}{T_{\mathrm{ad,i}}} \tag{2.9}$$

where $\tilde{T}_a = T_a/2 - T_{\mathrm{ad}} \ln[\{\mathrm{Le}\ (\lambda/\mathrm{c_p})\mathrm{B_c}/\mathrm{Ze}\}^{1/2}/\rho_u]$ is a modified activation temperature. $T_a = E_a/R$ is the activation temperature, E_a is the activation energy, R is the universal gas constant, Le is the Lewis number, λ is the thermal conductivity, B_c is the frequency factor, Ze is the Zeldovich number and ρ_u is the density of the reactants. Assuming that the flame speed of the fuel mixture can be related to the adiabatic flame temperature of the mixture using the same scaling, and that $\tilde{T}_{a,m}$ can be approximated in a similar fashion as ΔT_m, then the expression for flame speed of the mixture for constant T_u can be expressed as,

$$\ln S_{L,m} = \frac{\sum_i x_i n_i T_{\mathrm{ad},i} \ln S_{L,i}}{\sum_i x_i n_i T_{\mathrm{ad},i}} = \frac{\sum_i x_i n_i T_{\mathrm{ad},i} \ln S_{L,i}}{n_m T_{\mathrm{ad},m}} \tag{2.10}$$

Hirasawa et al. [38] reported that the adiabatic flame temperature based mixing rule (2.10) provided a good estimate (±5%) of flame speed for binary mixture of ethylene, n-butane and toluene. Ji et al. [39] further showed that this mixing rule also gives good flame speed prediction for binary mixtures of n-dodecane, methylcyclohexane and toluene. Based on the performance of the flame temperature based mixing rule, they suggested that the flame speed of these binary mixture is more sensitive to the flame temperature and that kinetic coupling at best has a second order effect.

CHAPTER 3

APPROACH

This chapter provides a detailed overview of the experimental facility and numerical simulations used for determining laminar flame speeds. The chapter also discusses some of the sources of uncertainties associated with the measurements and how they are accounted for in the experiments.

Since one of the primary goals of this work is to measure laminar flame speeds at high preheat temperature, it is necessary to employ a system which provides a low residence at high temperatures. This is important for avoiding any significant changes in reactant composition before it reaches the flame front. Flowing systems, like those used for Bunsen and stagnation flame techniques, are well suited for such applications because the fuel and oxidizer can be mixed at low temperature and then preheated quickly, to desired temperature, short distance upstream of the flame.

Further to facilitate the measurement of flame speed, over wide range of conditions, it was decided to use a modified Bunsen flame approach for unstrained flame speed measurement and the stagnation flame approach for strained flame speed measurements. Unstrained flame speed from extrapolation of stagnation flame data is used to provide an estimate of relative accuracy of modified Bunsen flame. This chapter covers the details on the implementation of these approaches and the comparison of results is presented in subsequent chapters.

3.1 Measurement approaches

3.1.1 Modified Bunsen flame technique

The modified Bunsen flame technique can be used with any burner capable of stabilizing an axisymmetric Bunsen flame. The subsequent chapter provides validation results from two such burners, viz. a straight tube and a contoured nozzle burner. The straight tube burner was used for atmospheric tests with no preheating. The primary selection criterion was the length of the burner to allow for sufficient distance for a parabolic exit velocity profile to develop. Two straight tube burners with inner diameter of 14.1 and 16.6 mm and length and length greater than 30× the diameter were used. These burners were limited to atmospheric pressure and room temperature mixtures with low flame speed and were later substituted by the contoured nozzle burner especially for measurements at pressure and/or preheat conditions. While both burners used the same supply (Section 3.1.1.2) and imaging (Section 3.1.1.3) system, the contoured nozzle burner was instrumented to measure the pressure and reactant temperature during run time. The following subsection provides the details of the contoured nozzle burner.

3.1.1.1 Burner assembly

Figure 3.1 shows a schematic of the facility used for producing axisymmetric Bunsen flames. The burner assembly consists of a contoured nozzle with exit diameter of 9 mm diameter and an area-contraction ratio of 72. The high contraction ratio ensures that the exit velocity profile is uniform and the flow is laminar even at relatively high Reynolds number (Re ~ 4000). A flat near stoichiometric (ϕ = 0.9–1.0) methane/air pilot flame is used to anchor the main flame at high flowrates. The pilot flame is set-up on a

co-annular sintered metal plate of width 5 mm, which is offset 1–2 mm upstream of the main burner exit. The flowrate of the pilot flame reactant mixture through the sintered plate is not metered but is estimated to be less than 8 slpm even during experiments at 10 atm. The pilot flame also serves an ignition source for the main flame. The pilot flame itself is ignited using a spark discharge close to the outer rim.

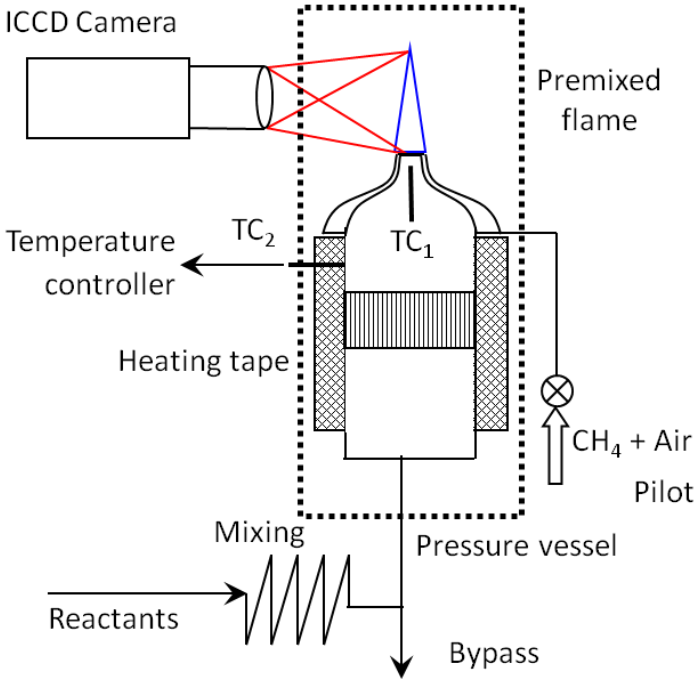

Figure 3.1. Schematic of experimental setup used for producing axisymmetric Bunsen flames.

The temperature of the reactants exiting the burner is monitored by a K-type thermocouple (TC_1) 25 mm upstream of the burner exit. The burner is attached to a plenum that is used for preheating the flow to the desired temperature and also to laminarize the flow. The coherent structure of the jet entering the plenum is broken by a ~60 mm deep bed of ball bearings (9.5 mm diameter). A ceramic flow straightener (90 mm length × 76 mm diameter and 2 mm cell size) downstream removes any large scale and transverse flow structures.

The reactant mixture is preheated to the desired temperature by two electric resistance heater (624 W rating) wrapped around the plenum. The temperature of the heating tapes, monitored by a thermocouple (TC_2), is controlled to be 100–150 °C higher than the required reactant temperature. The whole burner assembly is placed in a nitrogen ventilated pressure vessel. The vessel (15.24 cm diameter) is capable of withstanding pressures up to at least 30 atm and with a wall temperature of 500 K. Optical access for measurements and imaging is provided by three quartz windows (7.62 cm diameter × 1.9 cm thickness).

The different gases used for preparing the reactant mixture were ordered from Airgas. Table 3.1 lists the grade and associated purity of these gases as specified by the supplier. The low flowrates of propane, ethane and CO_2 needed resulted in single gas cylinders being used for each of these gases over the full set of experiments. [g]

Table 3.1. Purity grade of different gases used for preparing the reactant mixture.

Gas	Grade	Minimum Purity	Impurities[h] (ppm)
CH_4	Chemically pure	99.5%	$C_2H_6 \leq 1000$ $N_2 \leq 4000$
C_2H_6	Research	99.99%	Other HC ≤ 80
C_3H_8	Chemically pure	99.0%	
Air	Dry	O_2: 20–22%	
O_2	Zero	99.8%	
N_2	Zero	99.998%	
CO_2	Instrument	99.99%	$N_2 \leq 70$ $O_2 \leq 20$
He	Zero	99.998%	

[g] The flowrate for CH_4 was higher compared to other two fuels not only because it is forms the larger constituent of the fuel mixture (molar basis) but also because it was used for the pilot flame.
[h] Only impurities greater than 10 ppm are reported.

3.1.1.2 Flow metering

The volumetric flowrate of the reactants ($\dot{Q}$) entering the flame is determined with a bank of variable area rotameters, both to meter and control individual gas flowrates. Matheson high flow accuracy FM-1050 series rotameters (tube no: E100–E700) were used for the experiments. The rotameter tube was selected so as to maximize the range of movement of the floats during the experiment. The rotameters were calibrated at desired supply pressure using a wet-type drum (Ritter TG-50) calibration system. For very low flowrates (< 2 lpm) of fuel and diluents, a bubble flow calibration system (Sensidyne Gilibrator-2) was used.[i] Both the calibration systems have an accuracy of better than 1%. This implies that the accuracy in the equivalence ratio of the reactant mixture is ~2%. A more detailed discussion on measurement uncertainties is included in Section 3.2.

The reactant gases were allowed to mix thoroughly by passing them through a length of tubing ($L/D \sim 80$). After mixing, the reactant mixture can be split into two flows. This allows for better control over the total flowrate of a given mixture without having to adjust the individual reactant flowrates independently. The bypass flowrate is measured with a separate rotameter, which is then calibrated at the end of each day for the desired mixture. The flowrates were corrected for pressure and temperature in the test section to determine the total reactant flowrate $\dot{Q}$ passing through the flame.

A custom-built commercial steam generator (Bronkhorst) was used to control the steam addition over the range of pressures. The system uses a thermal mass flow controller (L23-AGD-22-K) to control liquid water flowrate (0–200 g/hr range) and has

[i] More details on the calibration procedure are included in APPENDIX A.

an accuracy of ±1% of full scale. A mass flow controller for air (F-201AV-50K-AGD-22-V) was also present but was set at full open during the experiments as the gas flow was prepared and controlled separately. The liquid and gas flows were mixed using a controlled evaporator mixer (W-303A-222-K) before being preheated to a set temperature. When working with steam, the supply lines were preheated to keep the reactant temperature above 400 K. This ensured no condensation occurred in the lines. The bypass line was not used under these conditions; instead, flowrates were adjusted individually at each condition. To verify the performance of the system a series of tests were performed. First the calibration for the liquid water flowrate was tested by measuring the actual flowrate. Since the flowrate of liquid water was of the order of 10–100 g/hr, it was necessary to perform the calibration over long time. Next the connections were tested for any leaks when the lines were heated. Finally, flame speed measurements were performed at different steam dilution level for known fuel/air mixture. The results are presented in Section 4.1.1.1.

The residence time of fuel and air mixture in the heated section of the setup was calculated to be ~1–3 s, with significant portion of the time spent at preheat temperatures less than 450 K. Calculation performed to check for the effect of possible chemical degradation of the reactant mixture in the heated lines, show that the effect of preheat on the flame speed is less than 1% for residence time of up to 10 s, at 750 K preheat temperature. Figure 3.2 presents calculations for propane and n-decane ($C_{10}H_{22}$) to highlight the fact that long residence time, at preheat, is an issue for heavier fuels. For current experiments propane was the heaviest fuel used and the results show that the effect of residence time is negligible. These calculations were performed by modeling the

experimental setup as a plug flow reactor (heated lines) followed by a flame speed reactor. The reactant mixture in the plug flow reactor was held at 750 K and atmospheric pressure while the residence time was varied from 0–10 s. The composition of the mixture at the exit of the plug flow reactor was used to initialize the reactant composition for the flame speed calculation. The final flame speed calculations were performed at reactant temperature of 650 K and atmospheric pressure.

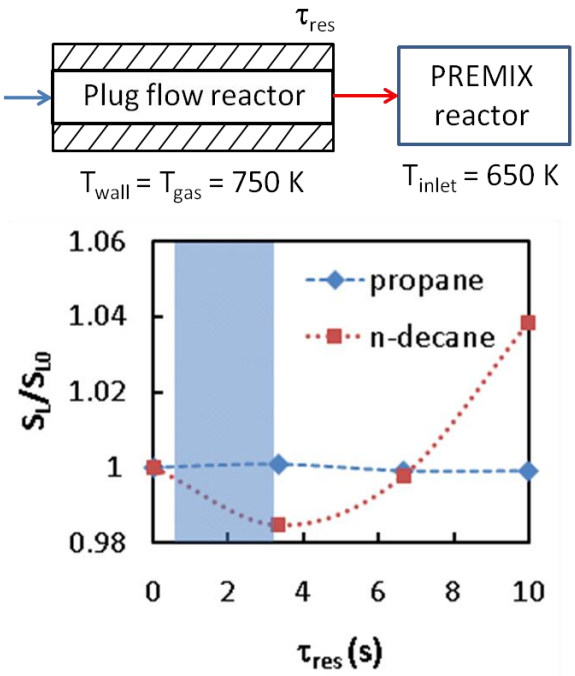

Figure 3.2. Effect of preheating on flame speed as a function of residence time of the reactants at high temperature. The calculation for propane/air mixture were performed using San Diego mechanism whereas for n-decane/air mixture JetSurf mechanism was used.

3.1.1.3 Chemiluminescence imaging

The reaction-zone area, A_b, of the flame can be determined by acquiring chemiluminescence images of the flame. For hydrocarbon-air flames, the chemiluminescence region is marked by visible and ultraviolet emissions primarily from CH^*, OH^*, C_2^* and CO_2^*. Broadband chemiluminescence images of the flame were captured using one of two 16-bit ICCD PI-MAX cameras (256×1024 pixels with a

25 mm Gen II intensifier, or 512 × 512 pixels with an 18 mm Gen III intensifier). A 105 mm f/4.5 UV Nikkor lens along with a 25 mm extension tube was used to get to a spatial resolution of 30–50 μm/pixel. The imaging system is sensitive to emissions in the ultraviolet and visible spectrum (~300–700 nm). This allows us to capture the emission from: the OH^* bands around 280 nm and 310 nm, CH^* bands around 390 nm and 430 nm, C_2^* bands around 430 nm, 460 nm and 520 nm and the broadband CO_2^* emission from 270–550 nm.

The chemiluminescence images were analyzed with a gradient-based edge-detection algorithm to determine the reaction-zone location. Since the background signal, from the products and other sources, was observed to be less than 10% of the signal from the flame and because the primary interest was in the gradient of the signal, the images were not background corrected. The edge-detection algorithm divides the image in two halves along the centerline and finds the inner edge (maximum gradient) of the reaction-zone for both the halves. Figure 3.3 illustrates the steps involved in determining the edge from one such half of the flame image. (A discussion on sensitivity of flame speed measurements to the definition of the reaction-zone location is presented later in Section 3.2.3.2.) The result from gradient based edge location is then passed to median filter to reduce the noise.

Next a robust polynomial curve-fit of fifth order is then used to smooth the location of the edge determined at each axial location. The reaction-zone area can then be determined by revolving the edge about the centerline. The reaction-zone areas from 50–100 realizations were averaged to determine the flame area (A_b) at each operating condition. Cases where the tip was observed to vary more than ±10% of the burner

diameter from centerline were discarded before taking an average. The movement of the tip was primarily due to the unsteadiness in flame anchoring resulting from non-uniform pilot flow. In the case of propane flames at high equivalence ratio, the flame tip is not observed due to extinction at high strain. The flame area for these cases only corresponds to visible area of the flame. The difference from actual total area of the flame due to discarding the area of the tip is calculated to be less than 1%.

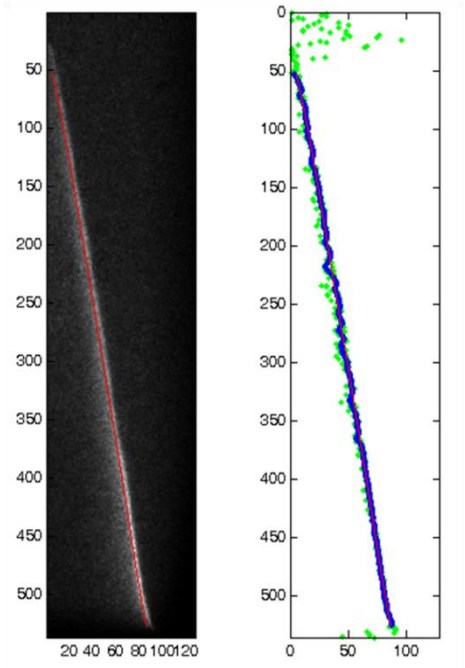

Figure 3.3. Steps involved in determining the reaction-zone location from the raw chemiluminescence image. The figure on the left shows the initial raw image and the final edge (red) used for further calculations. The plot on the right shows the edge locations at various steps of processing; green dots are the edge locations based on the intensity gradient, blue dots after median filtering and cropping the region outside the flame and red curve is the final edge location from the polynomial fit.

3.1.2 Stagnation flame technique

3.1.2.1 Burner assembly

The setup used for the stagnation flame approach is similar to the one used for the Bunsen data (Section 3.1.1.1) with the addition of a metal stagnation plug downstream of the nozzle and a seeder downstream of the bypass. The plug was positioned ~10–15 mm

downstream of the nozzle (9 mm) exit. A schematic of the setup is presented in Figure 3.4. Since the flame anchored in the stagnation flowfield is more resilient to perturbations, the use of a pilot flame, similar to one used during the Bunsen flames experiments, can be avoided. The only instance when the pilot flame is used was during high pressure experiments to ignite the reactant mixture, although the pilot flame was turned off during the velocity measurements.

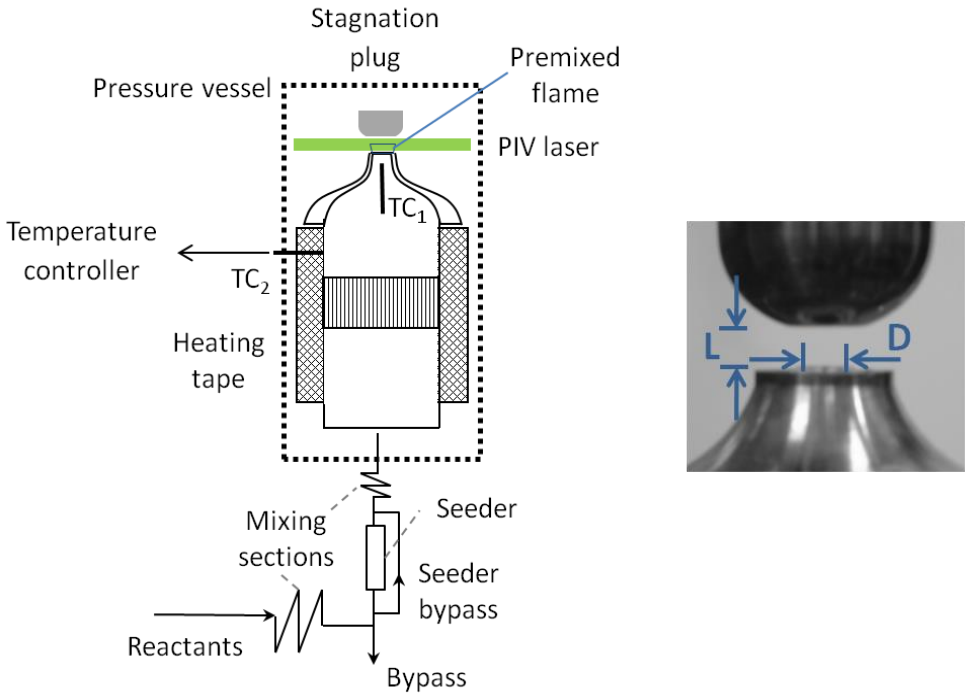

Figure 3.4. Schematic of the experimental setup used for stagnation flame approach. The insert on the right shows the actual image of the stagnation plug and its typical placement relative to the exit of the burner nozzle (D = 9 mm).

The reactant flowrates were metered using a bank of rotameters (see Section 3.1.1.2). As in the previous case, a bypass line was used to change the total flowrate through the nozzle without altering the settings on the rotameters during a given data set. This ensured that there was no change in the mixture composition for a particular data set. The reactant mixture then passed through a flow seeder to pick up seeding particles. Here the flow was split appropriately, with part of it bypassing the seeder, to control the

seeding level. For most experiments, it was more convenient to send the all the flow through the seeder and adjust the seeding level by changing the intensity of vibrations to the seeder.

3.1.2.2 Flow seeding

The flow was seeded with 1–2 μm aluminum oxide (Al_2O_3) particles. Various constraints were considered when deciding the seeding for the flow. Two important aspects considered while determining the size of the seeding for the current work were: (i) response time of the particles to changes in the flow (viscous drag forces), and (ii) thermophoretic effects due to large temperature gradient near the flame. Apart from these, particle size also affects the Mie scattering signal, i.e., larger particles provide a large scattering signal per particle. However the signal strength was not of concern for current setup.

Other than particle size, it is also important to consider the seeding density in the flow. Seeding density not only affects the accuracy of PIV results, but also influences the flame chemistry due to heat losses associated with the particles; the particles take energy from the gas, and radiate it to the surroundings. To obtain good cross-correlations (so that the probability that a measurement judged to be valid is actually valid i.e., with a valid measurement probability greater than 95%) while analyzing PIV data, it is desirable to have at least 10 particles in an interrogation window [67]. Different seeding densities were tested during test runs and a minimum density was assured visually during the experiments. At low seeding densities, multiple passes with decreasing size of interrogation windows, during the data reduction phase, resulted in better accuracy in velocity measurements. This process is described later in Section 3.1.2.3.1.

3.1.2.3 PIV setup

Two-dimensional velocity measurements of the flowfield, close to the jet centerline, were performed using a 15 Hz LaVision PIV system. The system consists of a dual-head, frequency-doubled, pulsed Nd:YAG laser (Big Sky). The energy of each 532 nm beam (one from each head) was 120 mJ/pulse. A 10 μs interval was used between the pulses to allow for sufficient movement of seeding particles (~5 pixel) within the interrogation window (32 × 32 pixel). The laser beam is shaped into a thin non-collimated sheet using a cylindrical (60 mm focal length) and spherical (250 mm focal length) lens. A 14-bit, 1600 × 1200 pixel Imager Pro X 2M CCD camera was used to capture the Mie scattering signal from the particles. The size of each pixel is $7.4 \times 7.4\ \mu m^2$. A 105 mm UV Nikkor lens along with two 25 mm extension tubes and two 2× teleconverters was used to get to a resolution of 2.65 μm/pixel (magnification of ~0.36). The camera field of view was $\sim 4.2 \times 3.2\ mm^2$. A narrow bandpass filter was used to remove light away from the laser wavelength. The lens was operated at f/8 to reduce the spurious signal produced due to diffraction from the small seed particles. Furthermore since only the region close to the centerline was of interest, the camera's region of interest (ROI) was restricted to 1600 × 400 pixels; this allowed data acquisition at 15 Hz over 1000 frames.

3.1.2.3.1 Data reduction

The DaVis 7.0 software package was used to determine the velocities from the PIV images. The particle images were first corrected for background noise by using a sliding background subtraction. The velocity field was then computed over four passes

starting with a 128 × 128 pixel window with no overlap, which was successively reduced to 64 × 64 and finally to a 32 × 32 pixel window. The final pass used 32 × 32 pixel interrogation windows with a 50% overlap between windows. An initial shift in the interrogation window, based on expected flow velocities, was specified for the first pass to improve the correlation. Thereafter each successive pass used the previous result as an initial estimate to shift the interrogation windows to get a better correlation. This practice ensured that same particles are correlated with each other even if there are less particles entering or leaving the interrogation window. A standard FFT-based correlation function [68] was used to determine the cross-correlation between the image pairs. The resulting velocity field has a spatial resolution of ~42 μm per velocity measurement which results in a flame speed uncertainty of less than 2%, as determined by model calculations described in Section 3.2.4.2.

Since the measurements were performed away from the stagnation plane and close to the central streamline, where the flow was primarily in the axial direction, a 2:1 elliptical Gaussian weight was used to look for flow vectors in the dominant flow direction. Velocity vectors were ignored from computations by median filtering if the velocity vector had an RMS greater than two times the neighboring points. Vectors were also ignored if the correlation peak ratio was less than 1.1. No interpolation was performed at this stage to fill in the removed vectors.

3.1.2.4 Flame speed and strain rate determination

As described in the previous chapter (Section 2.1.2), the minimum axial velocity before the preheat zone is considered to be the unburned strained flame speed ($S_{L,u}$) and the maximum gradient in axial velocity upstream of the minimum velocity location is

taken as the imposed strain rate (κ). The velocity profile from PIV measurements was reduced to determine the strain rate and the corresponding flame speed. First, the central streamline was identified by searching for region where radial velocity changes sign. The axial velocity profile was then conditionally-averaged over three velocity measurements (central streamline and one adjacent streamline on each side). Only locations where velocity measurements were available were considered for averaging. The resulting axial velocity profile was then used for determining the flame speed and calculating the strain rate.

The minimum axial velocity before the increase in velocity though the flame was identified as the strained flame speed. An alternate approach using a curve-fit for the velocity profile was also investigated. Here a rational function [69] of the form:

$$y = \frac{a_3 x^3 + a_2 x^2 + a_1 x + a_0}{x^2 + b_1 x + b_0} \tag{3.1}$$

was considered for the curve-fit. It was observed that this function captures the axial velocity profile accurately. Other curve fits to stagnation flame velocity profiles, like the one developed using two parabolas [70], have also been reported in literature. Using the curve fit is equivalent to low pass filtering for removing the high frequency noise in the data. The minimum velocity from the curve fit provided a good estimate of the actual value. However the curve fit was prone to error in the absence of sufficient measurements close to the flame and in product region, which is often the case for measurements at high pressure. At these conditions, using the actual velocity minimum from the PIV measurement was more accurate (lower uncertainty) than those reported by the curve fit model. Hence the curve fit approach was limited to cases where the axial velocity profile could be averaged over multiple instances and not used for analyzing instantaneous

velocity profiles. The two approaches were observed to predict similar minimum velocity for atmospheric pressure profiles averaged over multiple instances.

The slope of a robust linear polynomial fit upstream of the flame speed location was used to determine the strain rate imposed on the flame. For instantaneous velocity measurement the linear fit was performed over 30 velocity measurement locations (a region ~1.2 mm long), whereas for the average velocity profile, the linear fit was performed over 10 measurement locations (~0.4 mm). The number of points used for the curve fit was determined by empirically, based on a goal of minimizing the number of points while simultaneously minimizing the error due to noise in the velocity measurement and the change in slope near the velocity minimum location. In the case of instantaneous measurements, the strain rate and flame speed values were further filtered to remove measurements with significantly different values compared to the neighboring points.

3.2 Measurement uncertainties

This section discusses various sources of uncertainty introduced in the measurement of flame speed from both the Bunsen and stagnation flame approaches. The primary source of error is due to flowrate uncertainties, which affects not only the actual flowrate but also the composition of the mixture. Uncertainty introduced due to preheating, temperature and pressure measurements and data reduction techniques are also addressed in this section. This section does not address bias errors inherent in the techniques due to the assumptions made, such as those regarding strain and curvature effects on the Bunsen flame or the non-adiabatic nature of the stagnation flame.

3.2.1 Flowrate uncertainty

All gas flowrates were monitored using high accuracy rotameters with ±1% full scale accuracy. The rotameters were calibrated for desired gas flow at appropriate pressure using a drum-type (for flowrates more than 2 lpm) or bubble flow meter (flow flowrates less than 2 lpm) meter. The drum-type flow meter has an accuracy of ±0.2%, whereas the bubble meter is ±1% accurate. Oscillations in the flow or imperfections in the rotameter can cause the float to fluctuate ±0–2 divisions. This can lead to an error of ±1.3% (±2/150) in the recoded reading. It should be noted that higher oscillation are observed primarily at low flowrates of fuel, specifically propane, which is converted from liquid to vapor before it reaches the rotameter.

The individual gas flowrates are uncorrelated because the supply lines are choked and assuming normal distribution for each flowrate, the combined standard uncertainty in total volumetric flowrate can be determined by root sum of the squares (RSS) method. Furthermore for simplicity, assuming that all individual flowrates have same uncertainty, we can express the uncertainty in the total flowrate as,

$$u(\dot{Q}) = \sqrt{\sum_{i=1}^{n} u(\dot{Q}_i)^2} \approx \sqrt{n}\, u(\dot{Q}_i) \qquad 3.2$$

where the subscript i represents the i^{th} component in a mixture of n gases. Assuming an individual uncertainty of ±1.3%, the combined uncertainty is ±1.9–2.7% for mixtures of 2–4 gases. This is the upper bound on the uncertainties, as the uncertainties in air and diluent flowrates are generally lower than 1.3% (usually less than 0.7%).

Furthermore, day-to-day fluctuations in room temperature and pressure introduce an error in the total calibrated flowrate. The room temperature was observed to be

21±3 °C and room pressure was measured to be 0.96±0.02 atm. Room pressure and temperature uncertainties can be accounted in the measured flowrate uncertainty as follows[j],

$$\frac{u(\dot{Q}_r)}{\dot{Q}_r} = \sqrt{\left[\left(\frac{u(\dot{Q})}{\dot{Q}}\right)^2 + \frac{1}{2}\left(\frac{u(T_r)}{T_r}\right)^2 + \frac{1}{2}\left(\frac{u(p_r)}{p_r}\right)^2\right]} \qquad 3.3$$

where subscript r represents room conditions. Thus the uncertainties in the room temperature and pressure result in an uncertainty in measured flowrate of ±2.5–3.1% (for mixtures of 2–4 gases). The uncertainty in the mixture composition and equivalence ratio can be determined similarly.

The modified Bunsen flame technique uses total flowrate of the reactant to determine the unstretched flame speed. As a result, an error in total flowrate directly translates to an error in measured flame speed, i.e., the uncertainty in measured flame speed is ±2.5–3.1% based on flowrate measurement uncertainty. This error is not relevant for the stagnation flame technique, because total flowrate is not required to be known. The main effect here is in the reactant composition and equivalence ratio. For example the uncertainty in the equivalence ratio is ±1.9–2.3% based on the flowrate uncertainty of the fuel and oxidizer and not including the room temperature and pressure uncertainty.

3.2.1.1 Steam flowrate uncertainty

A mass flow controller with ±1% full scale accuracy was used to control the liquid water flowrate. During the testing and experiments, it was observed that the mass

[j] The rotameter flowrate correction for temperature and pressure is given by:

$$\dot{Q}_{\text{actual}} = \dot{Q}_{\text{calibrated}} \sqrt{\frac{P_{\text{calibrated}}}{\text{P}_{\text{actual}}} \times \frac{\text{T}_{\text{actual}}}{\text{T}_{\text{calibrated}}}}$$

flow controller for the steam generator system controlled the water flowrate within ±0.2 g/hr of the set flowrate. This oscillation was present over the full range of the controller (10–200 g/hr) and leads to an uncertainty in water flowrate of ±2% at a minimum flowrate of 10 g/hr and less than ±0.15% at the highest flowrates employed here. At sufficiently low flowrates (0–10 g/hr), the mass flow controller has difficulty maintaining a constant flowrate and had typical oscillation of more than ±2 g/hr. To avoid uncertainty due to these oscillations, this range (0–10 g/hr) was not used during the experiments. Furthermore the controller also has difficulty in controlling the flowrate if sufficient pressure head is not available to atomize the liquid water jet. To avoid these fluctuations in the flowrate, the water tank pressure was maintained ~150 psig above the pressure downstream of the steam generator.

3.2.2 Reactant temperature uncertainty

Laminar flame speed is a strong function of initial temperature of the reactant mixture. As such any uncertainty in initial reactant temperature will introduce an uncertainty in the measured flame speed. The effect of reactant temperature on laminar flame speed of hydrocarbon fuels is often expressed as $S_L \propto T_u^m$, where $m \approx 1.5$–2.5 [71–73]. Since the experiment facility has a huge thermal inertia, the reactant temperature was controlled within ±3 K of the desired temperature to reduce the amount of reactant flowrate and the time required for data acquisition. This is equivalent to a temperature uncertainty of 1% at 300 K and 0.5% at 650 K, which results in ~1–2% uncertainty in the measured flame speed. As discussed in Section 4.1.2, it is possible to correct for the uncertainty in the reactant temperature. However for small temperature fluctuation, the actual temperature is still uncertain (within ±2–3 K) due to the limitations in the accuracy

of the thermocouples used. Hence no corrections are made for small variations in the measured reactant temperature instead an overall uncertainty in the flowrate (0.5–1%) and flame speed (1–2%) was included in the error bars for the final results.

3.2.3 Uncertainties in Bunsen flame approach

3.2.3.1 Flame surface area

Unsteadiness of the flame surface can result in fluctuations in the measured reaction-zone area of the flame. Variation in the measured flame area can also result from the inability of the processing code to accurately determine the edge location near the base and tip of the flame. These fluctuations are quantified by the standard deviation of the measured mean surface area of the reaction-zone. The mean reaction-zone area was calculated by averaging the area determined from the two axisymmetric halves of the flame over 50–100 flame images (100–200 flame area values). The standard deviation of the fluctuations in the mean area was generally less than ±5%, which gives an uncertainty in the mean area of ±1% at a 95% confidence level. The uncertainty in mean area is determined from the expression, $\pm 1.96 \times \sigma/\sqrt{n}$, where $\sigma = 5\%$ and $n = 100$. Thus the overall combined uncertainty in the flame speed from the flowrate, reactant temperature and mean flame area uncertainties is less than ±3.3–3.8%.

It is worth noting that the uncertainty in the measured flame area may not fully account for any stretch effects introduced due to the assumption that the measurements are performed on a stationary flame. While small unsteadiness in the flame surface is observed to have negligible effect on the measured flame speed, as discussed in Section

4.1.2, large movements in the flame surface might be responsible for increased errors in the measured flame speed under certain condition (such as helium dilution).

3.2.3.2 Flame edge definition

The finite thickness of the reaction-zone allows one to select different locations within the reaction-zone for measuring the flame speed. In this study, three different reaction-zone edges were considered based on broadband chemiluminescence imaging. These are: (i) the inner edge of the reaction-zone (corresponding to the maximum gradient in the chemiluminescence signal), (ii) the outer edge of the reaction-zone (corresponding to the minimum gradient), and (iii) the maximum signal intensity from an Abel inverted image. Other edge definitions such as those based on chemiluminescence signal from selective species or other signal thresholds were not investigated. Also both the inner and outer edges are determined from a raw (non-Abel inverted) image.

The results presented in this work are based on the reaction-zone area determined from the inner edge location. This was chosen because this edge is closer to the C_2^* chemiluminescence based edge used in the analysis by Choi et al. [57] and also because it was observed during the validation runs presented in Chapter 4 that the flame speed determined based on this edge location provided better agreement with the stretched corrected flame speed values reported from other techniques. However due to the geometry of the Bunsen flame, the inner edge location is more sensitive to the changes in flame thickness, which can introduce error in the measured flame speed. On the other hand, the outer edge is less susceptible to these changes. Since the most flames are relatively thin (compared to their width and height), changing the definition of flame

edge from inner to outer edge generally results in a small (~6%) *decrease* in the measured flame speed.

The flame edge determined from Abel inverted image is located between the inner and outer edges. Calculations show that the flame area determined from Abel inverted images results in flame speed generally ~2% *lower* than the one determined from the inner edge. As will be shown in Chapter 4, differences of up to 10% in measured flame speed values are common between different experimental approaches. Since the added accuracy from the Abel inversion is small, it was decided to not pursue determining edges from Abel inversions to simplify the data reduction process.

3.2.3.3 Lifted flames

Another source of error in the flame speed determination results from the region considered for determining the flame area. During the experiments, it was observed that some flames were anchored a short distance ($\lesssim 1$ mm) downstream of the burner exit instead of very close to the burner exit. Figure 3.5 shows an example comparison between a lifted and an attached (regular) flame.[k] This distance is primarily affected by the equivalence ratio and the flowrates of the reactant mixture and pilot flame. At low flowrates for the pilot flame, the pilot flame is situated further upstream from the main burner exit and closer to the porous plate. As such it is more likely to lose heat to the burner which will result in the main flame being anchored further downstream where heat losses are reduced. On the other hand at high flowrates, the pilot flame can be non-uniform due to the imperfections in the porous plate. This will affect the separation

[k] The slight tilt in the burner (~2–3 deg) was always present in the contoured nozzle setup.

distance of the main flame from the burner due to change in the anchoring locations along the base of the flame. While it is possible to improve the pilot flame condition, it is not always possible to reduce the lift-off distance while trying to keep the flame height above a desired value. As such, it was necessary to consider the lift-off issue during the data reduction.

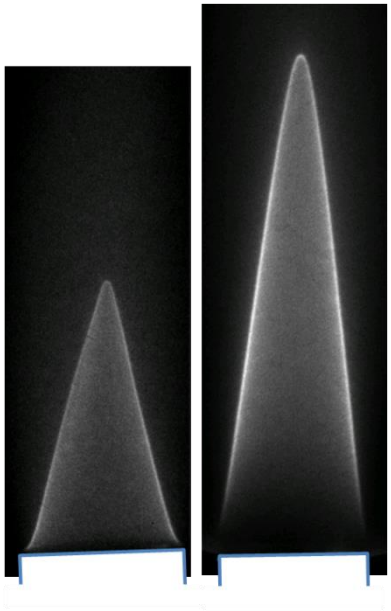

Figure 3.5. Instantaneous image of typical attached (left) and lifted flame (right). The burner exit plane location is shown by the blue border. The images are for ϕ = 0.8, 60:40 CH_4:C_3H_8 flames with H_2O dilution at 650 K. The image on the left is for 15.7% H_2O dilution at 5 atm and the one on right is for 11.1% H_2O dilution at 1 atm. The flowrate for the two cases is respectively 12.0 and 12.9 slpm which correspond to an average jet exit velocity of 1.37m/s and 7.37 m/s.

The algorithm used for determining flame area only considers the visible region of the flame edge. The flame area thus determined is less than the area if the edges were to be extended upstream to the burner exit. The effective flame speed determined using this area, with extended edges, will be less than the one reported. The main reason for using the extended edge in determining flame area is to ensure that the unburned reactant flow escaping at the base is accounted for. However because the lifted flame tends to be wider at the base than at the burner exit, it is not straightforward to account for unburned

reactant flowrate. Hence it was decided to use only the visible edge for consistency. No methodical test was performed to check for variation in the measured flame speed if the flowrate was decreased to reduce the flame lift-off distance.

Lifted Bunsen flames can also be affected by buoyancy effects which can lead to entrainment of surrounding air thereby changing the local equivalence ratio and hence the flame speed. However if the measurements are performed in a nitrogen environment, the change in the equivalence ratio can be ignored. Although the flame speed can still change due to nitrogen dilution, the change in flame speed is lower when compared to the effect of equivalence ratio change. For flame attached to the burner, diffusion of surrounding air across the flame, if any, will be negligible. Furthermore as shown in Chapter 4, the measurements performed in the absence of nitrogen co-flow[l] are in good agreement with the results reported from other techniques, which suggests that at those conditions any ambient air entrainment effect is either negligible or at best assists the flame speed measurement. Further analysis is required to quantify the effect of air entrainment on the flame speed result especially at rich equivalence ratios.

3.2.4 Uncertainties in stagnation flame approach

3.2.4.1 Flow seeding

As noted before, the two main factors affecting how accurately the seed particles follow the streamlines are the thermophoretic effect and particle inertia. The thermophoretic effect results in a net force on a particle in the direction opposite to the

[l] These are the measurements performed on a straight tube burner which lacks the provision for nitrogen shrouding.

temperature gradient in the flow. In a flame front, the temperature gradient can reach a value on the order of 10^7 K/m. Since the thermophoretic force is proportional to the magnitude of the temperature gradient and the particle size, it can lead to significant lag in particle velocity relative to the actual flow velocity [74]. However because this effect is important primarily in the high temperature gradient zone of the flame, the net effect on velocity and strain rate measurements upstream of the flame preheat zone is small. This, along with the small seed particles, makes it possible to use the current measurement approach for laminar flame speed determination without applying any correction for thermophoretic effects.

The seeding particle's inertia determines how accurately it will follow the flow streamlines and is quantified using the Stokes number (St). The Stokes number is defined as the ratio of a particle's momentum response time to the flow-field time scale and can be expressed as, $\mathrm{St} = \mathrm{Re}\,(\rho_p d_p^2)/(\rho_f L^2)$, where subscripts p and f refer to the particle and fluid, Re is the Reynolds number of the flow, ρ is the density, d_p is the particle diameter and L is the characteristic PIV window dimension. For Stokes numbers much less than unity, particles will follow the flow streamlines closely. More specifically, for Stokes numbers less than unity, the error in the velocity measurement due to particle response time is less than 1%. In the current experiments, $\rho_p = 3950\ \mathrm{kg/m^3}$, $\rho_f = 2.7\ \mathrm{kg/m^3}$ (for air preheated to 650 K at 5 atm pressure), $d_p = 1\ \mu\mathrm{m}$ and $L = 0.01$ m, $\mathrm{St} = 1.5 \times 10^{-5}\,\mathrm{Re}$. Since the Reynolds numbers for the laminar flow studied varies from 10^3–10^4, it is expected that the error due to viscous drag will be less than 1% of the actual flow velocity.

During PIV data processing, a minimum seeding density of ~10 particles per interrogation window is desirable. This would result in an ~10% particle mass loading for the current setup with a final interrogation window size of 32 × 32 pixels. While this can affect the measured velocities, the results (presented in Section 4.2) show that the current measurements are in good agreement with the results reported in the literature, indicating a negligible effect on flame chemistry. The effect may be small because the measurement primarily focuses in the earlier part of the preheat zone, where the temperature change is small; this reduces the heat transfer to the particles and any radiation loss from the particles. In many cases, the seeding density in the final interrogation window was lower than 10 particles. This is allowed because the velocity calculations were performed in passes with decreasing interrogation window size (Section 3.1.2.3.1). Thus even though the particle density is low (producing a lower mass loading and reduced heat losses), the accuracy of the velocity calculation is not reduced.

3.2.4.2 Spatial resolution of velocity measurements

Use of PIV for mapping the velocity field introduces a bias error when measuring flow with large velocity gradients. Also the spatial resolution of the velocity measurements is limited by the PIV interrogation window size. Decreasing the interrogation window size lowers the bias error and provides higher resolution, but results in significantly higher seeding density requirement. A limited spatial resolution can introduce error in the final flame speed result. The error in final flame speed result was estimated by modeling an expected experimental velocity profile and then processing it using the same algorithm used for determining the flame speed from actual experimental

results. The expected experimental velocity profile was generated from an actual velocity profile, as predicted by numerical flow simulation using OPPDIF routine.

The model of expected experimental velocity profile was derived by averaging the stagnation velocity profile of a methane/air flame, at high pressure and temperature, over different interrogation window size (and hence different spatial resolution). This reduces the resolution of the actual profile to that expected from the experiments. Next Gaussian noise was added to the new velocity profile to account for noise in experimental results. The final resulting velocity profile was analyzed to determine the flame speed and strain rate, using the same algorithm that was employed for reducing the PIV measurements. The analysis results, presented in Figure 3.6, show that for a spatial resolution of ~85 μm per velocity measurement, the uncertainty in the flame speed is less than 5% and for ~50 μm per velocity measurement resolution the uncertainty is less than 2%. The measurements reported in this work were made at spatial resolution of ~42 μm per velocity measurement, which translates to an uncertainty of less than 2% in the flame speed result.

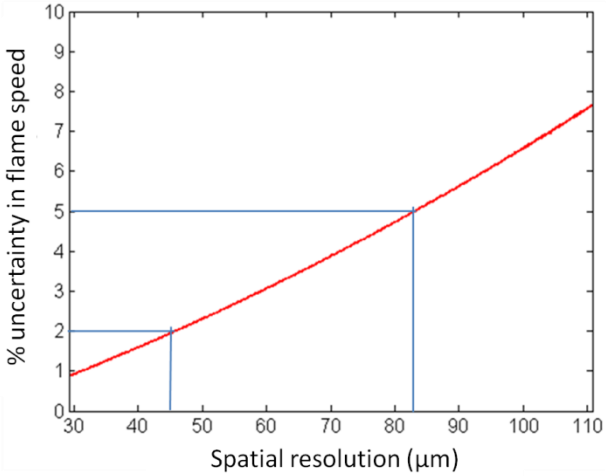

Figure 3.6. Uncertainty in actual flame speed due to limited spatial resolution of PIV measurements.

3.2.4.3 Flame speed and strain rate uncertainties

Determining the flame speed (velocity minimum) and imposed strain rate (velocity gradient) are the largest sources of uncertainty for the stagnation flame technique. The uncertainties in the flame speed and strain rate values are introduced due to the inherent noise in the instantaneous PIV velocity data and the definition of the region considered for linear regression to determine the strain rate. For instantaneous measurements, the uncertainty in flame speed is equal to the uncertainty in the PIV velocity measurement whereas the uncertainty in the strain rate is equal to the uncertainty in the coefficient of the linear regression. On the other hand, for averaged data, the uncertainty in the flame speed is determined from the root sum of squares of the uncertainty in the PIV velocity measurement and the RMS of the averaged values, while the uncertainty in the strain rate is determined from the root sum of squares of the uncertainty in the coefficient of the linear regression and the RMS of the averaged values.

The stagnation flame speed data is further reduced to determine the strain sensitivity (Markstein length) and unstretched flame speed of the mixture at a given condition. This is done by means of linear regression and extrapolation to zero strain rate. The uncertainty in the unstretched flame speed and Markstein length are then calculated based on a 95% confidence interval band for the linear regression. This assumes a normal distribution in flame speed and strain rate data.

3.2.5 Summary

This section provided a detailed analysis of the uncertainties introduced in the final result due to the different sources of uncertainty both in data acquisition and data

reduction processes. Table 3.2 provides a brief summary of these uncertainties. Here the flowrate and temperature uncertainty are applicable to both measurement techniques, while other sources are specific to the technique.

Table 3.2. Overview of uncertainties associated with the flame speed measurement.

Type of uncertainty (Section #)	Explanation	Effect on the final measurement
Reactant flowrate (3.2.1)	Unsteadiness in rotameter reading and fluctuations in the room conditions	S_L: ±2.5–3.1% ϕ: ±1.9–2.3%
Reactant temperature (3.2.2)	Variation in temperature between different cases and uncertainty in thermocouple measurements	S_L: ±1–2% ϕ: none
Specific to Bunsen flame technique:		
Flame surface area (3.2.3.1)	Movement in flame edge location	A_b: less than ±1% S_L: less than ±2%
Overall uncertainty in S_L^0, presented in the plots, due to uncertainties in flowrate, reactant temperature and flame surface area: ±3.3–3.8% Other uncertainties are not accounted for in the error bars for the plots.		
Flame edge definition (3.2.3.2)	Various edge locations that can be defined from the raw and Abel inverted flame images	Decrease in S_L due to, Outer edge: ~6%. Abel inversion: ~2%
Lifted flame (3.2.3.3)	Stand-off distance between the flame and the burner exit	Not corrected for.
Specific to stagnation flame technique:		
Flow seeding (3.2.4.1)	Seeding particles not being able to follow the flow streamlines accurately (thermophoretic and inertia effect)	U: less than 1%
	Effect of flow seeding density on accurate determination of flow velocity and effect on flame chemistry	Not observed to be significant
Velocity measurement resolution (3.2.4.2)	Bias error introduced in PIV measurements for flows with high velocity gradient	S_L: less than 2%

Type of uncertainty (Section #)	Explanation	Effect on the final measurement
Flame speed and strain rate (3.2.4.3)	Noise in PIV measurements (affects S_L) and region considered for linear regression (affects κ)	Based on RMS of measured U and the uncertainty in linear regression coefficient
	Linear regression affects S_L^0 and l	Generally less than 1–3%.

3.3 Modeling approaches

Flame speed measurements were compared with predictions from different chemical kinetics mechanisms. The calculations were performed using a commercial chemical kinetics software package, Chemkin [75]. The PREMIX [76] and OPPDIF [77] routines were used to model unstrained and strained one-dimensional adiabatic laminar flames, respectively. Multi-component and thermal (Soret effect) diffusion was accounted for in the final step of calculations. In case of PREMIX calculations, the computation domain was extended far upstream and downstream of the flame to ensure that no noticeable change in profile is present. For OPPDIF calculations, the nozzle separation was fixed at 20 mm to match the experimental settings. Both these routines use the Twopnt boundary value solver [78] to solve a discretized set of equations. This solver allows for adaptive grid refinement, controlled by the parameters GRAD and CURV, which account for the gradient and curvature of the solution and vary from 1 (coarse grid) to 0 (fine grid).

In the current computations, grid independence was assured by decreasing the value of GRAD and CURV parameters to 0.1. Further decreasing the value of these parameters (to 0.01) has a small effect on flame speed (< 5%) but increases the

computation time requirement by almost ten-fold. This trade-off is presented in Figure 3.7, which shows a typical PREMIX calculation convergence through flame speed and increase in computational requirements (through number of grid points) as a function of GRAD parameter value. The results presented in the figure are for calculations performed using GRI 3.0 mechanism for stoichiometric methane–air mixture at atmospheric pressure and 300 K temperature.

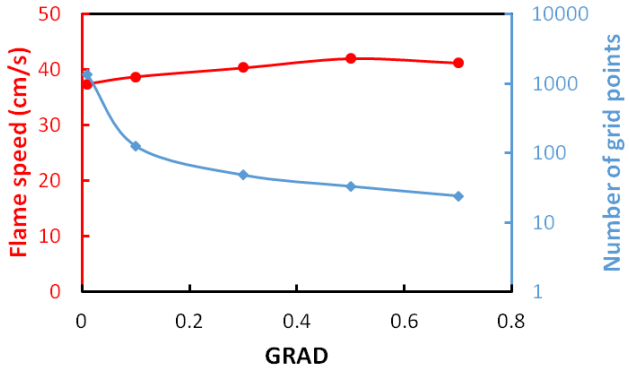

Figure 3.7. Trade-off between the accuracy of flame speed prediction and computation requirement.

Various leading chemical kinetics mechanism considered for comparison purpose are listed in Table 3.3. The GRI mechanism [79] has been widely validated presented for methane and natural gas combustion. Since the fuel mixtures, considered in this work, contained significant proportion of higher hydrocarbons, GRI mechanism results were only used for methane flames. Other mechanisms, viz. San Diego [80], USC II [81] and NUI C_3 and C_5 [37], have been developed to model combustion of higher hydrocarbons (up to C_3–C_5). Of these mechanisms, the flame speed predictions from USC II mechanism were observed to be similar (< 2% difference) to those predicted by the San Diego mechanism for the cases considered. Hence only a limited number of flame speed predictions are presented for the USC II mechanism.

Table 3.3. Chemical kinetics mechanisms considered for flame speed predictions.

Mechanism	Version	Species	Reactions
GRI	3.0	53	325
San Diego	20051201	46	235
USC	II (2007-09)	111	784
NUI	C3 High Temp 2009-09	96	588
	C5 v52 High Temp 2010-11	167	1064

The San Diego mechanism is hierarchically derived from a simplified chemical system and then slowly increasing the complexity of system while keeping the number of species and reactions to minimum to minimize the uncertainty in rate parameters. The mechanism focuses on conditions relevant to flames, high temperature ignition and detonations. The mechanism version used in this work does not account for nitrogen chemistry. However it is possible to include the nitrogen chemistry by including the appropriate reactions and species specified separately. The absence of nitrogen chemistry is favored due to the fact that it has small effect on predicting flame speed and it helps keep the size of the mechanism small.

On the other hand, the NUI mechanism, which is also derived hierarchically, tries to account for detailed fuel and nitrogen chemistry. Two versions of this mechanism were used in this study due to the updates being made during the course of the work. Since the newer version primarily addresses fuel chemistry for higher hydrocarbon, the results on flame speed for lower hydrocarbon did not differ significantly[m] from the previous version for the few cases that were compared. Furthermore since we are only interested in flame

[m] The flame speed generally differ by less than 5% except at significantly rich conditions ($\phi > 1.5$), where flame speeds differ by up to ~10%.

speed predictions, only the high temperature chemistry option is considered for both versions. These versions also do not account for nitrogen chemistry, since it has a negligible effect on the flame speed predictions.

3.3.1 Modeling uncertainty

While comparing stagnation flame results with the prediction from OPPDIF routine of Chemkin, it is worth noting that the boundary conditions at the nozzle exit and the stagnation plane are not same between the experiment and the model. The difference is in the slip boundary condition and heat transfer rate at the stagnation plane and in the velocity profile at the nozzle exit.

In opposed flow flame simulation the slip boundary condition at the stagnation plane results in a non-zero radial velocity gradient, whereas in the experiments the no-slip boundary condition imposes a zero radial velocity gradient. Furthermore while the opposed flow flame configuration has an adiabatic stagnation plane, in the experiment the presence of a relatively cooler plug can result in a non-adiabatic stagnation plane. The effect of the slip boundary condition and non-adiabatic nature of the wall, on the strain rate variation and hence the flame speed was studied by Natarajan [55]. He reported that while there is a significant change in the strain rate variation close to the wall in the product region of the flame, the predicted flame speed with non-adiabatic wall and no slip condition is lower than that for the opposed flow flame configuration by less than 3%. Also the strain sensitivity of the reactant mixtures under different conditions is essentially the same.

OPPDIF models the nozzle exit using plug flow boundary condition. However the exit velocity profile in the experiments can deviate from the ideal plug flow boundary

condition due to presence of boundary layer and pressure gradient from the stagnation condition. For large deviations this profile can approach a potential flow. Natarajan's [55] analysis showed that while flame is situated closer to the stagnation plane for the potential flow boundary condition, the flame speed (minimum axial velocity) is lower than that for the plug flow boundary condition by less than 2%. Furthermore the strain sensitivity of the reactant mixture is similar for both boundary conditions.

Overall the differences in boundary condition between the OPPDIF modeling and actual experiments can lead to slightly lower flame speed values begin reported from the measurements. However the difference in measured speed is expected to be less than 2 – 3% from the predicted value.

CHAPTER 4

VALIDATION RESULTS

One of the primary goals of this thesis is to extend the application of the modified Bunsen technique, for unstretched flame speed measurement, to hydrocarbon fuels. The goal is to be able to accurately measure flame speeds over ranges of fuel and oxidizer composition, pressure and temperature relevant to gas turbines. Another goal is to implement a bluff-body stagnation flame technique and use high resolution PIV for strained flame speed measurements. In this regards, the application of these techniques is experimental validated by comparing the measurements with results reported in literature. These comparisons also serve as an estimate for the fidelity of the current measurements.

This chapter also provides a comparison of measurements using the current approaches with flame speed predictions from leading chemical kinetics mechanisms. These comparisons help provide a guideline for estimating the difference between the current measurements and model predictions. The first section presents measurements from the Bunsen flame technique and compares it to results reported in literature and predictions from chemical kinetics mechanism. Results are presented for a range of fuels (C_1–C_3 alkanes), pressures and temperatures. This section also explores the reproducibility of the results under different conditions and discusses the effect of some of the approximations made during the measurements.

Next validation results are presented for implementation of PIV and the stagnation flame technique, along with comparison to literature results and mechanism

predictions. Since stagnation flame techniques have been used by a number of investigators for measurement of laminar flame speeds, the main goal here is to experimentally verify the current implementation, including the use of a stagnation body as opposed to counter-flow jets, and the use of high-resolution PIV and the analysis approach for faster data acquisition. Finally a brief comparison is presented between the validation result measurements from the two approaches. A more detailed comparison is presented in Chapter 6.

4.1 Bunsen flame technique

The modified Bunsen flame technique had been validated and used extensively for flame speed measurement of syngas fuel at lean equivalence ratios [55]. Natarajan also reported measurements of flame speed for lean to slightly rich methane–air mixtures at room temperature and pressure for validation. Since one of the goals of this work is to extend the range where Bunsen flame technique can be used for hydrocarbon fuels, validation results are presented for C_1–C_3 alkanes over a wide range of equivalence ratios, pressure and temperature. Measurements are also presented for methane–air mixtures with steam dilution.

4.1.1 Atmospheric pressure results

Flame speed measurements were performed for methane–air mixtures at room conditions over an equivalence ratio range of ~0.8–1.3. These measurements were performed using a Bunsen flame stabilized on a straight tube (16.6 mm inner diameter). The flame is anchored by adjusting the total flowrate and without the help of a pilot flame. Figure 4.1 shows the comparison of the measurements with stretch-corrected

results from spherical [19, 21] and counter-flow flame [18] configurations. The comparison shows that the current measurements are almost same as those from opposed flow flame configuration, which in general tend to be slightly higher than spherical flame configuration results (for lean and close to stoichiometric conditions). Overall, the measurements are in good agreement (±5%) with each other over the range of equivalence ratios, except the spherical flame results which tend to be lower but are still within ±10%.

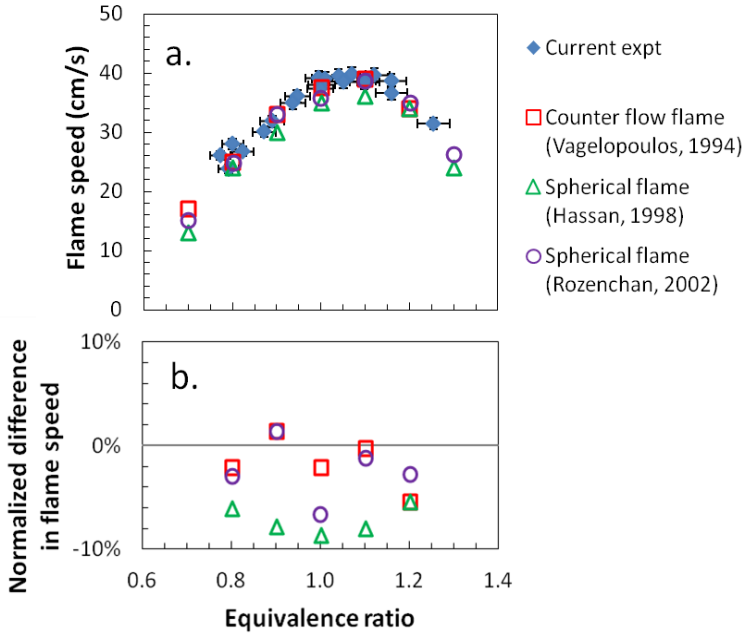

Figure 4.1. Bunsen flame technique validation for measuring unstretched laminar flame speed of methane–air mixtures at room temperature and pressure. (a) Actual measured laminar flame speed values and comparison to stretched corrected values reported in literature. (b) Normalized difference in flame speeds between reported measurements using other techniques and current measurements using Bunsen flame technique.

The figure also shows that there is a scatter in the current flame speed results close to a stoichiometric equivalence ratio and at lean conditions. The scatter is due to the oscillations in the flame shape arising from the difficulty in anchoring the flame at high flowrates. Since the setup did not have a provision for a pilot flame to anchor the main flame, the flow velocity had to be reduced to avoid lifted flames that are highly unsteady.

Figure 4.2 shows fluctuation in instantaneous measured flame speeds for a few different equivalence ratios. For the two cases at similar equivalence ratio, the flowrate for ϕ = 0.82 increases by roughly a factor of two compared to ϕ = 0.80. Although decreasing the flowrate reduces the unsteadiness in the flame, it also results in a decrease in the flame height (e.g., h/D ~ 1.15 for the low flowrate case as compared to >1.5 for most of the cases). This can increase the systematic uncertainty in the measured flame speeds due to increased fraction of the flame that experiences significant stretch.

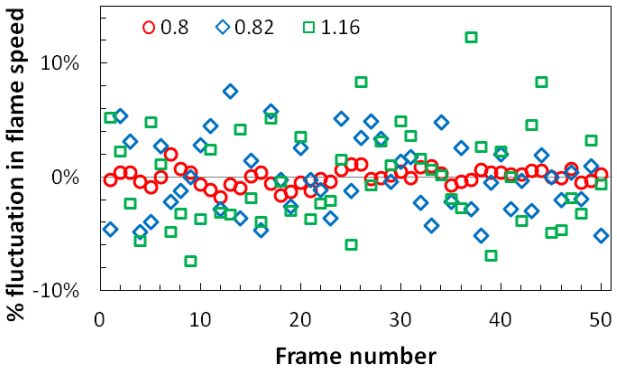

Figure 4.2. Fluctuation in instantaneous flame speed at different conditions. The measured flame speed, at a given condition, is an average over all the frames.

Figure 4.3 compares a few instantaneous flame images at different equivalence ratios. The images are for methane–air flames, except for the rightmost one, which is for a propane–air mixture. For the short methane–air flames, the curvature at the base of the flame is also significant, in addition to the flame tip. Since the base of the flame contributes a significant proportion of the flame surface area for short flames, it can lead to increased uncertainty in the flame speed for such flames, because the technique assumes negligible curvature effects on the flame speed. This effect is reduced when a pilot flame is used to anchor the main flame, because now the base of the main flame is relatively straight compared to the unpiloted case.

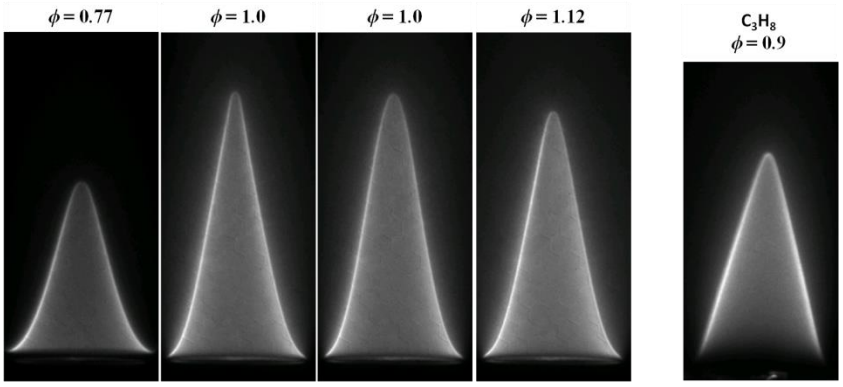

Figure 4.3. Instantaneous images of methane–air Bunsen flame at different equivalence ratios. The right most frame is for a propane–air flame. The methane–air flames are stabilized over 16.6 mm unpiloted burner, whereas the propane–air flame is stabilized on a 9 mm piloted burner.

Since the measurements presented in Figure 4.1 were acquired over separate days, they provide a means to check for reproducibility of the results. Figure 4.4 presents this comparison of current measurements, acquired on two subsequent days, with measurements reported by Natarajan [82] using the same approach but with a different experimental setup. The current measurements were performed on a 16.6 mm burner, whereas Natarajan used an 18 mm burner. The measurements show roughly same flame speeds (within ±5%) for a given equivalence ratio, with a slightly higher difference (~10%) at rich equivalence ratio.

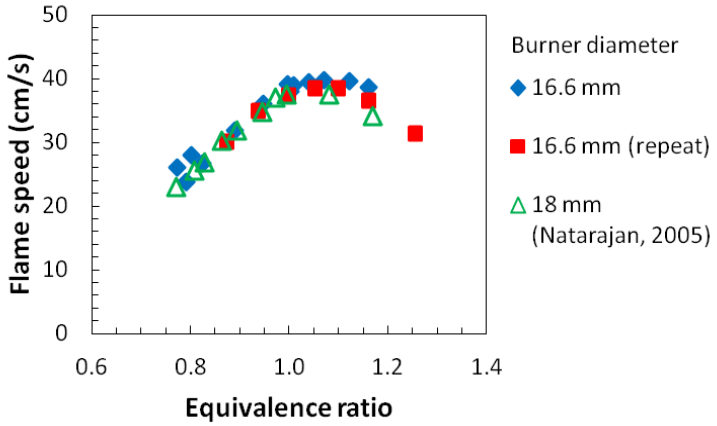

Figure 4.4 Repeatability and reproducibility of flame speed measurements using Bunsen flame technique over different diameter burner. Measurements are for methane–air mixture at room conditions.

Flame speed measurements were also performed for ethane–air mixtures at room conditions. Figure 4.5 shows the comparison of these measurements with stretch-corrected results from a counter-flow flame [29] and a spherical flame [83] configurations. The measurements, presented in Figure 4.5, were acquired from Bunsen flames stabilized on straight tube burners, one with a 14.1 mm inner diameter and the other with a 16.6 mm diameter. Similar flame speeds (within ±5%) were measured for both burners, which indicates that the measured flame speed is not sensitive to the burner diameter.

From Figure 4.5, we observe that the measurements are in good agreement (within ±4%) with the stretch-corrected results from the literature over most of the equivalence ratio range. Interestingly at lean equivalence ratios ($\phi \approx 0.75$), the current measurements seem to level-off. This was also observed for results with a larger diameter tube and for flames with different heights (i.e., *h/D* ratio). Also closer to stoichiometric conditions, it was observed that the flame speed values from the spherical flame configuration are slightly lower than the current measurements and the counter-flow flame results. This behavior is similar to the methane–air results (Figure 4.1), where the spherical flame produced slightly lower flame speeds than the other measurement approaches. Overall, the comparisons show the current measurement approach results in flame speeds that are within 5–10% of those from other established approaches, and these other approaches differ from each other by a similar amount.

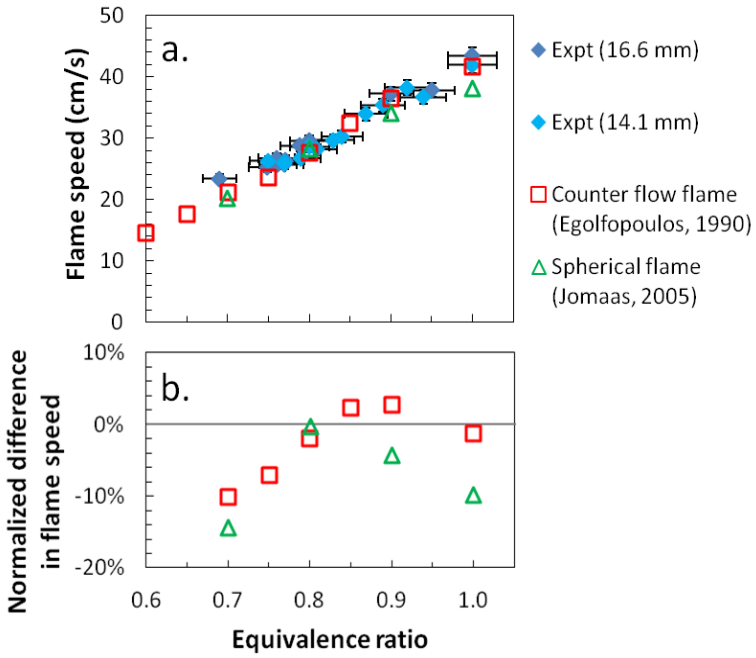

Figure 4.5. Measurements of unstretched laminar flame speed of ethane–air mixture at room temperature and pressure for validating applicability of Bunsen flame technique. (a) Actual flame speed measurements using Bunsen flame technique and comparison with stretch corrected results from other techniques. (b) Normalized difference in flame speed between current measurements and other reported values.

A validation test was also performed at high preheat temperature and atmospheric pressure using a propane-air flame. These measurements were performed with a Bunsen flame stabilized on a piloted contoured nozzle (9 mm diameter). A piloted burner allows for extending the range of equivalence ratios where flame speed measurements can be performed accurately. This is because the pilot flame allows for stabilizing the main flame over wider range of equivalence ratios and at higher flowrates (hence higher flame height). Also subsequent measurements were performed on the 9 mm contoured nozzle burner because the flame was observed to be more unsteady (susceptible to oscillations) on a larger diameter burner. A few high pressure measurements were also performed on a smaller 6 mm contoured nozzle burner due to the lower flowrate required.

Figure 4.6 shows a comparison of propane–air flame speed measurements with stretch-corrected results from a stagnation flame configuration [32]. The measurements

were performed over three separate days, at atmospheric pressure and 650 K reactant temperature. The Bunsen flame measurements are within ±5% of the stagnation flame results over most of the equivalence ratio range.

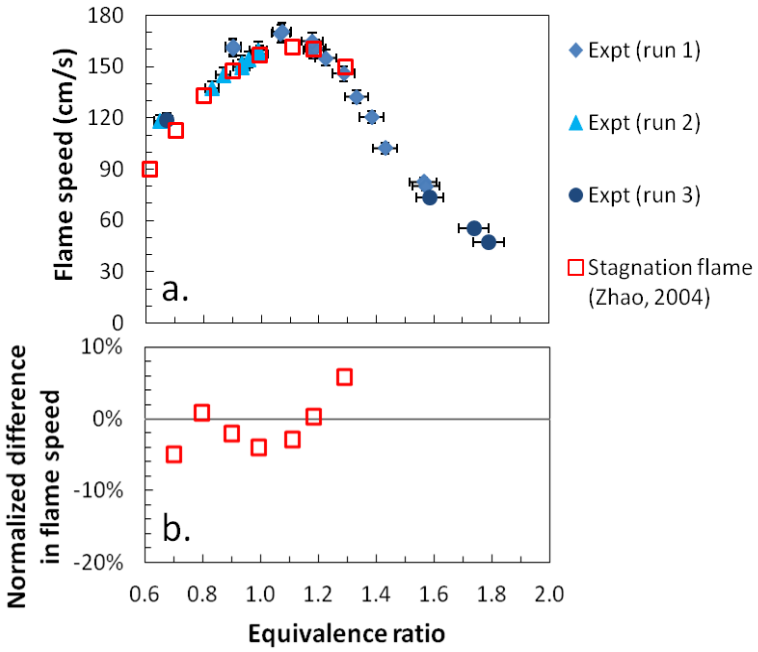

Figure 4.6. Unstretched laminar flame speed measurements of propane–air mixtures at 650 K and atmospheric pressure for validating applicability of Bunsen flame technique. (a) Actual measurement (separated by day) and comparison to stretch corrected results from stagnation flame technique. (b) Normalized difference in flame speed between current measurements and reported values.

At the significantly lean and rich equivalence ratios, the difference in flame speeds is slightly higher than 5%; however it is not possible to conclude from the current data whether the difference will increase at other equivalence ratios. It was also observed that short flames ($h/D < 1.3$) tend to predict higher flame speeds than that for tall flames. As such these measurements are not presented here. Instead the experiment was repeated at higher flowrates.

4.1.1.1 Steam dilution

Vitiation studies with steam dilution required implementing a new vaporizer system and modification to the reactant supply lines. The performance of this system and handling of steam dilution was tested by a series of sanity checks (as mentioned in Section 3.1.1.2). A final check was carried out by comparing the flame speed measurements for a known reactant mixture to those reported in the literature and to those predicted from standard chemical kinetics mechanisms. To this effect, atmospheric pressure flame speeds of a stoichiometric methane–air mixture were measured at 477 K preheat temperature. The measurements and comparison with literature data are presented in Figure 4.7. The measurements show that the measured flame speed is in good agreement (within ±10%) with similar measurements from a spherical flame technique [84] and a Bunsen flame technique with schlieren imaging to determine flame area [54]. The differences in the flame speed, between the Bunsen flame results by Mazas et al. and the current measurements are slightly larger at high steam dilution levels. However they are still reasonable given the reported uncertainty of ±5% for Mazas's data. It is worth noting that flame speed measurements from the current reaction-zone area based Bunsen flame technique are in better agreement with the stretch corrected results than the measurements from schlieren imaging based Bunsen flame technique. This indicates that using the reaction-zone edge is better for measuring unstretched flame speed than the unburned edge from schlieren imaging.

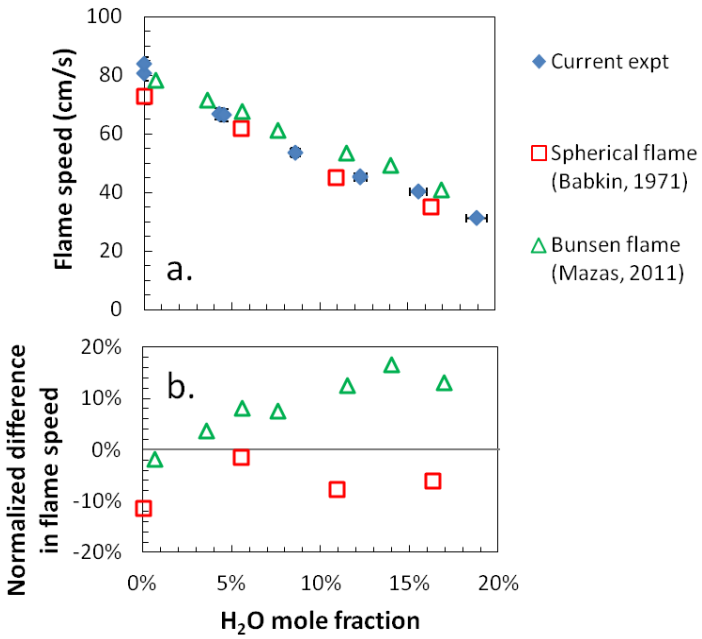

Figure 4.7 Atmospheric pressure laminar flame speed of stoichiometric methane–air mixture as a function of steam dilution at 477 K preheat temperature (473 K for literature results). (a) Actual measurements and (b) normalized difference in flame speed between current measurements and other techniques.

To briefly summarize, the atmospheric pressure validation results show that flame speeds measured with the modified Bunsen flame technique are within ±10% of stretch-corrected results from other accepted techniques. The measurements are shown to be reproducible. While the technique is not sensitive to burner diameter, a significant decrease in the non-dimensional height (h/D) of the flame was found to affect the measurements. In general, short flames ($h/D < 1.3$) can result in higher than expected flame speed values. To conclude, the modified Bunsen flame technique can be used to accurately measure the atmospheric pressure flame speed of different alkanes over a range of equivalence ratios and preheat temperatures.

4.1.2 High pressure results

The accuracy of the Bunsen flame speed technique was also examined at high pressure through a series of validation tests. Figure 4.8a presents flame speeds measured for ethane–air mixture at room temperature and 5 atm on 6 mm and 9 mm piloted-burners. The measurements are compared with stretch-corrected results from outward propagating spherical flames [29]. At fuel rich conditions, the flame surface was observed to be susceptible to instabilities, which leads to wrinkling of the flame surface and introduces error in the measured flame surface area. Reference flame images at different equivalence ratios are shown in Figure 4.9. To avoid erroneous results due to uncertainty in the flame surface area, no measurements are presented at rich conditions.

Also during the experiments, it was observed that the reactant mixture temperature was higher than the room temperature by ~25–35 K. This is because at high pressure there is an increased heat transfer to the burner, from both the main flame and the pilot flame, which are anchored closer to the burner. This results in higher burner temperatures, and therefore heating of the reactant mixture flowing through it. Furthermore because different equivalence ratio mixtures are stabilized at different flowrates and have different adiabatic flame temperatures (hence different heat transfer to the burner), they do not get preheated to the same reactant temperature. As a result, the reactant temperature variation is high for these mixtures. This is not a significant issue for the atmospheric pressure cases, where the both the flames are stabilized further downstream of the burner. In case of high pressure measurements with reactant preheating, it is possible to control the external heat source so that reactant temperature is held constant. This is not possible for cases with no preheating. Due to the difference in

reactant temperature, direct comparison to other measurements reported in the literature can be misleading. Instead, the current measurements are corrected to account for the preheat temperature and then compared with literature results. The reactant temperature correction is performed by first determining a best fit power-law (based on $S_L \propto T_u^{\alpha}$ scaling) for the flame speeds at different reactant temperatures.[n] The final temperature corrected flame speed at the desired equivalence ratio is then estimated by using a third-order polynomial fit for flame speed as a function of equivalence ratio.

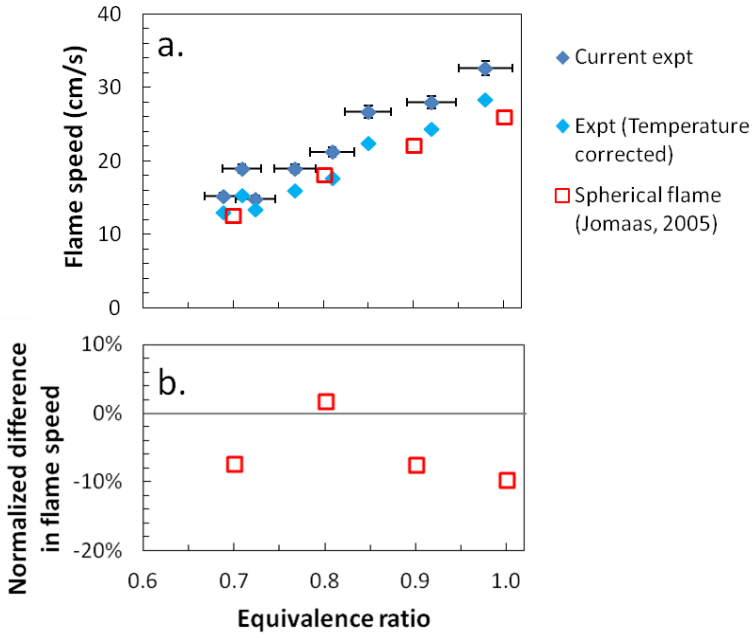

Figure 4.8. Validation results for flame speed measurement of ethane–air mixtures at 5 atm pressure using Bunsen flame approach. (a) Experimental measurements at actual conditions and those corrected to 300 K reactant temperature along with stretch corrected results from spherical flame configuration. (b) Normalized difference in flame speed between current temperature-corrected measurements and spherical flame results.

The reactant temperature corrected flame speed results presented in Figure 4.8 show that the current measurements are in good agreement with the stretch-corrected spherical flame results. As seen for the atmospheric pressure results, the measurements in

[n] Flame speed values predicted by San Diego mechanism, at different preheat temperatures (300–500 K), are used as reference for determining the power-law fit.

general tend to be higher than the spherical flame results, but are within 10% of the reported flame speeds.

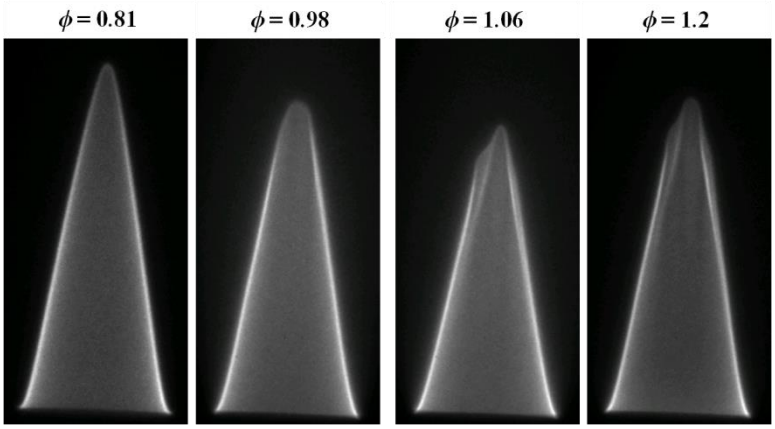

Figure 4.9. Instantaneous images of ethane–air flames, at 5 atm pressure, showing wrinkling in flame surface at rich equivalence ratio conditions. The flames were stabilized on a 6 mm piloted burner. Signal intensity is not normalized across the images.

As noted previously, the flame surface at high pressure is more susceptible to hydrodynamic and thermo-diffusive instabilities due to reduced flame thickness. As a result, the flame surface develops wrinkles, which limits the applicability of the Bunsen flame technique for flame speed measurement at high pressure. It has been shown that replacing nitrogen in the oxidizer with helium reduces the susceptibility of the flame surface to form wrinkles [21]. Helium dilution suppresses the hydrodynamics instabilities by decreasing the density gradient across the flame as a result of increase in the flame thickness from the higher thermal and mass diffusivity of helium. Furthermore helium dilution increases the Lewis number of the mixture, which is useful in suppressing the thermo-diffusive instabilities.[o]

Figure 4.10 presents flame speed measurements at room temperature for methane/oxygen/helium flames at 10 atm pressure. Here a 1:5 O_2:He molar mixture was

[o] Steam dilution also has similar effect as helium dilution on suppressing the instabilities. Therefore, helium dilution is not necessary when studying steam dilution cases.

used as oxidizer to allow for comparison with results presented in the literature for outwardly propagating spherical flames [21]. Similar to the room temperature ethane–air flames, the reactant mixture was observed to be preheated by a few degrees. Therefore, the comparison is again indirect, between the temperature corrected results from the current experiments and the literature data. As evident in Figure 4.10, the current measurements are in good agreement with the literature results for lean and stoichiometric mixtures. However at rich conditions, the measured flame speed is significantly lower than the results from the spherical flame technique.

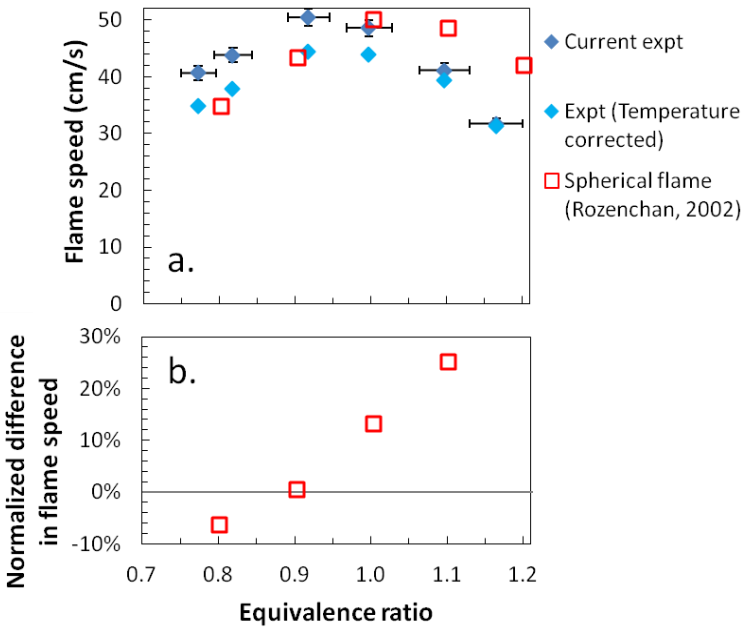

Figure 4.10. Validation results at 10 atm pressure for Bunsen flame technique for methane–O_2/He mixture. O_2:He = 1:5 by volume. (a) Current experimental measurements are at actual conditions and those corrected to 300 K reactant temperature along with results for spherical flame configuration. (b) Normalized difference in flame speed between current temperature-corrected measurements and spherical flame results.

To understand the large differences at rich equivalence ratio, the experiments were repeated by varying the flowrate (with the 9 mm burner) and also with a larger diameter (12 mm) burner. Increasing the flowrate (by ~10–40%) resulted in an increase in the flame speed (by ~5–10%) primarily for lean cases. However the flame was

observed to be more susceptible to instabilities and oscillations for the higher flowrates, which leads to weak wrinkles in the flame surface. Since the measured area of a wrinkled flame is lower than the actual area, wrinkling will result in a measured flame speed that is higher than actual. Similarly, increasing the diameter resulted in a significant increase in the oscillations in the flame surface along with an increase in the instabilities. Therefore the results from these cases were deemed unhelpful due to these inaccuracies and are not presented further.

A possible reason for the significantly lower flame speed value at the rich condition (presented in Figure 4.10) could be due to the unsteadiness in the flame surface. At the rich condition, there was a significant lateral motion in the flame surface, with the flame tip moving by ~15% of the burner diameter to the either side of the centerline of the burner. In this work, the flame motion is assessed by measuring the RMS in the measured flame area. However this may not fully capture a stretch effect on the flame speed due to the motion of the flame surface. One of the assumptions in the modified Bunsen flame technique is that the measurements are performed on a stationary flame; this is clearly not valid for this case. However for small motions in the flame surface, the effect on the flame speed is generally observed to be negligible. This may not be the case for mixtures with helium, which has a significantly higher diffusivity and hence the effect of the flame motion maybe pronounced at these conditions. It is also worth noting that the flame height for these mixtures is ~1.5–1.8 diameters, which is on the lower side, and that the flame is anchored close to the burner, i.e., no error is expected due to flame lift-off.

4.1.3 Conclusions on Bunsen flame technique validation

To summarize, it has been shown that laminar flame speed measurements from the modified Bunsen flame technique can provide a good estimate of the unstretched laminar flame speed of hydrocarbon fuels. The measurements show good accuracy and repeatability over a wide range of reactant compositions, equivalence ratios, pressures, and preheat temperatures. The measurements are generally within a ±10% agreement with other stretch-corrected measurements presented in the literature. However at high pressure and for rich mixtures, the measured flame speeds were significantly lower than values reported in the literature (at least for the methane/oxygen/helium mixture studied). This is possibly due to large oscillations observed in the flame at these conditions. The results also show scatter at different conditions due to uncertainties arising from short flames. For instance, reducing flame height significantly ($h/D < 1.3$) leads to over-prediction in measured flame speed. These effects are discussed in more detail in subsequent chapters.

4.1.4 Mechanism comparison

Since one of the goals of this work is to develop a database of flame speed values for validating chemical kinetics mechanisms, it is useful to compare the results of validations tests with predictions from different chemical kinetics mechanisms. These comparisons are useful in understanding the differences that may be present between the measurements and the models. To this effect, Figure 4.11–4.16 present the comparison for each of the validation cases presented earlier. The figures also present a normalized difference between the measured and predicted flame speed.

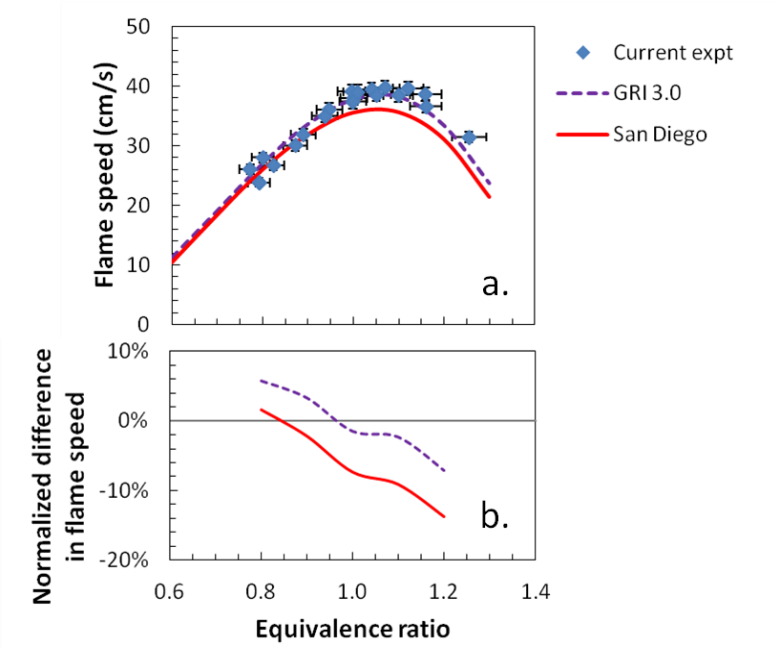

Figure 4.11. (a) Measured and predicted flame speed for methane–air mixture at atmospheric pressure and room temperature. (b) Normalized difference between the measured and predicted flame speeds.

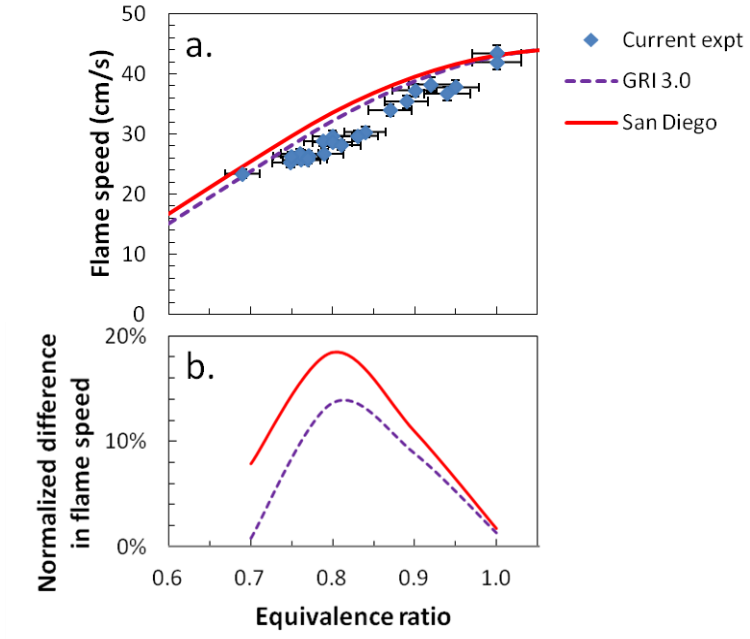

Figure 4.12. (a) Measured and predicted flame speed for ethane–air mixture at atmospheric pressure and room temperature. (b) Normalized difference between the measured and predicted flame speeds.

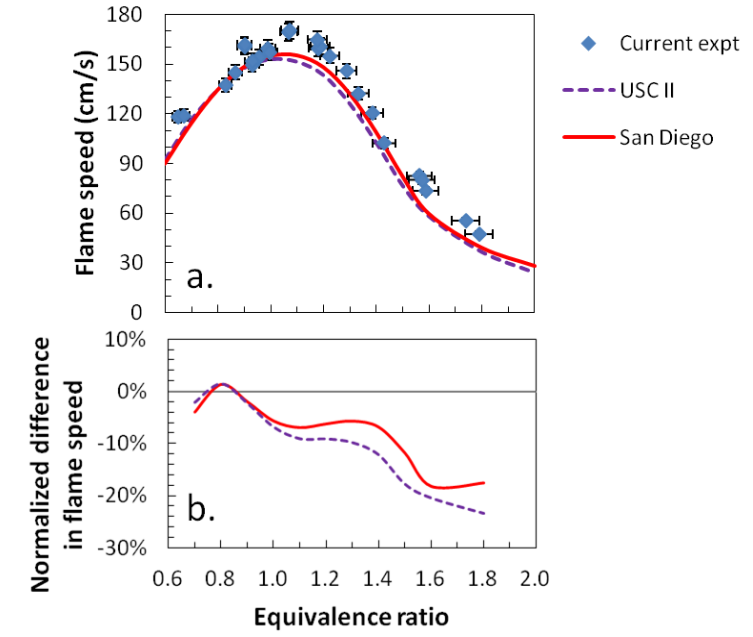

Figure 4.13. (a) Measured and predicted flame speed for propane–air mixture at atmospheric pressure and 650 K preheat temperature. (b) Normalized difference between the measured and predicted flame speeds.

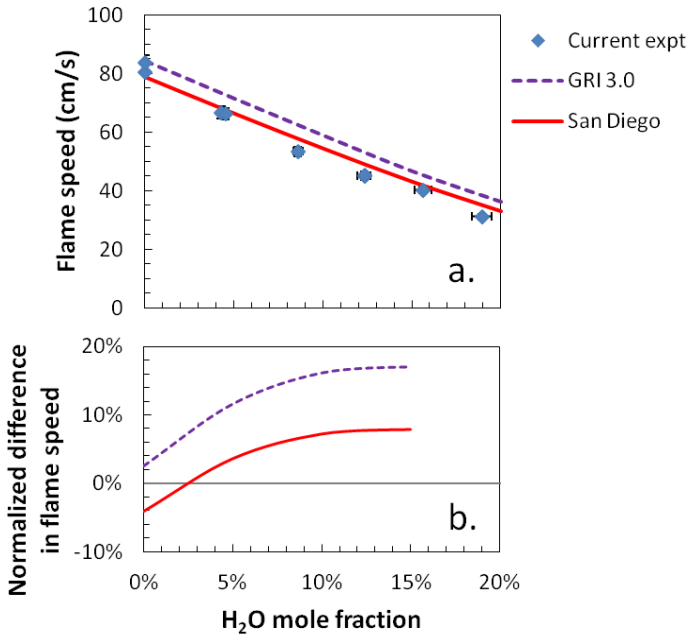

Figure 4.14. (a) Measured and predicted flame speed for stoichiometric methane–air mixture with steam dilution at atmospheric pressure and 477 K preheat temperature. (b) Normalized difference between the measured and predicted flame speeds.

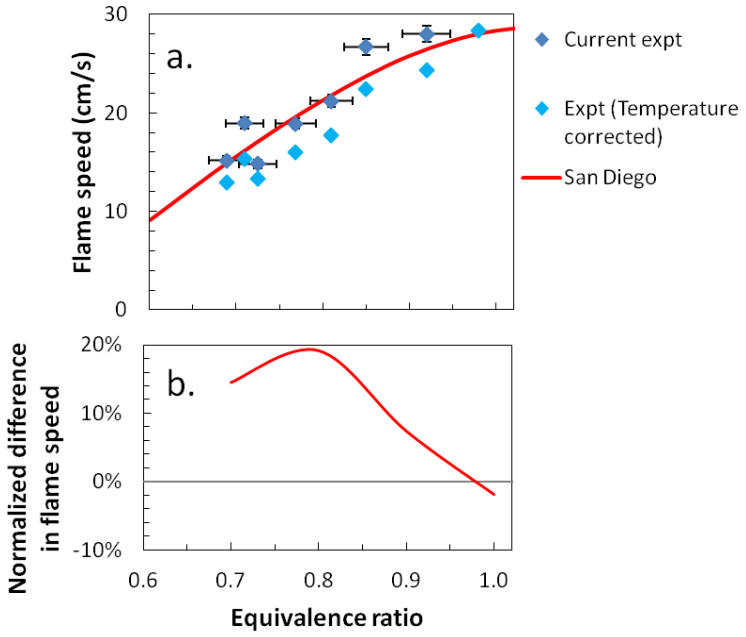

Figure 4.15. (a) Measured and predicted flame speed for ethane–air mixture at 5 atm pressure and 300 K. (b) Normalized difference between the measured and predicted flame speeds. Measurements are at actual experimental conditions and those corrected for 300 K reactant temperature.

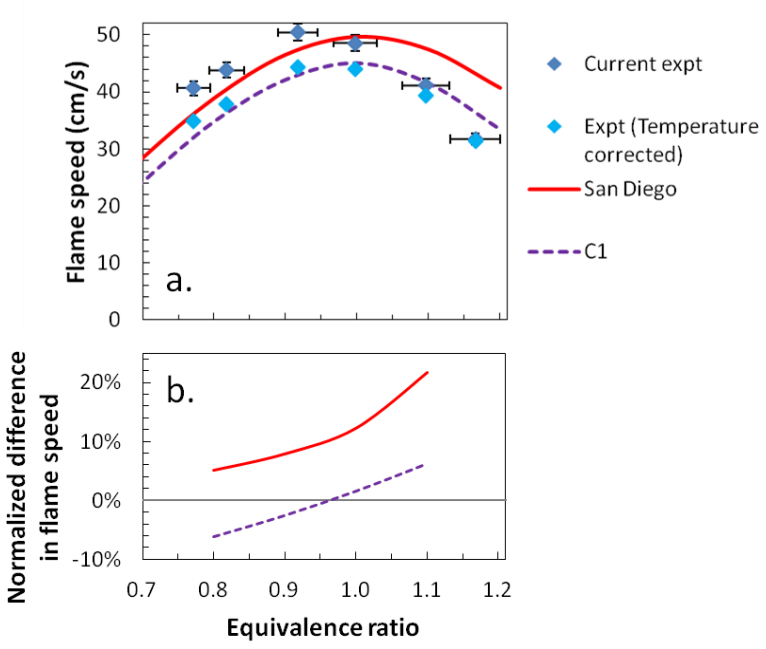

Figure 4.16. (a) Measured and predicted flame speed for CH_4/O_2/He mixtures at 10 atm pressure and 300 K. (b) Normalized difference between the measured and predicted flame speeds. Measurements are at actual experimental conditions and those corrected for 300 K reactant temperature. Oxidizer composition is O_2:He = 1:5 by vol.

Calculations are primarily presented for the San Diego and GRI 3.0 mechanisms. However, GRI 3.0 does not contain helium and is not optimized for pure propane, therefore it is not employed for those cases. Instead, USC II and a C1 [85] mechanism are employed. Multiple mechanisms are considered to provide an estimate of spread in flame speed predictions from different standard mechanisms. The differences between the mechanism predictions and the current measurements can be significant (±30%), even though the measurements are in good agreement (±10%) with other stretch-corrected flame speed results. Furthermore even between the mechanisms themselves, there is a spread in the flame speed predictions (5–10%). The uncertainty in mechanism flame speed predictions, due to inherent uncertainties in the heat of formation of the species and in the rate coefficients of elementary reactions, can be of the order of 10–20% for methane–air mixtures [86]. Furthermore the differences in the flame speed predictions are also because the mechanisms are typically optimized to achieve various performance goals, and may be adjusted to match different flame speed data sets. The spread in flame speed predictions is comparable to the spread in the stretch-corrected flame speeds from experimental measurements, which is around 10%. There is no systematic trend in the differences with equivalence ratio, although they tend to be small (< 10%) for near stoichiometric fuel/air mixtures.

4.2 Stagnation flame technique

Since the PIV technique was implemented here with a goal to improve on the spatial resolution, the current setup was validated by measuring flame speeds for stoichiometric methane–air mixtures at room conditions. The comparison of strained flame speed measurements to counter-flow flame results from the literature [33, 87] is

presented in Figure 4.17, along with strained flame speed predictions from different chemical kinetics mechanisms. The strain rate range for the current measurements is limited on the lower end by seeding density requirement and on higher end by limitations on the experimentally available flowrates. Since the primary goal was to validate the implementation of PIV measurements and data reduction, the higher strain rate range was not explored for this data set. For reference, an unstretched flame speed measurement from the Bunsen flame configuration is also presented in Figure 4.17.

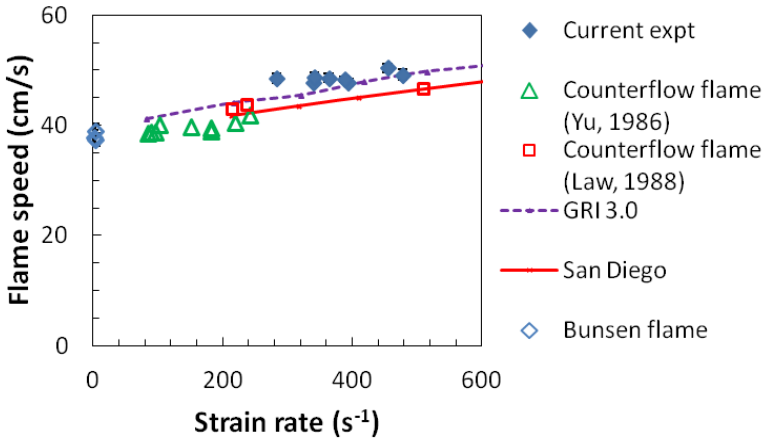

Figure 4.17. Validation of stagnation flame speed technique implementation by comparing results for room condition stoichiometric methane–air mixture from current experiments (closed symbols) to those from literature (open symbols) and mechanisms (lines). The open symbols at zero-strain are flame speed measurements by current modified Bunsen flame technique. The counterflow flame results are at equivalence ratio 0.98 and 1.04 for Yu et al. and Law et al. respectively.

The comparison shows that the current strained flame speed measurements are in good agreement, though generally higher than the literature results by 5–10%. The current uncertainty in the measured flame speed due to error in PIV measurement is roughly ±1 cm/s (so only 2-3% of the measured speeds). The result also indicates that the strain sensitivity from the current measurements is lower compared to the literature

results. The Markstein length from current measurements is – 77 μm whereas that from counterflow flame results by Law et al. is – 125 μm.

Since the focus of the stagnation flame experiments is to measure the stretch sensitivity of the reactant mixture over a range of strain rates, and because PIV allows for simultaneously measurement of the velocity and strain rate, the stagnation flame experiments can be modified to allow for faster data acquisition. This is achieved by slowly varying the flowrate of the reactants while the PIV data is being acquired. Varying the flowrate changes the strain rate imposed on the flame and hence the flame speed. Thus from a single run the stretch sensitivity measurements may be obtained over a range of strain rate as opposed to the averaging method where measurements are obtained at a fixed strain rate and averaged before changing the strain rate. To validate this instantaneous measurement approach, results were compared with those obtained by averaging the measurements at fixed strain rate.

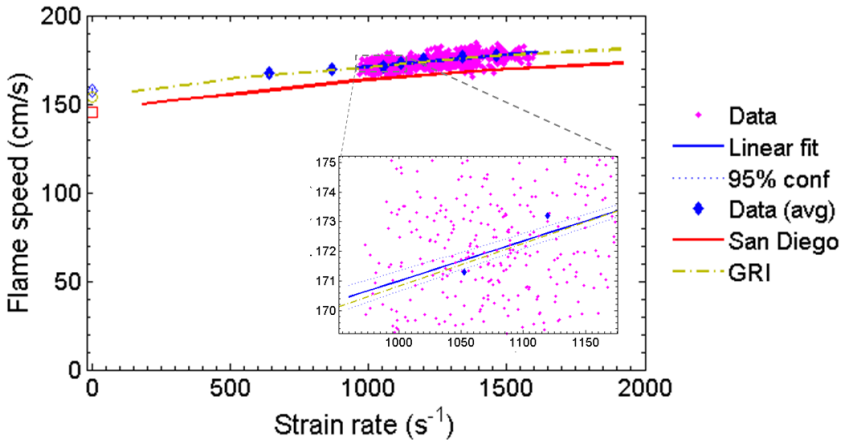

Figure 4.18. Averaged and instantaneous strained flame speed measurements for stoichiometric methane–air mixture at room pressure and 650 K. The flame speed at zero strain rate are from linear extrapolation of instantanous data and mechanism predictions.

Figure 4.18 compares results from these two measurement approaches, along with predictions from chemical kinetics mechanism and a linear fit to the instantaneous (scanned) measurements. The measurements are in excellent agreement with each other,

both in terms of the measured strained flame speeds and the stretch sensitivity. The mechanisms also predict similar stretch sensitivity but show slight differences in the actual flame speed value (~4%). The coefficients of linear regression,[p] $S_L = S_L^0 - l\,\kappa$, are presented in Table 4.1, along with the associated 95% confidence interval for the linear fit to experimental results. The uncertainty in the coefficients for the fit is better than 2%. The averaged measurements show a slightly higher uncertainty due to the number of data points available for the linear regression.

Table 4.1. Linear regression coefficients for data presented in Figure 4.18.

	S_L^0 (cm/s)	l (μm)
Data (averaged)	158.0±2.9	– 136 ± 26
Data (instantaneous)	157.5±1.5	– 135 ± 13
GRI 3.0	156.3	– 137
San Diego	148.5	– 136

Figure 4.18 shows that the instantaneous approach has a significant scatter in flame speed and strain rate values. However, the stretch sensitivity as measured by the slope of the linear regression has significantly smaller uncertainty due to the high sampling rate and strain rate range for data acquisition. The 95% confidence interval for the linear fit to the instantaneous measurements is less than ±1% of the actual fit. The linear regression and its confidence interval, for the instantaneous measurements, are presented only over the range where measurements were performed. This approach will be used in later chapters to present results where strain flame speed measurements are

[p] The linear regression was performed over the whole range of available data in the same manner for the experimental data sets and simulation results. Since the range of κ range over which the linear regression is performed is different, it can introduce some uncertainty in the regression. This is important if S_L behaves non-linearly over the range of κ. For example see results presented in Table 6.2. However for most of the data presented S_L varies linearly with κ and the regression was performed over the whole range.

performed in similar manner, as it helps convey both the extent of data acquisition and the corresponding linear fit, thereby reducing the clutter due to the actual data points.

4.3 Chapter summary

This chapter presented a comparison of flame speed measurements with the modified Bunsen flame with literature results over a range of conditions. The current measurements are within ±10% (generally higher) of other stretch-corrected values reported in literature over range of equivalence ratio (0.6–1.3). No correlation is observed between the difference in flame speed and equivalence ratio. The measurements are shown to be repeatable and independent of burner size, with systematic uncertainty due to fluctuations in the flame area and flowrate calculated to be less than 3.5%. These uncertainties do not account for the stretch effect due to the motion of the flame surface, which along with other sources of stretch (strain and curvature) remains the largest un-quantified source of uncertainty in the measurements. The effect of stretch, in terms of the influence of flowrate and hence the flame height, on the flame speed measurements is explored in more detail in subsequent chapters. The current Bunsen flame speed measurements also show differences up to ±20% in comparison to the mechanism predictions. Such differences in flame speed with mechanism predictions are seen in previous stretch-corrected results too and provide a reference when looking at differences in flame speed at conditions where no measurements have been performed before.

The chapter also presented strain flame speed measurements using a stagnation flame configuration. The results serve to verify the implementation of current setup and also show the feasibility of acquiring instantaneous strain rate sweeps of flame speed data with high accuracy.

CHAPTER 5

FLAME SPEED OF PURE FUELS WITH VITIATION

Vitiated air combustion is encountered in modern gas turbines and other combustion applications due to techniques such as exhaust gas recirculation, inter-turbine combustion, and staged combustion, which are used for improving efficiency and reducing emissions. Vitiated air from hydrocarbon combustion can contain significant proportion of combustion products, e.g., CO_2, H_2O, CO, NOx and unburned hydrocarbon, in addition to N_2. Moreover steam is sometimes added to reactant mixtures to reduce NOx emissions and improve life and efficiency of gas turbines for power generation. The presence of combustion products causes a decrease in the O_2 mole fraction in the oxidizer.

This chapter studies the influence of diluents on flame speed of fuel–air mixtures. The first half of this chapter focuses on the effect of N_2, CO_2 and H_2O dilution on the flame speed of propane–air mixtures. The second half of the chapter investigates flame speeds of methane–air and propane–air mixtures at constant adiabatic flame temperature. This is achieved by varying the dilution level and equivalence ratio of the mixture while keeping the flame temperature constant. The measurements reported here were performed at atmospheric pressure using the 9 mm contoured nozzle burner and the modified Bunsen flame technique. The oxidizer mixture, with O_2 mole fraction as low as 15% of oxidizer (by vol.), is formed by adding diluent to air. Since vitiated air is often

encountered at high temperatures, this study focuses on high reactant preheat temperature (~650 K).

5.1 Effect of diluents on flame speed of propane–air mixture

5.1.1 Nitrogen dilution

Nitrogen is the least chemically active of the three diluents considered (viz. N_2, CO_2 and H_2O). Since N_2 chemistry occurs primarily in the high temperature product region of the flame, the effect of N_2 dilution on flame speed should be limited to changes caused due to its heat capacity and changes in O_2 concentration in the reactant mixture. Figure 5.1a presents the measured flame speeds for propane–air mixtures, as a function of equivalence ratio at three different O_2:N_2 volumetric ratios, specifically 21:79, 16.7:83.3 and 15:85, which correspond to added N_2 mole fractions (compared to air) of 0%, 20.6% and 28.6%. As expected, increasing the amount of dilution decreases the flame speed of the mixture. The largest reduction in flame speed with dilution occurs near the stoichiometric condition, which is not surprising as this is also near the peak flame speed location. Furthermore at sufficiently rich equivalence ratios, the flame speeds appear to be approaching similar values for the two dilution cases, though this may be a result of the measurement uncertainty. Also at sufficiently rich equivalence ratio (1.4–1.6) the flame speed of the mixture shows a marked change in slope. The equivalence ratio where this change occurs decreases with increase in the dilution level (and hence a decrease in the peak flame speed and O_2 mole fraction in the oxidizer).

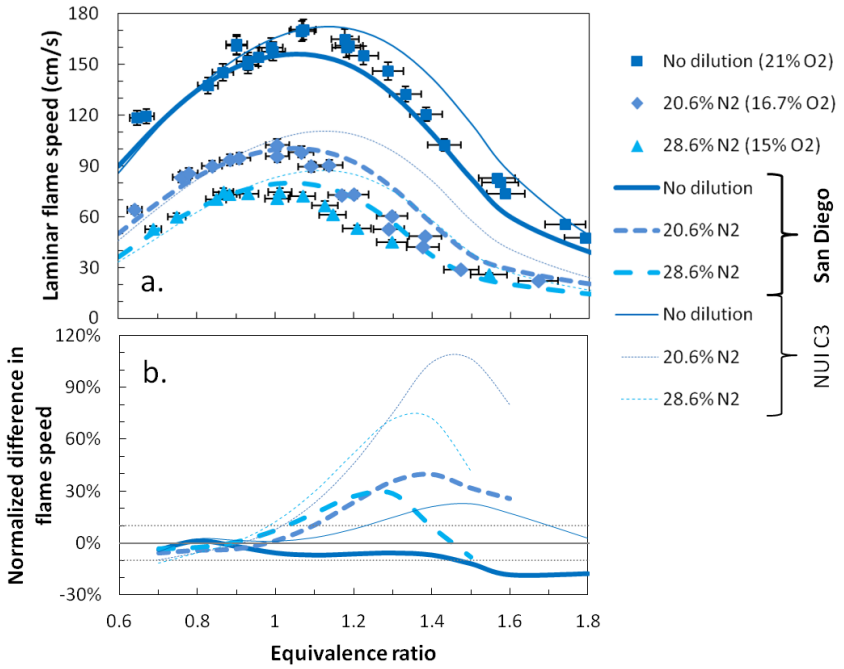

Figure 5.1. Atmospheric pressure laminar flame speed of propane–air mixture with N_2 dilution at 650 K. (a) Bunsen flame measurements and mechanism predictions. (b) Normalized percentage difference between measured and predicted flame speeds. The lines are for San Diego (thick) and NUI C3 (thin) mechanisms. Oxidizer mixture consists of standard air and excess N_2. The legend specifies the added N_2 (and O_2) mole fraction in the oxidizer mixture.

Figure 5.1a also includes the flame speed predictions by the San Diego and NUI C3 mechanisms, which are in good agreement (within ±10%) with the measurements, for the two dilution cases, at lean and stoichiometric conditions. However at moderately rich equivalence ratios, the mechanisms predicts significantly higher (> 20%) flame speed than the measured values, with the NUI mechanism predictions being much higher than the San Diego results. Figure 5.1a also shows that both mechanisms under-predict the change in peak flame speed with N_2 dilution. Additionally, the rich mixture, where the flame speed slope changes, is predicted correctly by the San Diego mechanism but the NUI mechanism predicts it at a higher equivalence ratio.

Figure 5.1b, which shows the normalized fractional difference between the predicted flame speed from a best fit curve (fifth-order polynomial) to the experimental results, provides a better visualization of the differences in flame speed. It is interesting to

note that, for a given mechanism, similar fractional differences in the predicted and measured flame speeds are observed over a wide range of equivalence ratio, for both N_2 dilution levels. The difference in the flame speeds for rich mixtures is much greater than the expected experimental uncertainties (±5–10%), indicating a possible limitation in the flame speed prediction from the mechanisms at these conditions. This observation is discussed further in subsequent sections.

Both the mechanisms considered here viz. San Diego and NUI C3 are based on species up to C_3 only. It has been observed that, especially at rich conditions, recombination of methyl, ethyl and propyl radicals can be important in capturing the fuel chemistry correctly and on accurately predicting flame speed [88, 89]. This could be one reason for the large difference in flame speed observed at rich conditions. In order to assess this possibility, a simulation was performed for propane/air mixtures with nitrogen dilution using the NUI C5 mechanism, which includes higher order species than the C3 mechanism. The C5 mechanism predictions are higher than those obtained with the C3 mechanism by ~0–9% over ϕ = 1.3–1.8. The difference is slightly higher (~2–11%) for nitrogen dilution cases. Since the predictions from the C5 mechanisms show a larger disagreement with the measured flame speeds, it is unlikely that the lack of higher order hydrocarbons is the source of the disagreement.

Figure 5.2 shows the effect of N_2 dilution on the flame speed of a rich (ϕ = 1.1) propane–air mixture. The flame speed measurements, from the current Bunsen flame technique,[q] are within +3% to –15% of the stretch corrected measurements from the

[q] The Bunsen flame speed measurements were interpolated to correct for the equivalence ratio.

stagnation flame technique [32]. Furthermore both the techniques and mechanisms indicate that the flame speed of the mixture decreases nearly linearly with dilution.

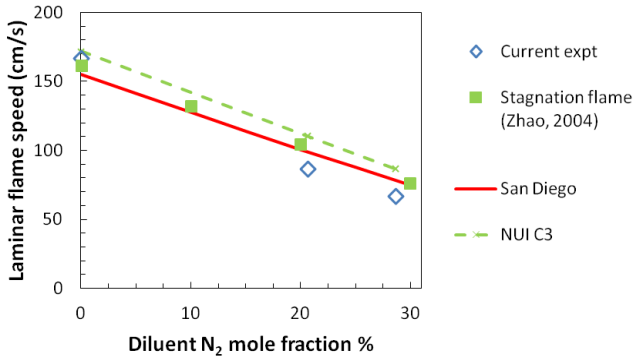

Figure 5.2. Laminar flame speed of rich (ϕ = 1.1) propane–air mixture as a function of N_2 dilution. Results are for atmospheric pressure and 650 K preheat. Current experiment results were interpolated to correct for the equivalence ratio.

The effect of N_2 dilution is studied further by analyzing simulated (San Diego mechanism) flame speeds of propane–air mixtures, with the N_2 diluted results normalized by the undiluted flame speed at the corresponding equivalence ratio (Figure 5.3a). The different equivalence ratio mixtures considered show similar nearly linear decreases in normalized flame speed. However, the rate of change in the flame speed is slightly higher for equivalence ratios further from a stoichiometric condition. This quasi-linear variation of flame speed with dilution and the increase in slope away from a stoichiometric equivalence ratio were also observed by Zhao et al. [32] in simulations for the propane–air with nitrogen dilution, at atmospheric pressure and over a range of preheat temperatures (300–650 K). The decrease near ϕ of 1 may be closer to linear because for the same amount of dilution, the fractional decrease in the adiabatic flame temperature is lower. To examine the influence of temperature, Figure 5.3c presents semi-log plots for the variation of flame speed with dilution level and temperature change.

As discussed in more detail in Section 5.1.5, N_2 dilution does not have a direct chemical effect on the flame speed of propane–air mixture. The effect of N_2 dilution on the flame speed is due to the decrease in the adiabatic flame temperature of the mixture and the decrease in the O_2 concentration.[r] Standard scaling models for flame speed suggest a dependence on flame temperature due to its influence on both the (assumed) Arrhenius rate kinetics and the diffusivity [73] viz. $S_L \propto T_{\mathrm{ad}}^m \exp(-E_a/2RT_{\mathrm{ad}})$, where E_a is the activation energy and R is the gas constant. The dependence of flame speed on the adiabatic flame temperature is seen in Figure 5.3b, which shows normalized flame speed (S_L/S_L^0) as a function of normalized change in flame temperature $(\Delta T_{\mathrm{ad}}/T_{\mathrm{ad}}^0)$, where $\Delta T_{\mathrm{ad}} = T_{\mathrm{ad}}^0 - T_{\mathrm{ad}}$ is the change in adiabatic flame temperature from the reference, undiluted condition (represented by superscript 0).

With the semi-log scaling used in Figure 5.3b, the drop in normalized flame speed is nearly linear with the fractional decrease in adiabatic flame temperature. Moreover, all the equivalence ratios cases considered here show essentially the same variation in flame speed when the dilution effect is scaled by the fractional decrease in flame temperature. Expanding the flame speed expression above in a Taylor series and truncating the result to first order in $\Delta T_{\mathrm{ad}}/T_{\mathrm{ad}}^0$, the variation in the flame speed can be expressed as,

$$\ln\left(\frac{S_L}{S_L^0}\right) \approx -\left(m + \frac{E_a}{2RT_{\mathrm{ad}}^0}\right)\frac{\Delta T_{\mathrm{ad}}}{T_{\mathrm{ad}}^0} = -m\frac{\Delta T_{\mathrm{ad}}}{T_{\mathrm{ad}}^0} - \frac{E_a}{2R}\frac{\Delta \mathrm{T_{ad}}}{\left(\mathrm{T_{ad}^0}\right)^2} \qquad 5.1a$$

[r] During numerical simulations, it is possible to modify the heat capacity of N_2 such that the effect of flame temperature is isolated from the changes in O_2 concentration, thereby separating the thermal and indirect chemical kinetics effect of N_2 dilution. However this was not done in the present study.

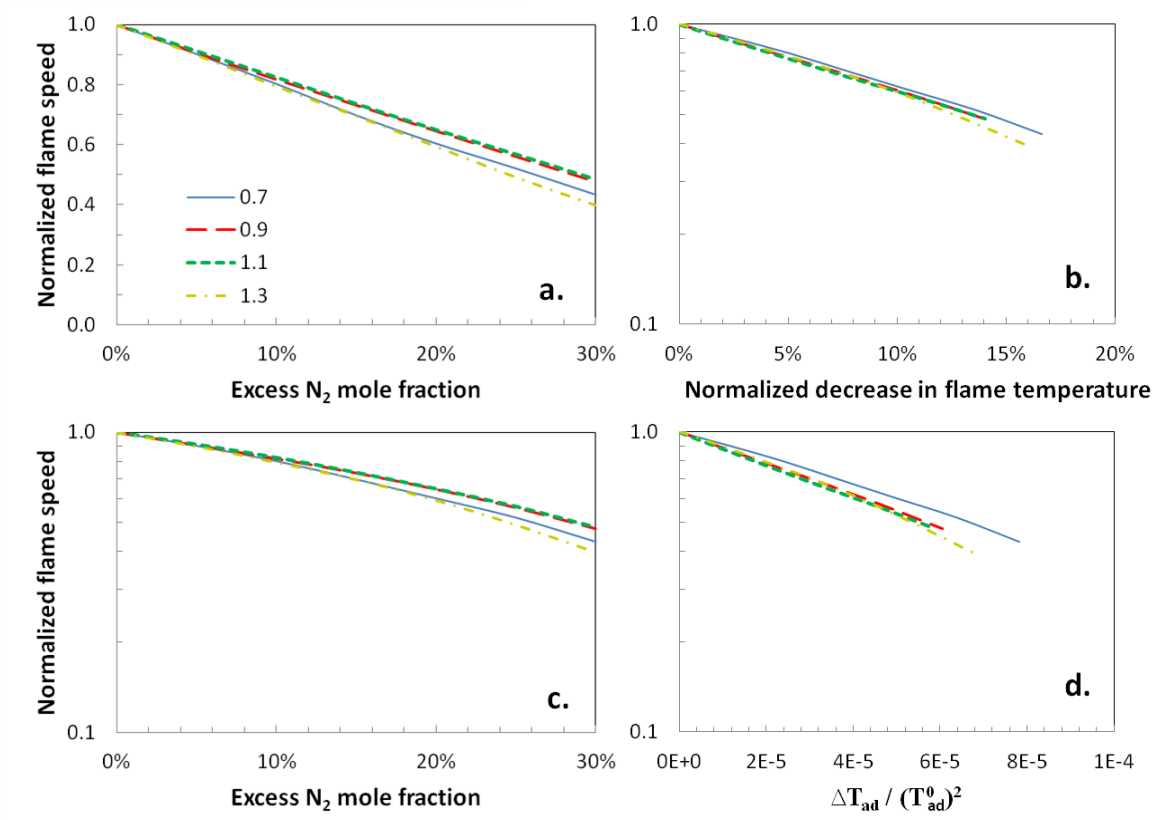

Figure 5.3. Laminar flame speeds of propane–air mixture with N_2 dilution (normalized by the flame speed of the undiluted mixture) at atmospheric pressure, 650 K and different equivalence ratios. Linear (a) and semi-log (c) plot of flame speed as a function of added N_2 mole fraction. Variation of flame speed as a function of change in flame temperature normalized by (b) the flame temperature of undiluted mixture and (d) square of the flame temperature of undiluted mixture. Calculation performed using San Diego mechanism.

The second term in the expression above (5.1a) scales inversely with $T_{\mathrm{ad}}^{0\,2}$. However when the normalized flame speed is plotted against $\Delta T_{\mathrm{ad}}/\left(T_{\mathrm{ad}}^{0}\right)^{2}$ (Figure 5.3d), the flame speeds at different equivalence ratios do not collapse as well as when the $\Delta T_{\mathrm{ad}}/T_{\mathrm{ad}}^{0}$ scaling is used. The fact that the results for different equivalence ratios nearly collapse to one curve indicates that the effective m (the value based on fitting the results to a simple power law dependence[s]; subsequently referred to as m' in this thesis) is nearly the same for all the equivalence ratios examined. For the cases considered, the value of

[s] m' is defined based on the relation, $\ln(S_L/S_L^0) = -m'(\Delta T_{\mathrm{ad}}/T_{\mathrm{ad}}^0)$.

m' is found to be 4.8–5.5 based on linear regression, with $R^2 > 99\%$, over the range of data. The high value of m', compared to m[t], suggests that the second term in Equation 5.1a (due to the exponential dependence of S_L on T_{ad}) is also important and is captured to a certain extent with the current $\Delta T_{ad}/T_{ad}^0$ scaling. The nearly linear trend and the agreement among the different equivalence ratio cases begins to fail at high dilution levels, i.e., significant decrease (> 10–15%) in flame temperature. This is likely due to the influence of the higher order terms.[u]

5.1.2 Carbon dioxide dilution

The effect of CO_2 dilution on laminar flame speeds of propane–air mixtures was studied at two CO_2 dilution levels, viz. (i) 10 mol% CO_2 dilution in oxidizer (corresponding to O_2:N_2:CO_2 volumetric ratio of 18.9:71.1:10) and (ii) 5 mol% CO_2 and 15.5 mol% N_2 dilution in oxidizer (with O_2:N_2:CO_2 ratio of 16.7:78.3:5). These compositions were selected to explore different N_2 and CO_2 vitiation conditions as shown in Figure 5.4.

Figure 5.5a presents the flame speed measurements for propane–air mixtures with N_2 and CO_2 dilution. The addition of CO_2 results in a significant decrease in flame speed. Furthermore, CO_2 addition leads to a larger decrease in flame speed than N_2 addition, as observed by comparing the flame speeds for 16.7% O_2 cases for N_2 (Figure 5.1a) and CO_2 (Figure 5.5a) dilution. For example, the flame speed for a stoichiometric mixture

[t] m has a value generally less than 1 [73].

[u] For $S_L \propto T_{ad}^m \exp(-E_a/2RT_{ad})$, the Taylor series expansion results in:

$$\ln\left(\frac{S_L}{S_L^0}\right) \approx -\left[\left(m + \frac{E_a}{2RT_{ad}^0}\right)\frac{\Delta T_{ad}}{T_{ad}^0} + \left(\frac{m}{2} + \frac{E_a}{2RT_{ad}^0}\right)\left(\frac{\Delta T_{ad}}{T_{ad}^0}\right)^2 + \cdots\right] \quad 5.1b$$

with only N_2 dilution (O_2:N_2 = 16.7:83.3) is ~99 cm/s whereas that for N_2 and CO_2 dilution (O_2:N_2:CO_2 = 16.7:78.3:5) is ~77 cm/s.

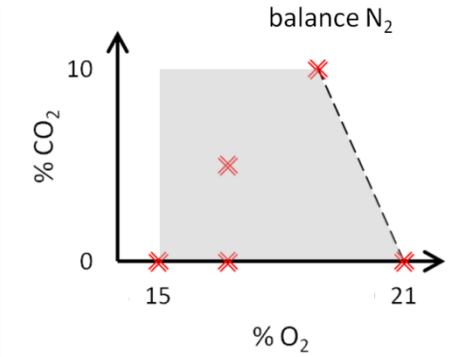

O_2	N_2	CO_2	H_2O
21	79		
18.9	71.1	10	
17.7	66.8		15.5
16.7	83.3		
16.7	78.3	5	
15	85		

Figure 5.4. Schematic showing the relationship between different N_2/CO_2 dilution cases studied (left) along with the actual mole fraction composition of the oxidizer mixture (right). The dashed line represents O_2:N_2 ratio of 21:79.

The greater decrease in flame speed, associated with CO_2 addition, is expected because CO_2 results in a higher decrease in flame temperature than N_2 for the same equivalence ratio.[v] This decrease in flame temperature is primarily driven by the higher (molar) specific heat capacity of CO_2 compared to N_2. CO_2 addition also leads to a reduction in the net oxidation of CO, due to a decrease in the extent of completion of the CO + OH ⇔ CO_2 + H reaction. Since CO oxidation is responsible for significant heat release in hydrocarbon combustion, more CO in the products means a decrease in the final temperature. Because the change in amount of un-oxidized CO can be small (few 100–1000's ppm), its effect on the final flame temperature is marginal for many mixtures. However, CO_2 dilution can still have a chemical effect due its effect on the CO oxidation rate within the flame and thus the heat release profile. The chemical effect of the diluents is discussed later in Section 5.1.5.

[v] For the stoichiometric propane–air mixtures, mentioned here, the flame temperature decreases from 2459 K (at no dilution) to 2254 K for N_2 dilution case and to 2217 K for CO_2 and N_2 dilution i.e. the temperature decrease for the latter case is ~20% higher.

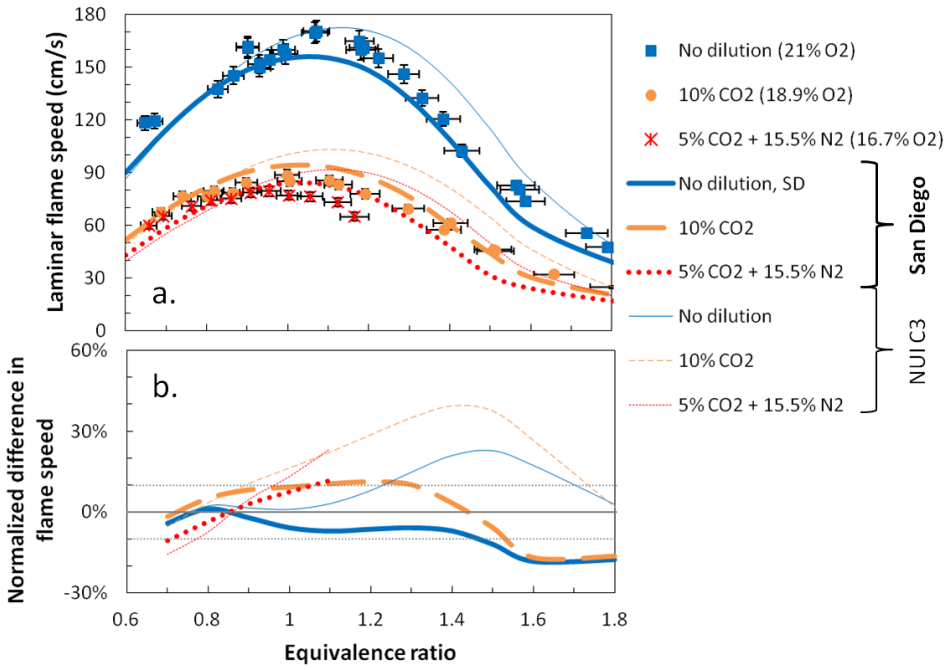

Figure 5.5. Atmospheric pressure laminar flame speed of propane–air mixture with N_2 and CO_2 dilution at 650 K. (a) Bunsen flame measurements and mechanism predictions. (b) Percentage difference between measured and predicted flame speeds. The lines are for San Diego (thick) and NUI C3 (thin) mechanisms. Oxidizer mixture consists of standard air, CO_2 and added N_2 (diluent and O_2 fraction are specified in the legend).

Figure 5.5a further shows that for 10% CO_2 dilution, the peak in flame speed is closer to a stoichiometric mixture, compared to the 5% CO_2 case, which peaks lean ($\phi \approx 0.9$). Interestingly for lean mixtures, the two dilution cases appear to have very similar flame speeds, although this is within the uncertainty of the measurements. Also similar to the N_2 dilution findings, the 10% CO_2 dilution case shows a change in the flame speed profile around $\phi \sim 1.6$; this is close to where the no dilution case also changes slope. Since the 10% CO_2 dilution case has a similar peak flame speed as 20.6% N_2 dilution (Figure 5.1a), it is likely the location where the flame speed changes slope is affected by the O_2 mole fraction in the oxidizer.

The flame speed predictions from the San Diego mechanism show a good agreement (within ±10%) with the measured flame speed for lean and close to stoichiometric mixtures. Figure 5.5b shows that good agreement is also observed for rich

mixtures for high O_2 content (18.9%). However for the low O_2 content (16.7%) mixture, the differences between the measured and predicted flame speed exhibits an increase similar to the one observed for N_2 dilution (Figure 5.1b). Figure 5.5 also includes predictions from the NUI C3 mechanism, which produces good agreement to the measurements over a very limited range of lean equivalence ratios (~0.7–0.9). For stoichiometric and rich mixtures, the NUI predictions show significant difference from the measured flame speed values. These differences are similar to those observed for N_2 dilution (Figure 5.1), though somewhat smaller in magnitude. The trend in the difference in flame speed, especially at low O_2 content and for rich mixtures, suggests a possible limitation in the measurement technique and/or the chemical kinetics mechanism at these conditions. Additionally, both mechanisms under-predict the change in peak flame speed with addition of CO_2. Since this was also observed for N_2 dilution, the under-predictions is more likely due to a general decrease in O_2 content rather than the specifics of the diluent used.

The effect of dilution on flame speed for a fixed equivalence ratio can again be examined using the simulation results. Calculations performed using the San Diego mechanism and presented in Figure 5.6a show that the different equivalence ratio cases follow the same trend. Unlike the N_2 results, the decrease in flame speed with increasing CO_2 dilution is not linear with dilution level; rather, the flame speed decrease is moderated at higher dilution levels. Like the N_2 dilution results, however, the decrease in flame speed is well correlated to the change in adiabatic flame temperature. As before, the log of the flame speed ratio scales nearly linearly with $\Delta T_{\mathrm{ad}}/T_{\mathrm{ad}}^{0}$ (Figure 5.6b), at least

until high dilution levels. Also, the different equivalence ratio cases nearly collapse with an effective exponent, m', for these conditions of 6.8–7.7.

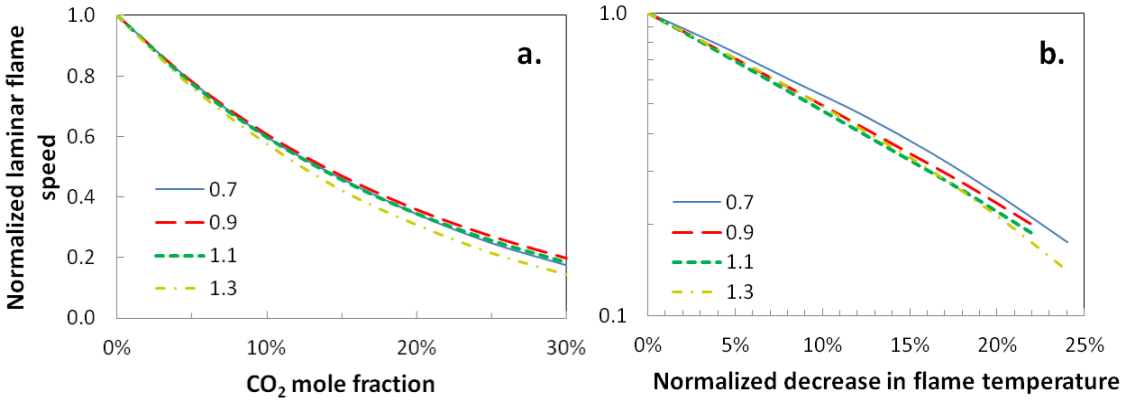

Figure 5.6. Normalized flame speed of propane–air mixture (a) as a function of CO_2 dilution and (b) change in adiabatic flame temperature normalized by the flame temperature of undiluted mixture, at 1 atm and 650 K for different equivalence ratios. Calculations performed using San Diego mechanism.

Compared to the N_2 results, the drop in flame speed is greater for the same fractional decrease in flame temperature and there is a slightly greater difference between the equivalence ratio cases (especially ϕ = 0.7). These observations may be a result of the direct chemical influence of CO_2. As noted previously, the presence of CO_2 inhibits the CO oxidation reaction (CO + OH ⇔ CO_2 + H), as well as lowers the adiabatic flame temperature. While these are separate influences on flame speed, they are correlated; additional CO_2 both lowers temperature and further inhibits the CO oxidation. The correlation can change, however, with equivalence ratio. For example, how much CO_2 inhibits the oxidation of CO also depends on the concentrations of OH and H, which should be different for lean and rich flames. Thus, while the success of the $\Delta T_{ad}/T_{ad}^0$ correlation indicates the thermal effect likely dominates (quantified later in Section 5.1.5), the direct chemical effects are also likely captured by the correlation.

5.1.3 Steam dilution

Flame speed measurements were also performed for atmospheric propane–air mixtures with fixed steam dilution. Figure 5.7 presents the flame speed measurements for propane–air–steam mixtures with 15.5 mol% of the oxidizer being H_2O (this corresponding to 17.7 mol% O_2 in the oxidizer). The flame speed profile changes slope at $\phi \sim 1.5$. Also around $\phi = 1.1$, the measured flame speed dips, though this could be due to experimental scatter.

Figure 5.7 also compares the measurements with predictions from the San Diego and NUI C3 mechanisms. As observed for other dilution cases, the San Diego mechanism predictions are in good agreement (within ±10%) with the measured flame speeds for lean and near stoichiometric mixtures. Although, they tend to be higher than the measurements for steam dilution, and lower for N_2 and CO_2 dilution. Furthermore, at rich conditions, the predicted flame speeds become progressively lower than the measured values, reaching a difference of ~40% at the richest condition examined. The trend is different for the NUI mechanism; there, the predicted flame speed values are *higher* by 10-15% compared to the measurements until $\phi \sim 1.5$, at which point the predicted flame speed decreases more rapidly than the measured data. The disagreement between the two mechanisms for rich mixtures is ~10–25%, which is similar to the results for the other diluents.

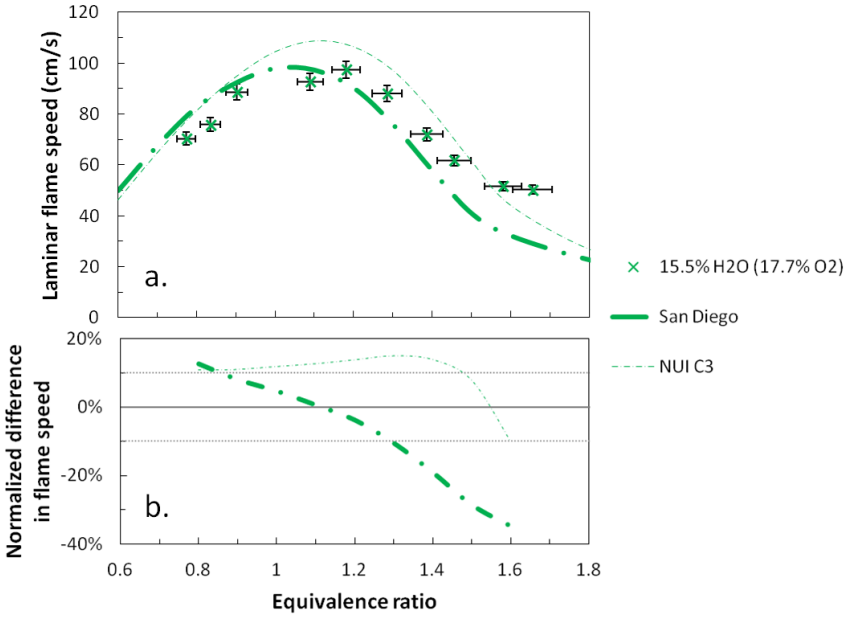

Figure 5.7. Laminar flame speed of propane–air mixture with steam dilution (15.5% of oxidizer by vol.) at atmospheric pressure and 650 K. (a) Bunsen flame measurements and mechanism predictions. (b) Percentage difference between measured and predicted flame speeds. Lines represent calculations from San Diego (thick) and NUI C3 (thin) mechanism.

To further investigate the effect of H_2O dilution, flame speeds of propane–air mixtures were calculated with the San Diego mechanism and normalized by the corresponding value for the undiluted mixture; these are presented in Figure 5.8. The flame speed decreases roughly linearly with increase in H_2O dilution, and like the N_2 (Figure 5.3b) and CO_2 (Figure 5.6b) results, the decrease in normalized flame speed correlates well with the fractional drop in adiabatic flame temperature. The sensitivity of the flame speed to fractional drop in temperature is greater compared to N_2 dilution, but less than for CO_2 dilution (m' ~ 5.7–6.6). However the R^2 value of the linear regression for H_2O dilution case is poor ($R^2 > 97\%$) compared to the N_2 and CO_2 dilution cases ($R^2 > 99\%$). This suggests that while the variation, in $\ln(S_L/S_L^0)$ as a function of $\Delta T_{ad}/T_{ad}^0$, is similar for different equivalence ratio conditions, it has a slight non-linear dependence. The non-linearity could be due to a change in the reaction chemistry with change in H_2O dilution level.

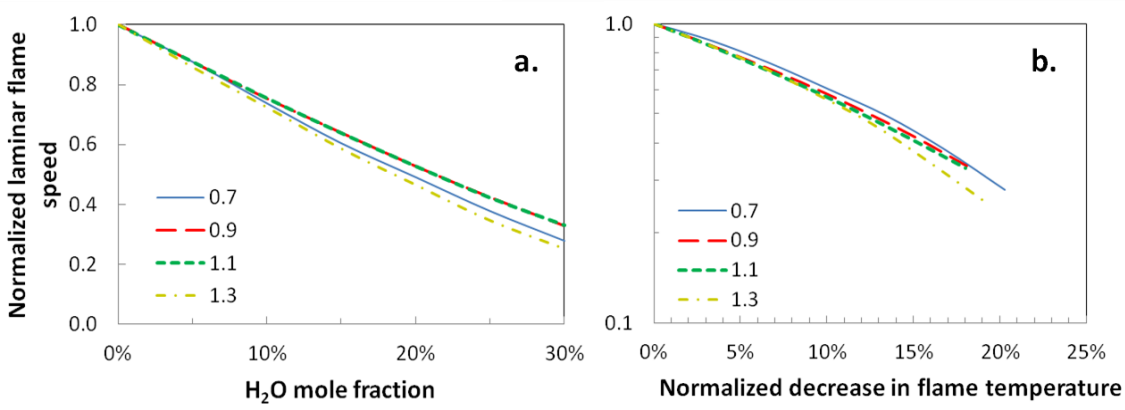

Figure 5.8. Normalized flame speed of propane–air mixture (a) as a function of CO_2 dilution and (b) change in adiabatic flame temperature normalized by the flame temperature of undiluted mixture, at 1 atm and 650 K for different equivalence ratios. Calculations performed using San Diego mechanism.

Figure 5.9 compares the differences between the measured and predicted flame speeds for the different dilution cases with propane–air mixtures. In general for both mechanisms, the lean and stoichiometric mixtures ($\phi = 0.7–1$) show good agreement (within ±10%) between the measured and predicted flame speeds. However for rich mixtures, specifically for low O_2 content and with N_2 or CO_2 dilution, the predicted flame speeds are significantly higher than the measured values. For rich mixtures and H_2O dilution, the agreement is better, though not as good as for lean and stoichiometric mixtures. The agreement with the measurements at rich conditions is closer for the San Diego mechanism than for the NUI predictions. The reason for the disagreement between the measured and predicted flame speed is expounded further in subsequent sections and in Chapter 6.

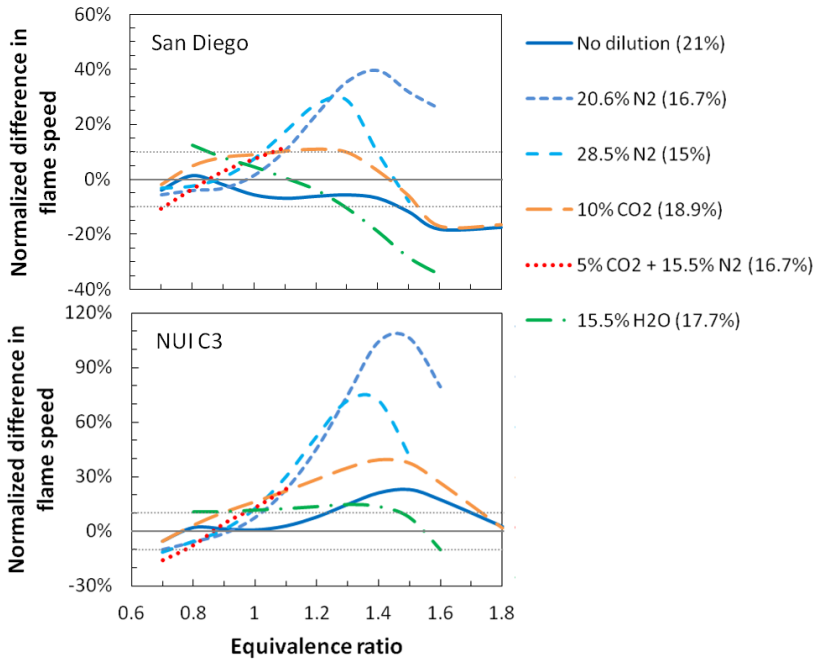

Figure 5.9. Normalized difference in measured and predicted laminar flame speed of propane–air mixture with different diluents. Differences for atmospheric pressure condition with reactants at 650 K. Legend specifies the mole fraction of diluent in oxidizer with remaining fraction being standard air,while the number in bracket are mole fraction of oxygen in oxidizer mixture.

5.1.4 Summary of flame speed measurements with vitiation

To summarize, flame speed measurements for propane–air mixtures with $N_2/CO_2/H_2O$ dilution show that flame is most affected by CO_2 addition followed by H_2O and N_2 respectively. The results also show that the equivalence ratio where the flame speed changes slope for sufficiently rich mixtures decreases with the decrease in the O_2 content of the oxidizer.

Flame speed predictions from different chemical kinetics mechanisms show good agreement with the measurements for lean and near stoichiometric conditions. However for rich mixtures, the mechanisms predict a significantly higher flame speed. The mechanisms also tend to under-predict the decrease in peak flame speed with the decrease in the oxidizer O_2 mole fraction. The flame speed simulations show that the decrease in flame speed due to dilution correlates well with the fractional decrease in

adiabatic flame temperature. Furthermore the effective slope of the $\ln(S_L/S_L^0)$ curve as a function of $\Delta T_{ad}/T_{ad}^0$ is around 4.8–5.5 for N_2, 5.7–6.6 for H_2O and 6.8–7.7 for CO_2, which suggest that it scales with the likely direct chemical effect of the diluent.

5.1.5 Chemical effect of diluent

As indicated above, the decrease in flame speed associated with dilution is not limited to the thermal (c_p) effect; some diluents are important actors in the chemical reactions. The relative effect of these processes can be separated by comparing the flame speeds with and without the chemical effects of the diluents. Figure 5.10 presents predictions from the San Diego mechanism[w] for a 90:10 (mole ratio) oxidizer mixture of air and diluent, either N_2 or CO_2. The chemical effect of the diluent species was "turned-off" by introducing an inert species (referred to as CO_2 (inert) and N_2 (inert)) with the same thermodynamic and transport properties of the actual diluent species. These inert species are allowed to participate in reactions as a third-body, with same third-body efficiency as the actual diluent.

Figure 5.10 shows that the direct chemical effects of nitrogen on flame speed are negligible (< 1%), whereas for CO_2 dilution the chemical effect accounts for almost 30% of the decrease in flame speed from the undiluted condition. The effect on flame speed is more pronounced near stoichiometric conditions. This is because artificially removing the direct chemical effect reduces the concentration of radicals available to react. Since the flame temperature is highest close to the stoichiometric conditions, the radical concentrations are also high at these conditions. As such by not allowing CO_2 to

[w] Additional species and reactions were added, as specified [80], to account for the nitrogen chemistry.

participate in the reactions, the radical concentrations are most affected at this condition and in turn produce a greater change in flame speed.

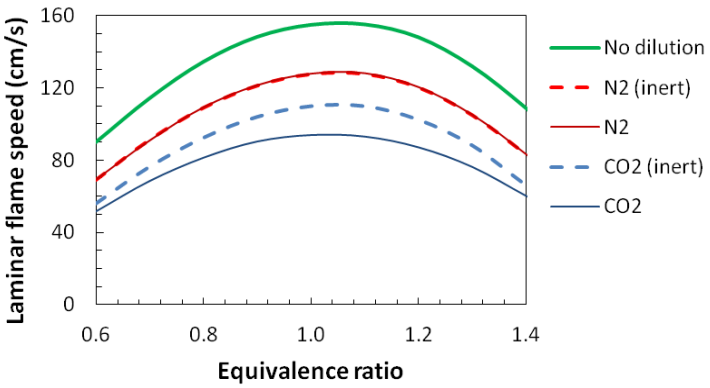

Figure 5.10. Laminar flame speed of methane–air mixtures with CO_2 and N_2 dilution, with (solid line) and without (dashed line) the direct chemical effect of the diluent. Predictions are from San Diego mechanism, for oxidizer with 10% vol. as diluent and a reactant mixture at 650 K and atmospheric pressure.

The chemical effect of CO_2 dilution on flame speed for propane–air mixture can be further understood by examining the sensitivity of the flame speed to variations in the pre-exponential factor of the reaction rate constant of the elementary reactions. A positive sensitivity indicates that flame speed increases with the increase in the reaction rate constant. Sensitivity analysis results indicate CO_2 has a significant effect on propane–air flame speed through the CO oxidation reaction:

$$CO + OH \Leftrightarrow CO_2 + H \qquad R1$$

Increasing CO_2 inhibits H radical production as observed from Figure 5.11. This in turn affects the rate of chain branching reaction:

$$H + O_2 \Leftrightarrow OH + O \qquad R2$$

Sensitivity analysis results show that propane–air flame speeds are highly sensitive to the rate of reactions R1 and R2; and since addition of CO_2 results in a decrease in the rate of these reactions, the flame speed of the mixture will decrease. Figure 5.11 also shows that

even chemically inert CO_2 reduces the rate of consumption of H radicals. This is due to the decrease in the temperature and the concentration of the species, thereby decreasing the rate of the reactions. The rate of H radical consumption decreases even more when CO_2 is chemically active, suggesting a further decrease in the flame speed of the mixture.

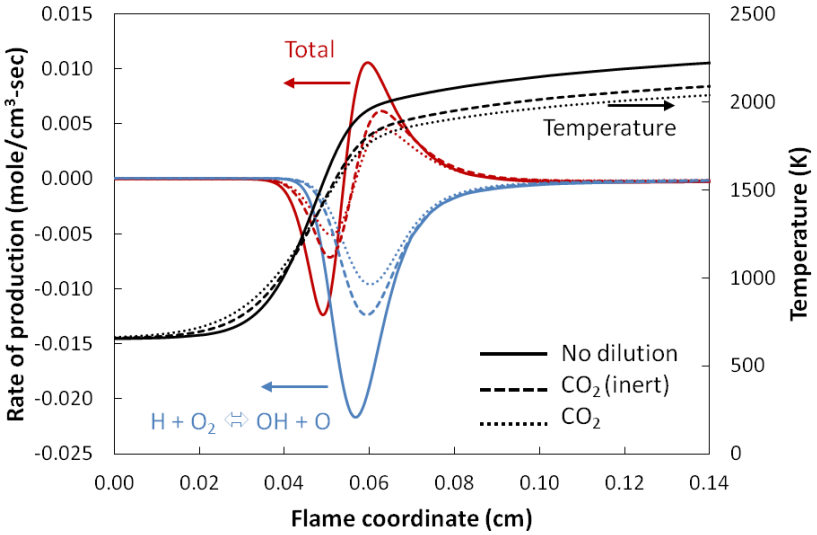

Figure 5.11. Profile of H radical rate of production (total and from reaction R2)in propane–air flame without (solid line), with chemically inert (dashed line) and with chemically active (dotted line) CO_2 dilution. Calculations are performed using San Diego mechanism for an oxidizer mixture with 90:10 vol% of air and CO_2 and reactant mixture at atmospheric pressure and 650 K preheat.

As in the case of CO_2 dilution, the decrease in flame speed due to H_2O dilution is also due to both thermal and chemical kinetic effects. However unlike CO_2, the chemical effect of H_2O does not always lead to a decrease in flame speed as shown in Figure 5.12. The figure presents fractional change in flame speeds of propane–air mixtures due to the direct chemical effect of the diluent species. The fractional change in the flame speed is defined as,

$$\text{Fractional change in flame speed} = \frac{S_{L,\text{inert}} - S_L}{S_L^0 - S_L} \times 100 \qquad 5.2$$

where S_L^0 is the flame speed of a fuel/air mixture with no dilution, S_L is the flame speed with dilution and $S_{L,\text{inert}}$ is the flame speed of the diluted mixture without the direct

chemical effect of the diluent. It should be noted that the change in flame speed for 5% CO_2 dilution case is primarily due to the chemical effect of CO_2 and not excess N_2. For the case of H_2O dilution at near stoichiometric conditions, the chemical effect of H_2O leads to a decrease in the flame speed. The change is greatest near $\phi \sim 1.3$, before decreasing to zero at $\phi \sim 1.45$. A further increase in equivalence ratio results in higher flame speeds due to the chemical effect of H_2O. The change in flame speed due to the chemical effect of diluent CO_2 also shows a decrease around similar rich conditions, $\phi \sim 1.3$–1.5. However for higher equivalence ratios, the chemical effect of CO_2 dilution results in a decrease in the flame speed of the mixture. It is also interesting to note that the equivalence ratio with minimum chemical effect on flame speed increases with increase in the O_2 content of the oxidizer.

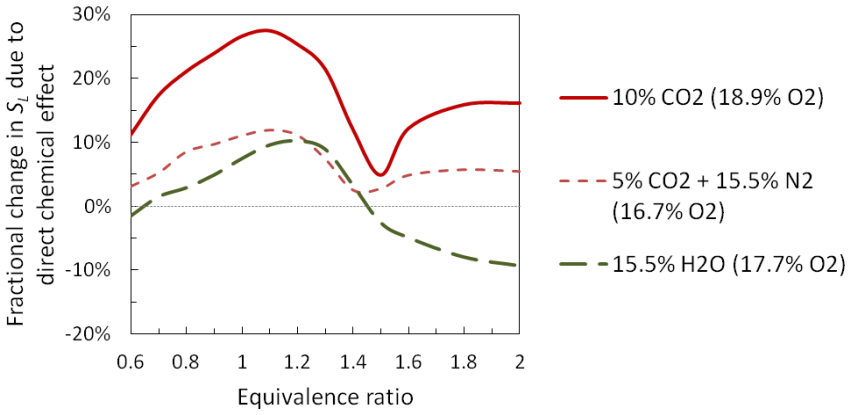

Figure 5.12. Fractional change in flame speed of propane–air–diluent mixture due to the chemical effect of diluent specie (CO_2 and H_2O). Calculation performed using San Diego mechanism at 1 atm and reactant temperature of 650 K. The numbers in the legend correspond to mole fraction of the diluent and corresponding final oxygen mole fraction in the oxidizer mixture.

Since the "inert" diluents are allowed to participate in the reactions as a third body, their interaction can be thought of as an "indirect" chemical effect. Furthermore because the third body efficiencies of CO_2 and H_2O can be significantly different from

N_2, this effect can be large. Preliminary calculations[x] show that including this effect in the overall chemical effect (i.e., setting the third body efficiency of inert CO_2 and H_2O to be the same as N_2), generally results in an increase in the flame speed, from the case where the third body efficiencies were modified to match the that of the actual diluent specie, by less than 1% for CO_2 and up to 8% for H_2O dilution. This translates to change in the percent value of chemical effect for CO_2 by ~2 and for H_2O dilution by up to 15. These calculations were performed for atmospheric pressure and it is expected that the changes in third body efficiency will have a larger effect at high pressure. The results suggest that how the chemical effect of the diluent specie is defined, is important.

5.2 Constant adiabatic flame temperature

Addition of diluent results in a decrease in the adiabatic flame temperature of a mixture. The flame temperature also changes with the equivalence ratio of the fuel–air mixture. It is possible to change the diluent fraction and the equivalence ratio independently while keeping the adiabatic flame temperature constant. This can be of practical interest in gas turbine design process where flame temperature is an important design parameter and in understanding how flame speed will change for different fuel/air mixtures at constant flame temperature.

Flame speeds were measured for nearly constant flame temperatures for a methane–air mixture with H_2O dilution and for a propane–air mixture with CO_2 and N_2 dilution. Figure 5.13a presents normalized flame speeds for the methane–air mixture at a constant adiabatic flame temperature of 1975 K. The flame speed is normalized by the

[x] The calculations were performed for atmospheric pressure propane/air mixture at 650 K with a diluent to air ratio of 10:90. These conditions are same to those for calculations presented in Figure 5.10.

corresponding value at a stoichiometric equivalence ratio to emphasize the change in flame speed. The adiabatic flame temperature was held constant by adjusting the H_2O mole fraction in the oxidizer mixture, shown in Figure 5.13b. This results in a change in the O_2 mole fraction in the oxidizer, also shown in Figure 5.13b. The results show an interesting trend in flame speed.

An undiluted methane–air mixture has a peak in flame speed at an equivalence ratio of ~1.1. To a large extent, this is influenced by the adiabatic flame temperature, which also peaks around the same equivalence ratio. However when the flame temperature is held constant, the flame speed has a local minimum near the stoichiometric condition. Also the flame speed increase on either side of stoichiometric mixture is asymmetric.

Figure 5.13a shows that predictions from the chemical mechanisms follow the same trend observed in the measurements.[y] The variation predicted by the San Diego mechanism is closer to the measured trend for lean mixtures, while the NUI mechanism trend is closer for rich mixtures. Furthermore, all the mechanisms predict a decrease in flame speed for rich mixtures ($\phi > 1.2$). Although no measurements were performed at these equivalence ratios, the drop in flame speed can be expected based on the agreement between the experiments and simulations. Also similar results are observed for propane–air–diluent mixture presented later.

[y]The non-normalized, predicted flame speeds were higher (~30%) than the measurements.

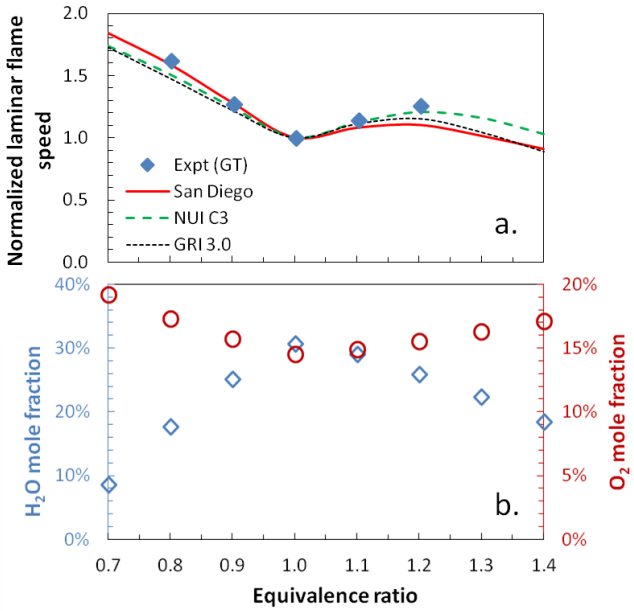

Figure 5.13. (a) Normalized laminar flame speed for methane/air/steam mixture at atmospheric pressure, 650 K preheat temperature and constant adiabatic flame temperature of 1975 K. (b) H_2O and O_2 mole fraction in the oxidizer mixture.

The flame speed of a mixture is driven by its diffusivity and reaction rate. However, the change in the thermal diffusivity, of $CH_4/O_2/N_2/H_2O$ mixtures over the range of equivalence ratio (0.7–1.4), is less than 2%, whereas the observed change in flame speed is ~60%. This indicates that the trend in the flame speed is driven by the change in the reaction rate. Furthermore since the reactant and flame temperatures are held constant, the change in reaction rate should be primarily due to the change in the concentration of the reacting species, specifically O_2 and CH_4.[z] Since H_2O needs to be added to keep the flame temperature constant, it results in a decrease in the concentration of O_2 and CH_4. The amount of H_2O added is driven by the adiabatic flame temperature of the undiluted mixture. As a result, the concentration of both O_2 and CH_4 are lowest at the

[z] The chemical effect of H_2O on flame speed is not sufficient to explain for the changes in flame speed because similar trend is flame speed is also observed for inert diluent such as N_2.

stoichiometric mixture (Figure 5.13b).[aa] Since flame speed is a function of reaction rate and hence the concentration of the reactants, it follows a similar trend as change in the concentration of the reactants. The decrease in the flame speed for rich equivalence ratio is discussed after presenting the measurements for propane–air mixtures.

A similar trend in flame speed at constant flame temperature was observed for propane–air mixtures with N_2 and CO_2 dilution (Figure 5.14a). The measurements included in the figure were selected from the propane–air results presented earlier in the chapter and at flame temperatures of 2150 ± 25 K. Since the experiments did not have exactly the same flame temperature, the difference in flame temperature is also presented in Figure 5.14b. Figure 5.14a also includes the flame speed predictions from the San Diego mechanism. Unlike the methane–air mixtures, which had a local minimum in flame speed close to an equivalence ratio of 1, the measured flame speeds for propane–air mixtures have a minimum at a slightly rich mixture, $\phi \sim 1.15$. On the other hand, the predicted flame speeds are relatively constant for $\phi = 1.0$–1.2. This difference is probably due to the change in the diluent from N_2 to CO_2, which results in a significant change in the reaction chemistry, as explained above. At sufficiently rich conditions ($\phi > 1.25$–1.3), the predicted flame speed shows a decrease similar to the methane–air results. The measured flame speed at the richest condition ($\phi = 1.3$) does not show the decrease, though this could be in part due to the higher flame temperature (nearly 25 K above the nominal value) for that point.

[aa] The amount of H_2O added to the mixture changes significantly in order to hold the flame temperature constant. As a result the effect of change in concentration of O_2 and CH_4, due to the change in the equivalence ratio of the mixture, is overshadowed.

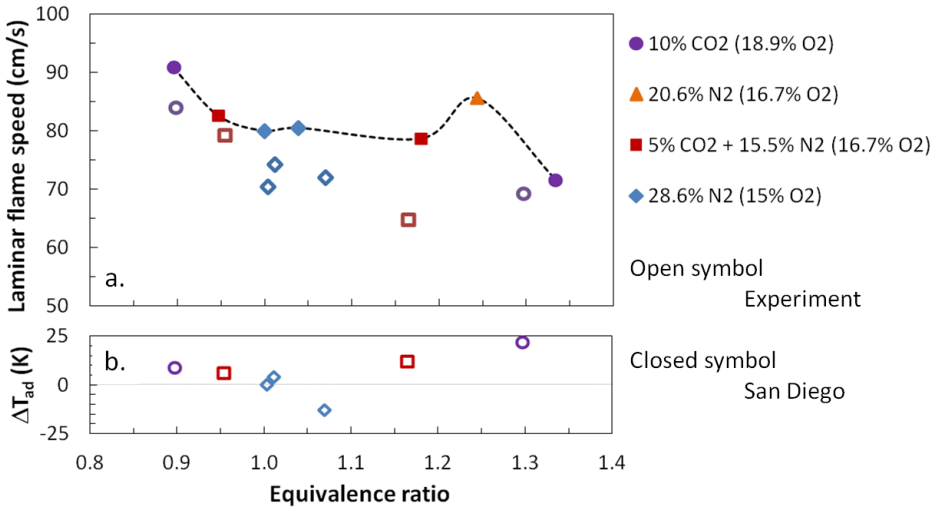

Figure 5.14. (a) Laminar flame speed of propane–air mixture with N_2 and CO_2 dilution at atmospheric pressure, 650 K preheat temperature and constant adiabatic flame temperature of 2150±25 K. (b) Calculated difference in adiabatic flame temperature of measurements due to difference in equivalence ratio. Open symbols are for the experimental measurements and closed symbols are predictions from San Diego mechanism.

The increase in flame speed at lean equivalence ratios is attributable to the increase in concentration of O_2 and C_3H_8 as the diluent is decreased. However this reasoning does not suffice to explain the decrease in flame speed at sufficiently rich equivalence ratios (> 1.25–1.3). To understand this, the sensitivity of the flame speed to the pre-exponential factor of the elementary reaction rates was calculated. The results show that the flame speed for these mixtures has a high sensitivity to reactions involving H radicals. This is because the H radicals that diffuse back are responsible for the initial chain branching reaction:

$$H + O_2 \Leftrightarrow OH + O \qquad R2$$

Figure 5.15 compares the calculated rate of production of H radicals from three flames: (i) $\phi = 0.894$, (ii) $\phi = 1.244$ and (iii) $\phi = 1.334$. All these cases have the same adiabatic flame temperature of 2150 K. Cases (i) and (iii) correspond to an oxidizer composition of O_2:N_2:CO_2 = 18.9:71.1:10, and case (ii) has an oxidizer composition of O_2:N_2 = 16.7:83.3. For case (i), there is significant consumption of H radicals through

reaction R2. However, the total rate of consumption of H radicals for the lean case (i) is less than for the rich cases (ii) and (iii). For the rich cases, the H radical is used in breaking up fuel molecules or in recombination reactions such as:

$$C_3H_8 + H \Leftrightarrow n\text{-}C_3H_7 + H_2 \qquad \text{R3}$$

$$C_3H_6 + H \Leftrightarrow C_3H_5 + H_2 \qquad \text{R4}$$

$$C_2H_3 + H \Leftrightarrow C_2H_2 + H_2 \qquad \text{R5}$$

$$H + CH_3 (+ M) \Leftrightarrow CH_4 (+ M) \qquad \text{R6}$$

The rate of these reactions is lower for the fuel-lean case. Also for the fuel-lean case, excess O_2 facilitates the rate of reaction R2. These competing reactions (which lead to decrease in the available H radical pool) result in a decrease in the rate of reaction R2 at rich conditions. Furthermore Figure 5.15 also shows that there is a decrease in rate of consumption of H radical from case (ii) to case (iii), which will result in a decrease in flame speed for case (iii) due to the high sensitivity of the flame speed to reaction R2.

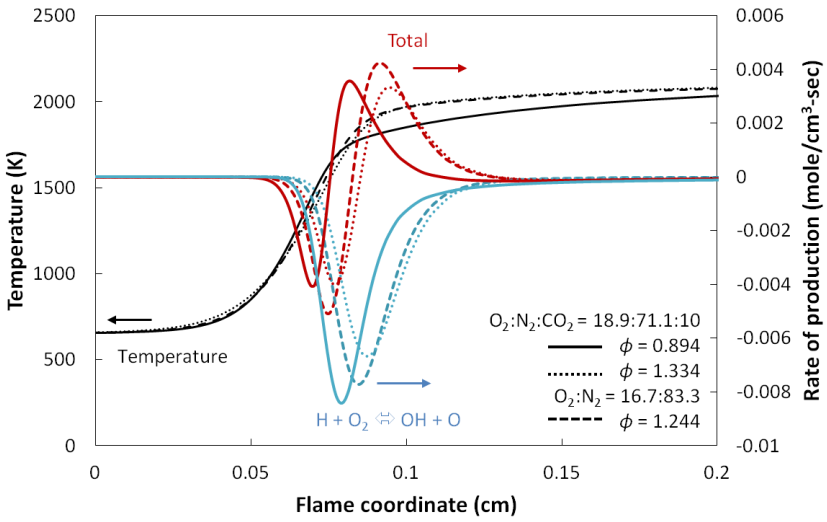

Figure 5.15. Rate of production of H radical (total and from reaction R2) and temperature profile for three different propane–air flames with same adiabatic flame temperature of 2150 K. Calculations performed using San Diego mechanism at equivalence ratio of (i) 0.894 (solid line), (ii) 1.244 (dashed line) and (iii) 1.334 (dotted line).

5.3 Relationship between flame height and measured flame speed

One of the approximations made during the modified Bunsen flame technique is that the flame is sufficiently tall that the contribution of the tip to the overall flame area is small. This is intended to reduce the effect of stretch on the measured flame speed. However it was not always possible to get to large flame height without significant instability in the flame surface. This introduces variations in flame height that can lead variability in the measured flame speed. To analyze possible systematic errors due to varying flame height, Figure 5.16 compares the difference between the flame speed predicted by the San Diego mechanism[bb] and the measured value as a function of normalized flame height (*h/D*) for different propane–air–diluent mixtures. The results are further grouped in three equivalence ratio ranges: lean ($\phi < 1.0$), slightly rich ($1.0 < \phi < 1.2$) and significantly rich ($\phi > 1.2$).

Figure 5.16 shows that most of the lean propane mixture data presented here are clustered around normalized flame heights of 1.5–2.5, whereas the rich mixtures have a greater variation in flame height (1.5–3.5). This is because it was possible to stabilize rich flames at high flowrates without any instability in the flame surface. In contrast for lean mixtures at high flowrates, the flame would either stabilize further downstream of the burner (thus being more susceptible to oscillations) or blow-off. As a result it was not always possible to establish a tall flame for lean mixtures. Overall there is no observable correlation in the flame speed differences (between measured and predicted values) and

[bb] The San Diego mechanism predictions were interpolated to equivalence ratio of experimental measurements using a 5th order polynomial curve fit.

the flame height. This suggests that either the flame speed is not sensitive to the flame height above some critical value or (more likely) the stretch effects are more prominent at certain mixture conditions and flame height alone is not sufficient to account for these effects.

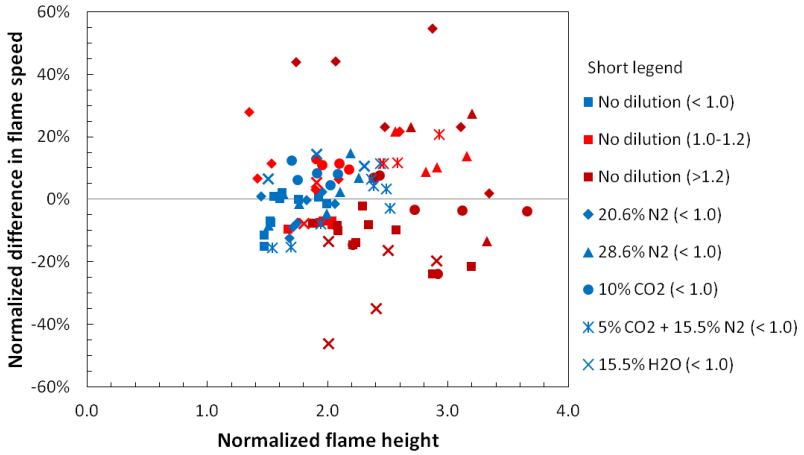

Figure 5.16. Difference in predicted and measured flame speed as a function of normalized flame height (*h/D*) for different propane–air–diluent mixtures. Results are for atmospheric pressure and reactant temperature of 650 K. Color indicates equivalence ratio: blue (ϕ < 1.0), bright red (1.0 < ϕ < 1.2) and dark red (ϕ > 1.2). Symbols indicate oxidizer composition in terms of mole fraction of diluent with balance being standard air: square (no dilution), diamond (20.6% N_2), triangle (28.6% N_2), circle (10% CO_2), cross with vertical strike (5% CO_2 and 15.5% N_2) and cross (15.5% H_2O).

CHAPTER 6

FLAME SPEED OF BINARY FUEL MIXTURES

Designing a fuel-flexible system requires understanding how flame speed is affected by changes in the fuel composition. This is important for systems operating on natural gas, which depending on it source can have significant variation in composition. Furthermore change in flame speed is not necessarily a linear function of the change in fuel composition. To this end, this chapter discusses the effect of fuel composition on the flame speed of fuel/air mixtures. Flame speeds of binary fuel mixtures of methane with ethane and propane are studied over a range of pressures (1-10 atm) and at high preheat temperature (~600–650 K). Flame speeds of these mixtures are also investigated for significant steam dilution (0-30% by vol.). The measurements were performed primarily with the Bunsen flame technique, with a few specific cases investigated the using stagnation flame technique. The results are used to validate the performance of leading chemical kinetics mechanisms, as well as investigate the relative accuracy of the measurement techniques.

This chapter first presents the flame speed results for binary fuel mixtures without steam dilution at atmospheric and high pressures. The next part of the chapter discusses the effect of fuel composition in the presence of steam dilution and provides a comparison of the measurements from the two techniques. Lastly, the performance of different mixing rules is studied for the binary fuel mixtures to help develop such rules especially in the presence of steam dilution.

6.1 Atmospheric pressure results

Laminar flame speed of two methane/ethane blends as a function of equivalence ratio, at 650 K preheat temperature and atmospheric pressure, are presented in Figure 6.1a. The results show that increasing the amount of ethane in the fuel mixture, from 20% to 40%, results in a marginal increase in the flame speed. In fact, the increase in flame speed is within the experimental uncertainty of the technique. The measurements suggest the peak flame speed for both fuel blends occurs close to a stoichiometric mixture, possibly slightly lean (ϕ = 0.95–1.0). This is in contrast to the expected result for alkane fuels, which tend to have a peak flame speed on the rich side (ϕ = 1.05–1.1).

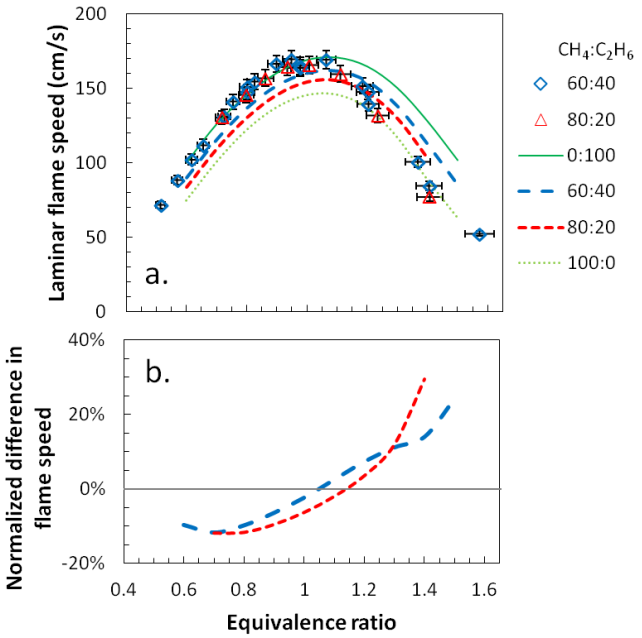

Figure 6.1. (a) Atmospheric pressure flame speed measurements of methane/ethane/air mixtures at 650 K preheat temperature. (b) Normalized difference between the measured and predicted flame speeds. Legend lists the mole fraction of methane and ethane in the fuel mixture. Symbols represent experiment data and lines are predictions from San Diego mechanism.

Figure 6.1a also includes predictions from the San Diego mechanism for the fuel blends; predictions for pure fuels are also presented for reference. As seen in Figure 6.1b, the mechanism predictions are in reasonable agreement (within ±12%) with the measured

flame speed values for lean and close to stoichiometric mixtures (ϕ = 0.6–1.25). However for sufficiently rich (ϕ > 1.3) mixtures, the predicted flame speeds are significantly higher (20–30%) than the measured values. It is also interesting to note that the measurements at lean conditions are close to the pure ethane predictions, while as the mixture becomes progressively richer, the experimental flame speeds approach the pure methane predictions. Furthermore the peak flame speeds predicted by the mechanism occur, as expected, at slightly rich equivalence ratios. These discrepancies were also observed in some of the high pressure measurements and are discussed further later in this chapter.

Figure 6.2 presents the strained flame speed of a 78:22 CH_4:C_2H_6 mixture, at equivalence ratio of 0.8, 1 and 1.2, for 650 K preheat and atmospheric pressure. Each measurement data point is an average over 400 instantaneous measurements. The ϕ = 0.8 and ϕ = 1.2 mixtures have similar flame speeds (within ±1%), while the stoichiometric mixture has a higher flame speed (~15%). Predictions from the San Diego and NUI C5 mechanism show good agreement (within ±8%) with the measurements for all the cases.

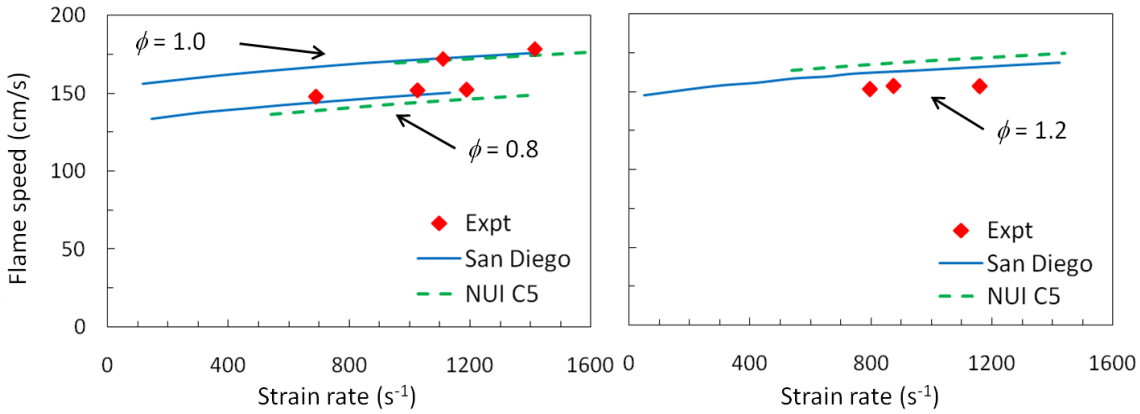

Figure 6.2. Flame speed of 78:22 CH_4:C_2H_6 mixture with air as a function of strain rate and equivalence ratio at 650 K and atmospheric pressure.

The largest differences are observed for the rich mixture, with the predictions higher than the measurements. Since the number of measurements is limited, it is difficult

to say conclusively that the mixtures show similar strain sensitivity, although the mechanism predictions do indicate this to be the case. Also these results suggest that for rich mixtures, the mechanism will over-predict the unstretched flame speed.

6.2 High pressure results

This section focuses on flame speed measurement at high pressure (5–10 atm). As discussed in Chapter 4, at high pressures a laminar flame is more susceptible to hydrodynamic and thermo-diffusive instabilities. These instabilities can be suppressed by addition of diffusive species such as helium or steam. As such the Bunsen flame results presented in this section are for an oxidizer mixture of oxygen and helium with no nitrogen. Helium dilution was not required for stagnation flames as they did not exhibit any instability in the flame surface.

The oxygen to helium ratio was chosen such that the adiabatic flame temperature of the mixture is similar to that for air. Maintaining the same adiabatic flame temperature ensures that there is no significant change in the fundamental fuel/oxygen chemistry compared to the cases where air is used as an oxidizer. The O_2:He volume ratio was held constant at 1:6 for different fuel mixtures. This corresponds to an O_2 mole fraction in oxidizer of 14.3%. Thus there is some impact on the fuel and oxygen concentration in the reactants; both are reduced, which can result in modestly reduced reaction rates compared to fuel-air mixtures.

6.2.1 Methane/ethane mixtures

Figure 6.3 shows the Bunsen-based laminar flame speed measurements for two methane/ethane mixtures at 5 atm and 600 K preheat. As expected, increasing the amount

of ethane in the fuel increases the flame speed of the mixture. The observed change in the flame speed is small, however, and within the precision uncertainty of the measurements. Furthermore for the 80:20 mixture, the flame speed changes little for $\phi = 0.9–1.0$.

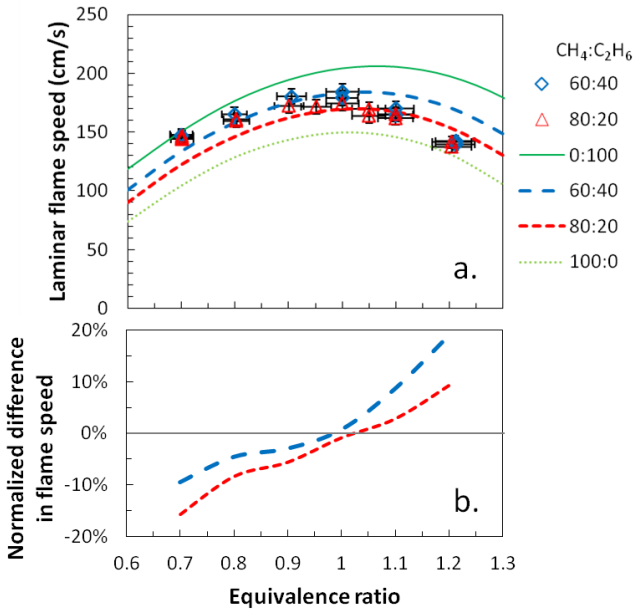

Figure 6.3. (a) High pressure (5 atm) laminar flame speed of methane/ethane fuel mixtures at 600 K preheat temperature. (b) Normalized difference between the measured and predicted flame speeds . The oxidizer is a 1:6 volumetric mixture of O_2:He. Legend lists the mole fraction of methane and ethane in the fuel mixture. Symbols represent experiment data and lines are predictions from San Diego mechanism.

Similar to the atmospheric pressure data, the peak flame speeds of these mixtures occur at slightly leaner equivalence ratios (0.95–1.0) compared to that expected for air (1.05–1.1). In this case, however, a shift of peak flame speed to leaner mixtures can be expected due to the replacement of nitrogen with helium. Addition of helium significantly increases the diffusivity of the mixture and hence the flame speed. Because helium is added to the oxidizer, its impact on flame speed will be biased toward leaner mixtures. To ensure that this is not due to an error in flow calibration,[cc] the experiment

[cc] An error in the flow calibration can cause the measured equivalence ratio to be lower than actual. This will shift all the measurements to leaner equivalence ratio.

was repeated after re-calibrating all the flow meters. No significant change in flame speed was observed between the repeated measurements.

Figure 6.3a includes predictions based on the San Diego mechanism. For reference, flame speed predictions for pure methane and ethane, at these conditions, are also included. Although the San Diego mechanism has not been validated at these conditions for these fuel/oxidizer mixtures, it shows trends very similar to those observed in the experimental data; though, the predictions show a greater change in flame speed due to the difference in fuel composition than that observed in the experiments.

Still, the predicted flame speeds are within ±10% for most of the equivalence ratio range (Figure 6.3b), with the best agreement at near stoichiometric conditions. The difference monotonically increases as the mixture becomes less stoichiometric. The most striking systematic difference between the predictions and measurements is that for lean mixtures the mechanism under-predicts the flame speed whereas for rich mixtures it over-predicts. As discussed above, repetitions of the experiments with re-calibrated flow meters rule out the possibility of errors in the measured equivalence ratios. Additionally, as will be shown in Section 6.2.2, similar disagreement is observed for methane/propane mixtures.

Figure 6.4 present the strained flame speed measurement for a $\phi = 1.4$ methane/ethane mixture at 5 atm and 650 K with air as the oxidizer. Since the flame speed and strain rate were determined from instantaneous velocity profiles, the result appear to have significant scatter in the measured values. However the 95% confidence interval for the linear fit to the data reveals that the uncertainties in the unstretched flame

speed and the Markstein length are small.[dd] The linear fit to the experimental data agrees quite well with the NUI C5 predictions of strained flame speed (within ±3%); however the San Diego mechanism predictions tend to be significantly lower (~15%). The measurements also have a 50% higher strain sensitivity compared to the mechanisms' predictions (see Table 6.1); though in both cases the sensitivity is small.

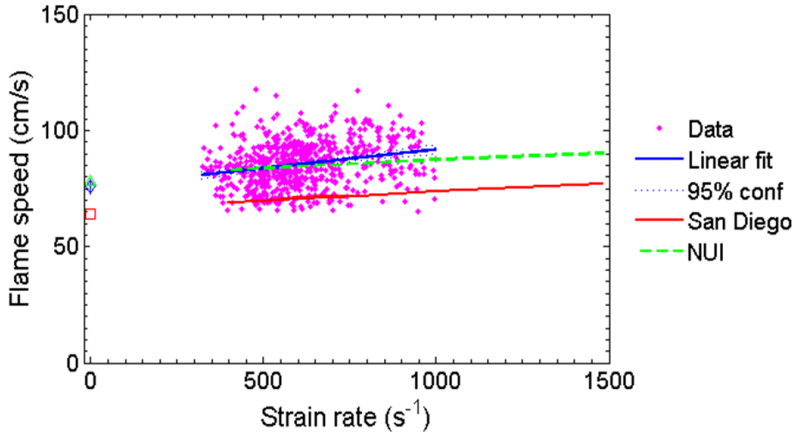

Figure 6.4. Instantaneous strained flame speed results rich (ϕ = 1.4) for 60:40 CH_4:C_2H_6 mixture at 5 atm and 650 K. Open symbols at zero strain rate indicate the unstretched flame speed from linear extrapolation of experimental data and those calculated using PREMIX routine.

Table 6.1 presents the Markstein lengths and unstretched flame speeds from linear extrapolation of the experimental and numerical data. It is interesting to note that the unstretched flame speed estimated from the strain flame measurements is slightly higher (~12%) than the San Diego mechanism prediction. In contrast, the Bunsen flame speed measurements (Figure 6.3) for the same fuel mixture at rich conditions (though with a He:O_2 oxidizer) were lower than the San Diego predictions. While this could be due to the difference in diluent (N_2 versus He), it is worth nothing that the atmospheric pressure results (with no helium dilution) also indicate that the flame speed predictions tend to be high for rich mixtures (Figure 6.1).

[dd] The 95% confidence interval is within ±2% of the actual flame speed value and therefore barely visible in the figure.

Table 6.1. Unstretched flame speed and Markstein length determined from linear regression for experiment and OPPDIF simulation. Results are for ϕ = 1.4, 60:40 CH_4:C_2H_6 mixture at 5 atm and 650 K.

	Unstretched flame speed (cm/s)	Markstein length (μm)
Experiment	75.6 ± 3.2	– 162 ± 51
San Diego	66.1	– 74
NUI C5	80.4	– 67

Figure 6.5a presents flame speed measurements for the same methane/ethane mixtures at 10 atm. As expected: (i) increasing the pressure for a given mixture results in a decrease in the flame speed of the mixture, and (ii) decreasing ethane content increases the flame speed at a given equivalence ratio. However, compared to the 5 atm results, these measurements show a larger percentage change in flame speed with change in fuel composition. For example, the flame speed at ϕ = 0.9 increases, as the amount of ethane is increased from 20 to 40%, by roughly 5% at 5 atm and 16% at 10 atm. Furthermore the peak flame speed of the 80:20 CH_4:C_2H_6 mixture occurs at a rich equivalence ratio (1.0–1.1). Although, no measurements are available for the 60:40 CH_4:C_2H_6 mixture close to stoichiometric conditions[ee], it appears to have a similar trend to the 80:20 mixture.

Figure 6.5a also provides a comparison of the measurements with the San Diego mechanism predictions. The overall trends are similar, e.g., (i) the predicted flame speeds show a similar variation with equivalence ratio, (ii) a higher fractional change in flame speed due to change in fuel composition at higher pressure, and (iii) similar peak flame speed location.

[ee] Measurements could not be performed due to the limitation in metering the required flowrates at the required conditions.

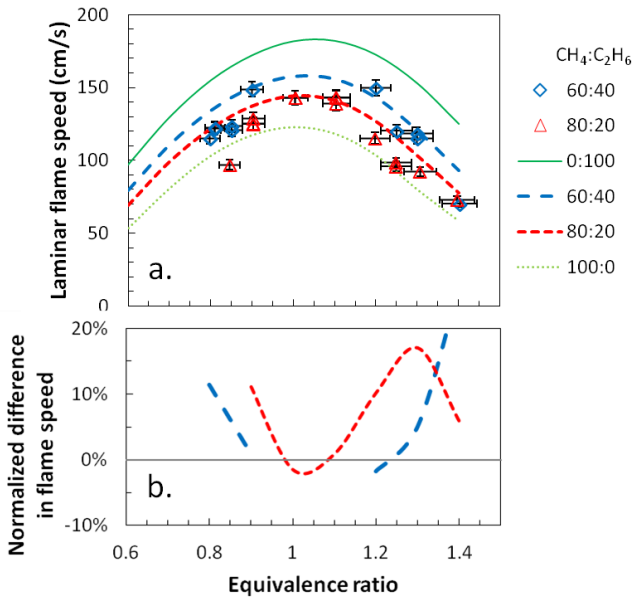

Figure 6.5. (a) High pressure (10 atm) laminar flame speed of methane/ethane fuel mixtures at 600 K preheat temperature. (b) Normalized difference between the measured and predicted flame speed. The oxidizer is a 1:6 volumetric mixture of O_2:He. Legend lists the mole fraction of methane and ethane in the fuel mixture. Symbols represent experiment data and lines are predictions from San Diego mechanism.

Quantitatively, the predictions are in reasonable agreement with the measurements over the complete range of equivalence ratios studied, within –2% to +20% (see Figure 6.5b). Excellent agreement is found for near stoichiometric equivalence ratio (differences of only a few %), but the predictions show a smaller decrease in flame speed away from near-stoichiometric conditions compared to the experiments. This leads to increasingly over-predicted flame speeds at off-stoichiometric condition, with a more rapid deviation between experimental and predicted results observed for lean mixtures.

6.2.2 Methane/propane mixtures

Flame speed measurements for methane/propane fuel mixtures at 5 atm and 650 K preheat temperature are presented in Figure 6.6a. The results, similar to the methane/ethane measurements at 5 atm (Figure 6.3a), indicate that increasing the mole

fraction of propane, from 20% to 40%, marginally increases the flame speed of the mixture over most of the equivalence ratio range. However for rich equivalence ratios, the measured flame speeds are essentially the same for the two fuel mixtures. Also, the observed increase in flame speed for the higher propane content mixture is within the precision uncertainty of measurements. Finally, the peak flame speed is shifted significantly toward lean equivalence ratios (close to 0.9) in the measurements.

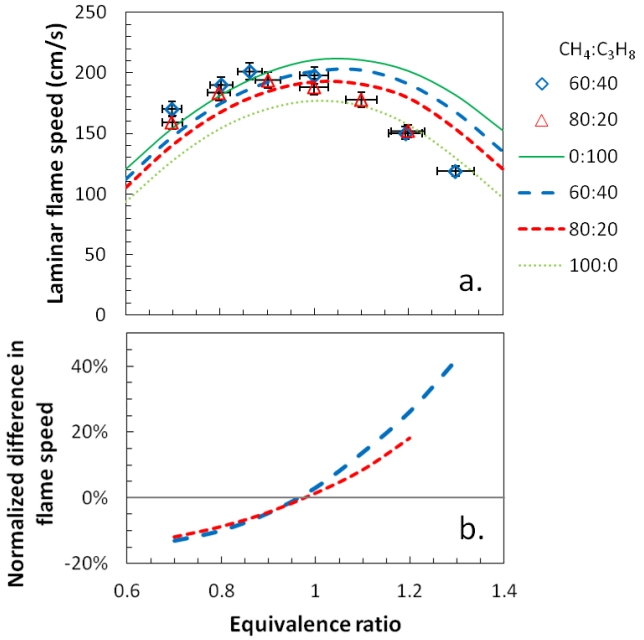

Figure 6.6. (a) High pressure (5 atm) laminar flame speed of methane/propane fuel mixtures at 650 K preheat temperature. (b) Normalized difference between the measured and predicted flame speed. The oxidizer is a 1:6 volumetric mixture of O_2:He. The ratios indicate the volumetric methane/propane composition of the fuel mixture. Symbols represent experiment data and lines are predictions from San Diego mechanism.

As in the methane/ethane results, the predicted flame speeds show good agreement with the measurements, within ±10%, for equivalence ratios close to one (see Figure 6.6b). However for rich equivalence ratios the mechanism significantly over-predicts the flame speed of the mixture (~20–40% for $\phi > 1.2$). Furthermore while the experiments and computations indicate similar peak flame speed values, the mechanism

predicts the peak flame speed location to be at rich equivalence ratio (~1.05 to 1.1) compared to the lean value (~0.9) observed in the measurements.

Much like the atmospheric pressure methane/ethane comparisons, the lean flame speeds are closer to those predicted for pure propane; while for increasingly richer mixtures, the results tend toward the pure methane predictions. Thus the differences in the flame speeds display a similar trend with equivalence ratio as observed for methane/ethane mixtures at 1 and 5 atm; the mechanism under-predicts the flame speed for lean mixtures and over-predicts it for rich mixtures.

The predictions also show that addition of even 40% propane shifts the flame speed of the mixture close to that of pure propane. This shows that propane has a strong effect on the methane/propane mixture flame speed. A similar change in flame speed (although to a smaller extent) is also observed with ethane addition in the methane/ethane mixtures. These changes in flame speed as a function of mixture composition are further discussed in Section 2.2.

6.3 Steam dilution results

This section presents stretched and unstretched (Bunsen) flame speed measurements for binary fuel mixtures of methane/ethane and methane/propane with significant steam dilution for a range of equivalence ratios. Results with steam mole fractions up to 30% of the oxidizer mixture are presented. The measurements were performed on a 9 mm burner at a preheat temperature of 650 K.

6.3.1 Atmospheric pressure results

6.3.1.1 Methane/ethane mixtures

Figure 6.7 presents the laminar flame speed for two methane/ethane mixtures, as a function of steam in the oxidizer and the equivalence ratio of the mixture, obtained with the Bunsen technique. As expected, increasing ethane fraction in the fuel mixture increases the flame speed for a given equivalence ratio and steam dilution. For a given equivalence ratio, the flame speed decreases nearly linearly with the amount of steam. Furthermore, the decrease in flame speed normalized by the no-steam-dilution value is similar for all the equivalence ratios considered. This is seen in Figure 6.8, along with the normalized flame speed predictions from the San Diego mechanism.

The predictions from the San Diego and NUI C3 mechanism are also presented in Figure 6.7. Both mechanisms predict flame speeds that are close to the measured values (mostly within ±10%) for the lean and stoichiometric equivalence ratios, though with a tendency to over-predict the measurements, especially at higher dilution levels. However, the mechanisms significantly over-predict the flame speed for the rich mixture ($\phi = 1.2$) by as much as 30% for the San Diego and 40% for the NUI mechanism. It is also worth noting that the flame speed predictions from the two mechanisms are nearly identical for stoichiometric mixtures, but for lean mixtures the San Diego results are higher and for rich mixtures the NUI results are higher. Overall though, both mechanisms show a similar decrease in the normalized flame speed with added steam dilution (Figure 6.8), and the decrease is a bit less than that observed in the experiments.

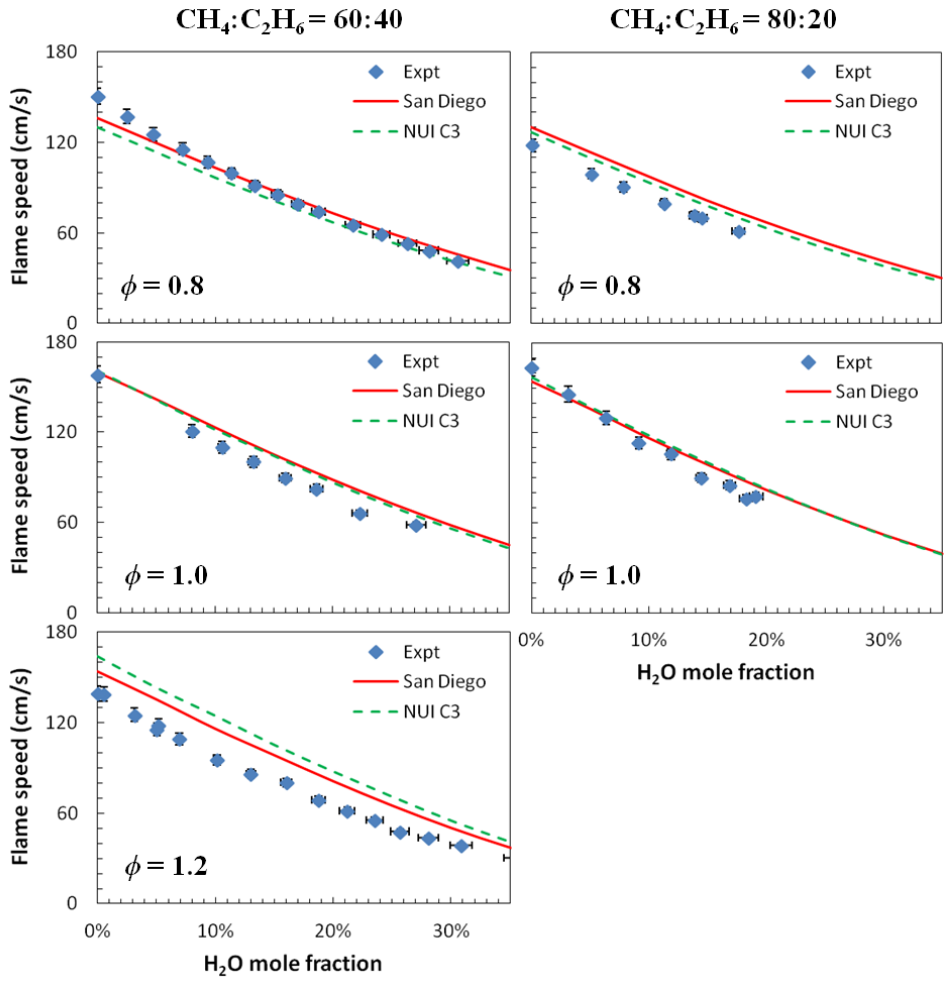

Figure 6.7. Laminar flame speed of methane/ethane/air/steam mixtures at atmospheric pressure and 650 K preheat temperature. The rows correspond to equivalence ratio of 0.8 (first), 1 (second) and 1.2 (third), whereas the columns correspond to CH_4:C_2H_6 mixture of 60:40 (first) and 80:20 (second).

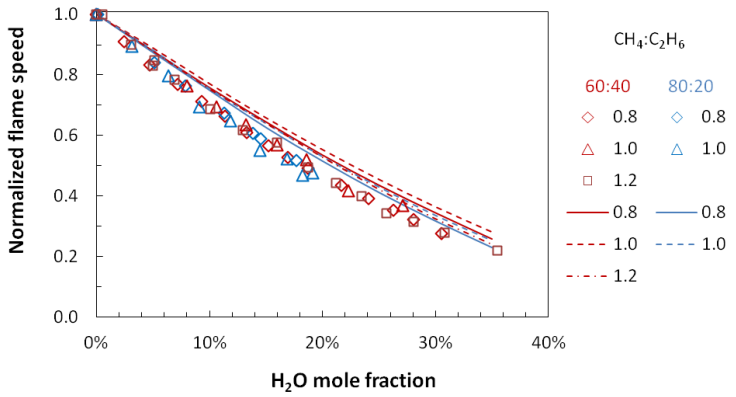

Figure 6.8. Measured (symbols) and predicted (lines) flame speed of atmospheric methane/ethane/air mixtures with steam dilution normalized by flame speed at no dilution. Results are color coded: red and blue for 60:40 and 80:20 CH_4:C_2H_6 mixture respectively. Predictions are for San Diego mechanism.

6.3.1.2 Methane/propane mixtures

Figure 6.9 presents the unstretched laminar flame speed measurements for two methane/propane mixtures as a function of steam dilution level and equivalence ratio. Normalized flame speed values are plotted in Figure 6.10. The flame speed decreases nearly linearly with steam dilution, with a steeper decline at low steam dilution.

However the flame speed measured for the lean ($\phi = 0.8$) 80:20 CH_4:C_3H_8 mixture at low steam dilution level (< 5%) is questionable because: (i) it is higher than the flame speed for the stoichiometric mixture of the same fuel blend, and (ii) because it is higher than the flame speed for the higher propane content mixture at the same ϕ. A more careful inspection of the flame images (Figure 6.11) and experimental conditions did not reveal any systematic differences for this data set in terms of flame height, flame thickness, oscillation of flame front or flow metering and calibration. As discussed in Section 3.2.3.3, it is possible that the measured area is lower than the actual flame area due to the stand-off distance of the flame from the burner nozzle (~1 mm). However, flames at other steam dilution levels were also lifted by a similar distance. Furthermore, systematic errors due to improper data processing or scaling of the images can be ruled out because the all the data for the $\phi = 0.8$ case were acquired on the same day and the discrepancies are only observed for low steam dilution levels.

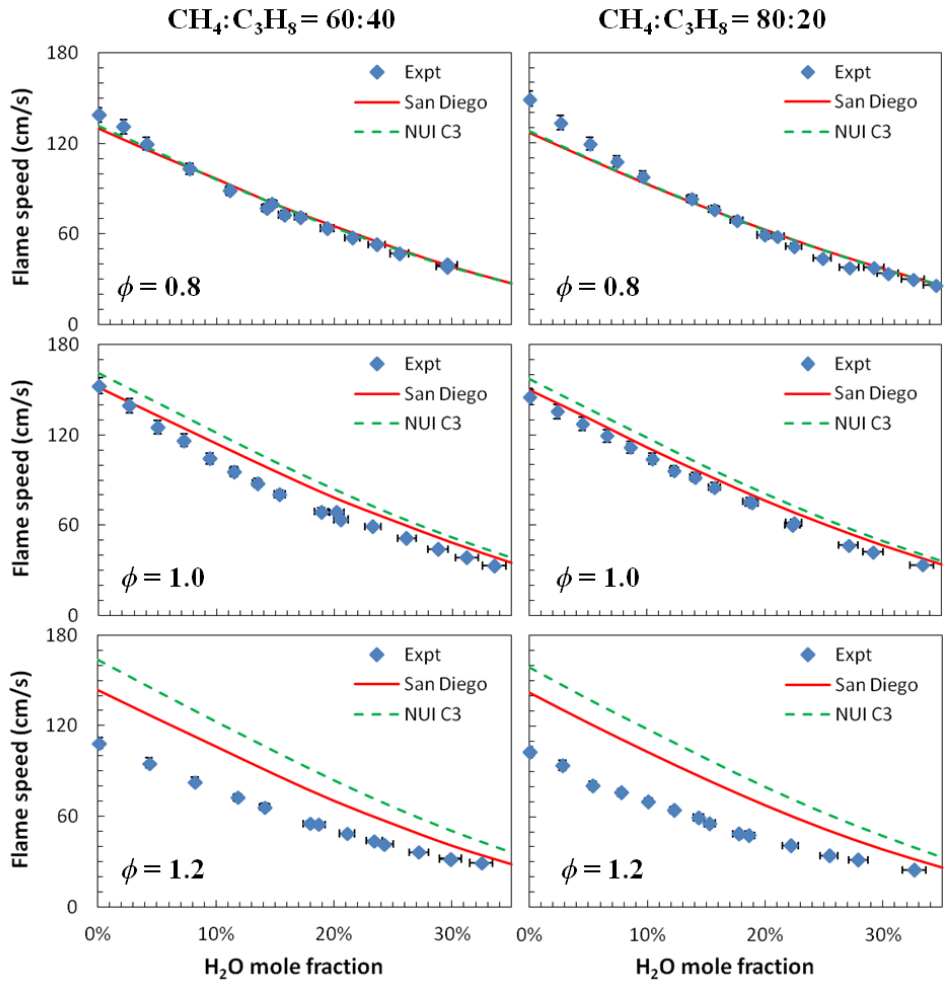

Figure 6.9. Laminar flame speed of methane/propane/air/steam mixtures at atmospheric pressure and 650 K preheat temperature. The rows correspond to equivalence ratio of 0.8 (first), 1 (second) and 1.2 (third) respectively whereas the columns correspond to CH_4:C_3H_8 mixture of 60:40 (first) and 80:20 (second) by volume.

Figure 6.9 also compares the measurements to the prediction from the San Diego and NUI C3 mechanisms. Similar to the methane/ethane case, the mechanisms predict nearly the same flame speeds (within 5–15%) as those measured for the lean and stoichiometric mixtures. However for rich mixtures, the mechanisms predict significantly higher flame speed values (by as much as 30–40%). Unlike for the ethane mixtures, the two mechanisms now agree best with each other (and with the experiments) for the lean

mixture, with increasing differences between the two mechanisms for the stoichiometric and rich conditions, with significant disagreement at the latter (ϕ = 1.2).

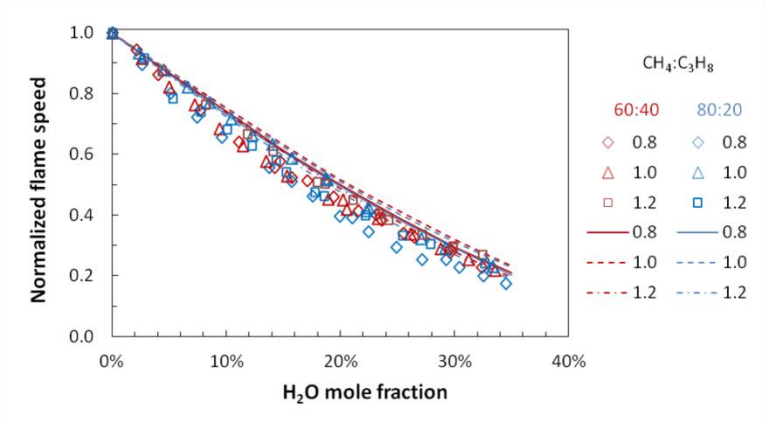

Figure 6.10. Measured (symbols) and predicted (lines) flame speed of atmospheric methane/propane/air mixtures with steam dilution normalized by flame speed at no dilution. Results are color coded: red and blue for 60:40 and 80:20 CH_4:C_3H_8 mixture respectively. Predictions are for San Diego mechanism.

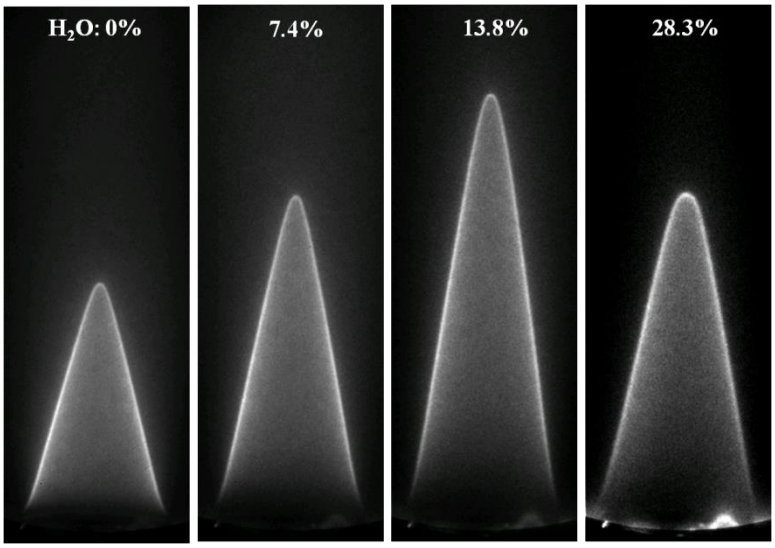

Figure 6.11. Typical instantaneous chemiluminescence image of the flame for ϕ = 0.8 CH_4:C_3H_8 = 80:20 mixture with steam dilution. Numbers indicate steam mole fraction in oxidizer. Images are not scaled to same signal intensity. The bright spot on the lower right corner is due to the pilot flame.

Focusing on the effect of dilution (Figure 6.10), the normalized results from both the experiments and simulations show that the relative decrease in flame speed is only a weak function of equivalence ratio, at least for the near stoichiometric range of conditions examined here (ϕ = 0.8–1.2). Also, the predicted decline in flame speed with added

dilution is less than observed in the experiments. These findings for the methane/propane mixtures are consistent with the methane/ethane results (Figure 6.8). When compared to the atmospheric pressure results for pure propane (Figure 5.7a), the San Diego mechanism predictions show a similar decrease in normalized flame speed with steam dilution level. Furthermore the variation in $\ln(S_L/S_L^0)$, for the two methane/propane mixtures (as shown in Figure 6.12), is roughly linear with the fractional change in adiabatic flame temperature and similar to that of pure propane for different equivalence ratios close to stoichiometric with m' ~ 5.9–6.9.

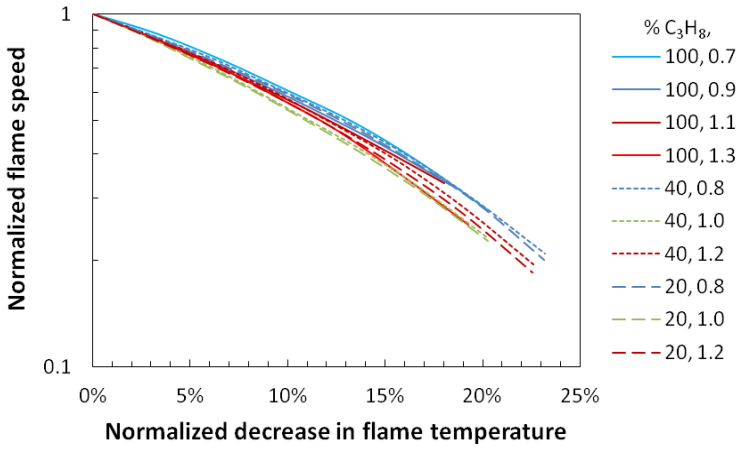

Figure 6.12. Normalized flame speed of different methane/propane mixtures with steam dilution as a function of change in flame temperature normalized by the flame temperature of undiluted mixture. The legend indicates the mole fraction of propane in the fuel mixture and the equivalence ratio.

The measurements presented in Figure 6.9 show that the measured flame speed of methane/propane mixtures at the rich equivalence ratio has a significantly lower value than at the lean and stoichiometric conditions tested, and also lower than that predicted by the two kinetic mechanisms. To investigate whether this is a systematic error associated with the measurement technique, strained flame speed measurements were also acquired, using the stagnation flame configuration, for the 60:40 CH_4:C_3H_8 mixture at the rich condition.

Linear fits to the measured flame speeds, presented in Figure 6.13, for an undiluted and 10% steam diluted mixture are in good agreement with the mechanism predictions for the strained flame, especially for the San Diego mechanism. Furthermore, extrapolations of the strained flame speeds (indicated along the left axis of Figure 6.13) to zero strain rate, and thus to the unstretched flame speed, also agree well. However, the unstretched flame speeds estimated from the Bunsen flame technique (indicated by the closed symbols along the left axis of Figure 6.13) are significantly lower than the extrapolations. Since none of the measurement uncertainties investigated in Chapters 3 and 4 can account for such a large error in the Bunsen-based flame speed, it is reasonable to conclude that the error is due to the failure of an underlying assumption of the method at these conditions, e.g., that the burned flame speed of this Bunsen flame is only weakly effected by curvature and strain except very close to the base and at the flame tip.

If this is true, however, this must somehow correlate to the specific conditions of these flames, as much better agreement was observed in Chapter 4 for pure methane and propane fuels at atmospheric pressure. The same systematic effect on flame speed is observed in Figure 6.13 for both diluted and undiluted oxidizers. Thus the cause can not simply be associated with dilution. Also, the atmospheric pressure results for methane/ethane mixtures (Figure 6.1) reveal the same trend at rich conditions. Therefore, the cause can not be associated solely with propane addition. If a greater portion of the Bunsen flame is being significantly impacted by flame stretch, it would have to be due to some combined impact of conditions that make these flames “different”, i.e., multi-fuel mixtures and preheating, combined with operation at rich equivalence ratios.

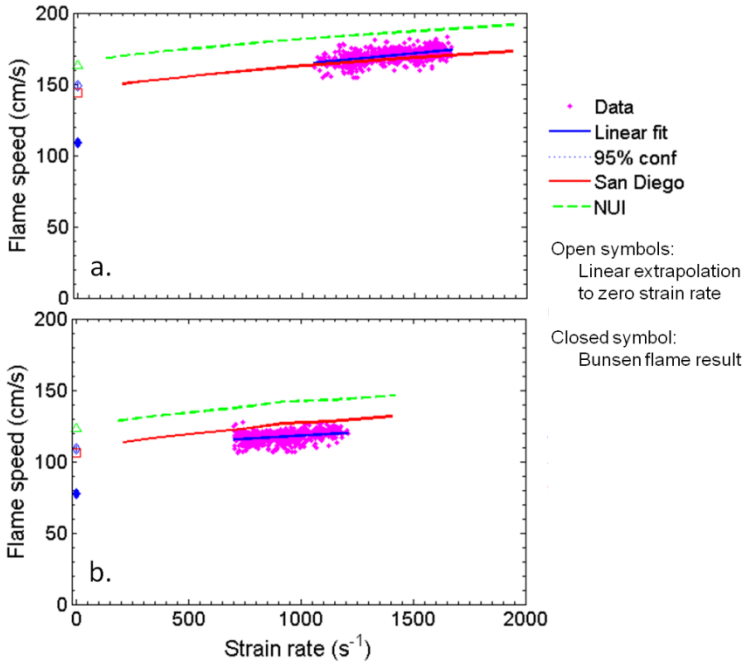

Figure 6.13. Strained laminar flame speed of 60:40 CH_4:C_3H_8 mixture without (a) and with (b) 10% steam dilution. [ff] Open symbols are linear extrapolation to zero strain rate and closed symbols are measurements from Bunsen flame technique (estimated to correct for steam dilution level).

Comparisons of the strained flame speed measurements and predictions, presented in Figure 6.13, also show a difference between the strain effect. The simulations indicate an increase in sensitivity of flame speed to strain rate (or increase in Markstein length) with increase in the steam dilution level. However, the experiments indicate a decrease in the Markstein length. The Markstein lengths for the different cases are presented in Table 6.2. The mechanism predictions show that the Markstein length for the 10% steam dilution case increases for strain rates higher than 900 s^{-1}. Since the measurements are performed around this strain rate, it is possible that measurements from the experiment are weighted towards the lower Markstein length conditions. Table 6.2 also presents, in parenthesis, the Markstein length estimated from the mechanism results with strain rate over 900 s^{-1}.

[ff] The 95% confidence interval for the linear fit is barely visible due to its proximity to actual fit. The difference between linear fit and the 95% confidence interval is less than ±3%.

Table 6.2. Markstein length for ϕ = 1.2, 60:40 CH_4:C_3H_8 mixtures with and without steam dilution. Values based on linear fit to strained flame speed results at atmospheric pressure and 650 K preheat.

	Markstein length (μm)		
	Experiment	**San Diego**	**NUI**
No dilution	– 149 ± 16	– 133	– 127
10% H_2O	– 92 ± 22	– 153 (– 106)[gg]	– 145 (– 91)

6.3.2 High pressure results

6.3.2.1 Methane/ethane mixtures

Figure 6.14 shows the flame speed measurements for methane/ethane mixtures at 5 atm. Here, instead of varying steam dilution level at fixed equivalence ratio, the steam dilution was fixed at 26% mole fraction of the oxidizer, in order to prevent flame instabilities, and the equivalence ratio was varied over a wide range. As expected, higher pressure decreases the flame speed of the mixture at a given ϕ and steam dilution level (cf. Figure 6.7 and Table 6.3). Also increasing ethane mole fraction in the fuel mixture, from 20% to 40%, results in a significant (15–25%) increase in the flame speed over the equivalence ratio range. This is in contrast to atmospheric pressure measurements, where increasing ethane results in an ~20% increase in flame speed for the lean mixture but less than a 5% change for the stoichiometric mixture. Furthermore at high pressure, the peak flame speed for the 80:20 CH_4:C_2H_6 mixture is at a slightly leaner equivalence ratio compared to the 60:40 mixture (0.95 compared to 1.0).

[gg] The value in parenthesis refers to the Markstein length based on results with strain rate higher than 900 s^{-1}.

Table 6.3. Effect of pressure on laminar flame speed of 60:40 methane/ethane mixture with 25.9% steam dilution. Values interpolated, from flame speed measurements, to correct for the equivalence ratio and steam dilution level.

ϕ	S_L (cm/s)		% change in S_L
	1 atm	5 atm	
0.8	54.3	40.6	25
1.0	59.9	46.8	22
1.2	49.3	34.8	29

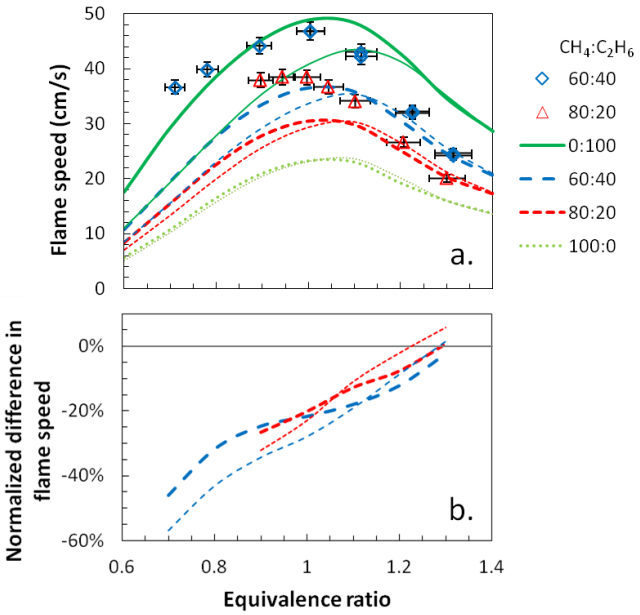

Figure 6.14. (a) Unstretched laminar flame speed of methane/ethane/air/steam mixtures at 5 atm pressure and 650 K preheat temperature. (b) Normalized difference between the measured and predicted flame speed. Oxidizer consists of 25.9% mole fraction of steam in air. The ratio in the legend indicates fuel composition as methane/ethane ratio. Current measurements are represented by symbols and mechanism predictions by thick and thin lines for San Diego and NUI C3 mechanism respectively.

The mechanism predictions are in good agreement with the measurements for rich mixtures, but predict significantly lower (20–60%) flame speeds for lean and near stoichiometric mixtures. This is in contrast with the trend observed at atmospheric pressure (Figure 6.7), where the mechanism predictions are in reasonable agreement with the measurements for ϕ = 0.8 and 1.0, but over-predict the flame speed for rich mixtures.

There is also a significantly larger difference in the predictions for the two mechanisms. The NUI mechanism predictions, which were lower than the San Diego results for lean mixtures, by ~7% at atmospheric pressure are now lower by ~15%. This disagreement between the mechanism increases with increase in the ethane content of the mixture. It should be noted that the mechanisms predict a peak in flame speed at a slightly rich equivalence ratio (between 1.0–1.15) for both the fuel mixtures.

6.3.2.2 Methane/propane mixtures

Flame speed measurements for two methane/propane mixtures at 5 atm pressure are presented in Figure 6.15. Measurements are not available at low steam dilution levels due to the wrinkling of the flame surface as a result of increased instabilities at this elevated pressure. As expected, the flame speed of the mixtures decreases in comparison to the atmospheric pressure case (Figure 6.9). The measured flame speed decrease with steam dilution is also less linear compared to the atmospheric pressure results. This is more evident in Figure 6.16, which presents a comparison of the normalized flame speeds for different equivalence ratios. The flame speeds were normalized by the value at 20% steam dilution due to the absence of undiluted data.

While increasing the amount of propane in the fuel mixture might be expected to increase the flame speed, this is clearly not the case for the lean condition ($\phi = 0.8$), where the 80:20 CH_4:C_3H_8 mixtures have higher flame speeds compared to the 60:40 mixtures. Furthermore the flame speeds for the lean 80:20 mixtures are higher than those for the stoichiometric mixtures at the same dilution. A higher flame speed can result either due to error in flowrate (actual flowrate being is lower than recorded) and/or error in the measured flame area (actual area being higher than measured). However, the same

results were obtained when the experiments were repeated, a month later, after recalibrating and making sure there were no gas leaks in the flow system. These are highlighted by data points with a lighter shade. An error in the measured flame area is unlikely due to the image processing algorithm used, which was also used for the all the other cases reported and has been thoroughly validated.

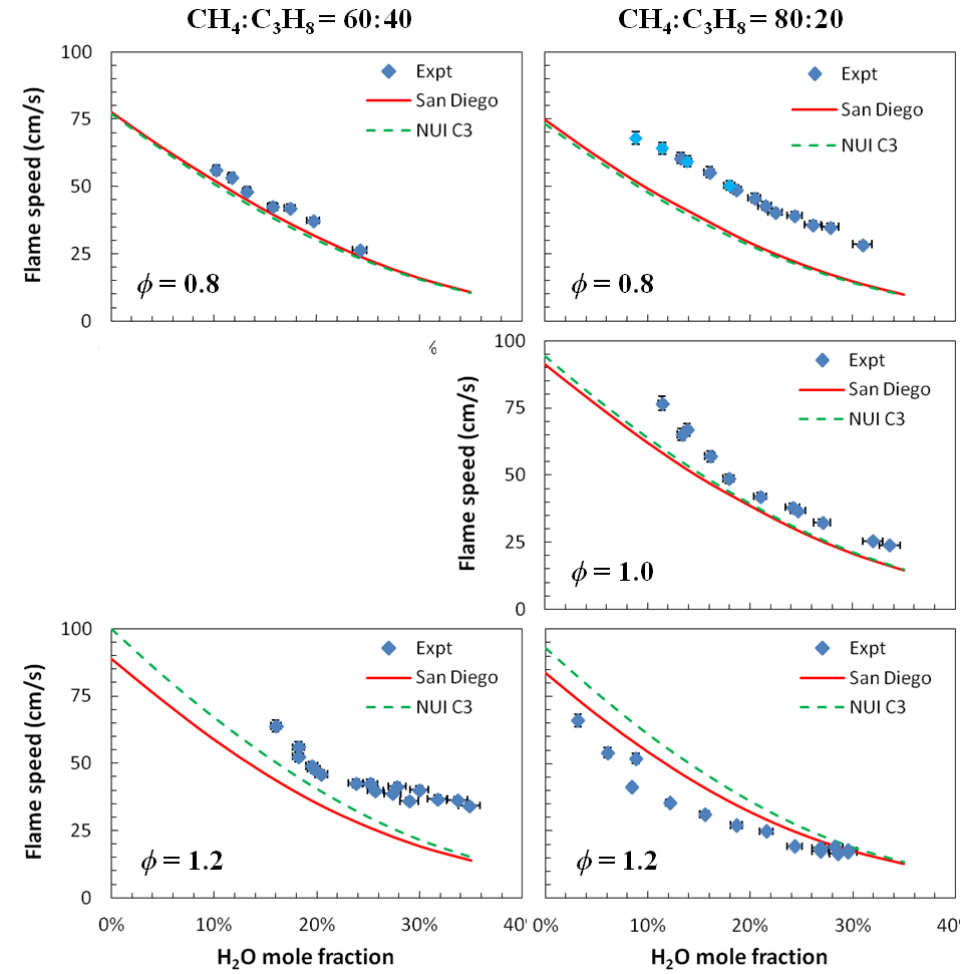

Figure 6.15. Unstretched laminar flame speed of methane/propane/air/steam mixtures at 5 atm pressure and 650 K preheat temperature. The rows correspond to equivalence ratio of 0.8 (first), 1 (second) and 1.2 (third) respectively whereas the columns correspond to CH_4:C_3H_8 mixture of 60:40 (first) and 80:20 (second) by volume. The lighter shade data for ϕ = 0.8, 80:20 mixture, corresponds repeat of experiment on a different day.

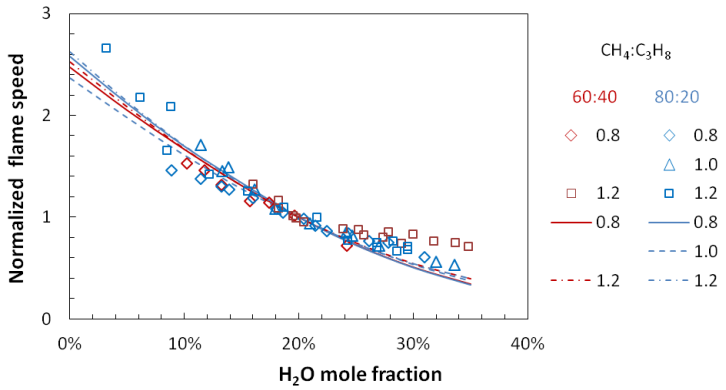

Figure 6.16. Measured (symbols) and predicted (lines) flame speed of atmospheric methane/propane/air mixtures with steam dilution normalized by flame speed for *20% dilution* case. Results are color coded: red and blue for 60:40 and 80:20 CH_4:C_3H_8 mixture respectively. Predictions are for San Diego mechanism.

Reference flame images at different steam dilution level are presented in Figure 6.17. Figure 6.17 also shows reference flame images at two steam dilution levels for the rich 80:20 mixtures. The images for the rich 80:20 mixtures are presented as a reference because the flame speeds measured at the two conditions, viz. 8.4% and 8.8% steam dilution, are significantly different (~20%). However no significant systematic difference is observed between the two images; the difference in flame height is due to the change in the total flowrate.[hh] These images indicate a possibility that significant difference in measured flame speed can exist even for cases with visibly similar and acceptable flame geometry.

Figure 6.15 also presents the flame speed predictions from the San Diego and NUI C3 mechanisms. The predictions show good agreement with the lean 60:40 and stoichiometric 80:20 mixtures over most of the measurement range. However for rich mixtures, the predicted flame speeds are lower by ~30–50% for the 60:40 case and higher by ~5–40% for the 80:20 case. At all other binary fuel mixtures conditions tested, the

[hh] The total reactant flowrate for the 8.4% and 8.8% mixture was 11.8 and 16.9 slpm respectively, which corresponds to an increase in the flowrate by ~40%..

mechanisms predictions are either higher or lower for both fuel compositions. However this is not the case for the methane/propane mixture presented in Figure 6.15. This indicates that the change in fuel composition has an effect on the flame speed measurement at these conditions. There is also significant difference between the measured and predicted flame speeds for the lean 80:20 mixtures. However this is expected due to the high flame speed measured for these mixtures.

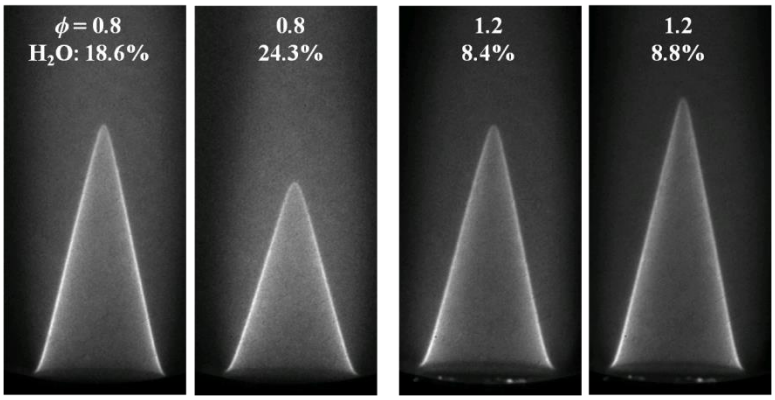

Figure 6.17. Instantaneous chemiluminescence image of the flame for lean and rich 80:20 CH_4:C_3H_8 mixtures with steam dilution. Numbers indicate equivalence ratio and steam mole fraction in oxidizer. Images are not scaled to same signal intensity.

6.3.2.2.1 Strained flame speed measurements

The 60:40 CH_4:C_3H_8 mixture is further investigated at lean and rich conditions, with and without steam dilution, with the stagnation flame approach. Figure 6.18 presents flame speeds for a lean (ϕ = 0.8) methane/propane mixture at 5 atm and 650 K preheat with no dilution and 10% steam dilution. Increasing the steam dilution results in greater strain sensitivity, though there is a significant uncertainty in the measured strain sensitivity for the no dilution case (–2 ± 56 μm). Also for 10% steam dilution, the unstretched flame speeds estimated from the stagnation and Bunsen flame technique are in good agreement (less than a 10% difference). Furthermore the predictions from both chemical kinetics mechanisms are also in good agreement with the measurements at both

dilution levels. The mechanisms, however, predict a smaller change in strain sensitivity with steam dilution level. The Markstein lengths for these mixtures are presented in Table 6.4. The apparent higher change in measured Markstein length could be due to the higher uncertainty in the undiluted case data, which indicates that a linear fit is not able to correctly capture the strain flame speed variation.

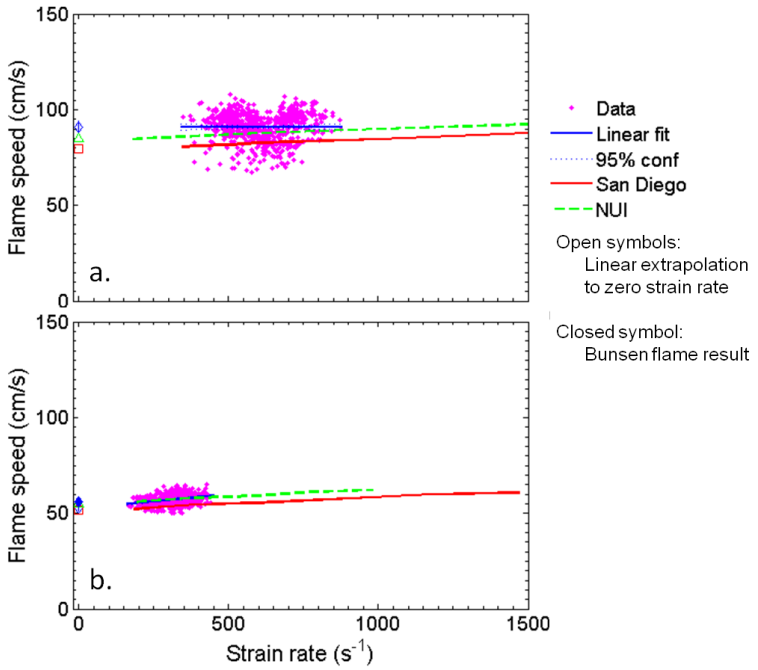

Figure 6.18. High pressure (5 atm) strained laminar flame speed of lean (ϕ = 0.8) 60:40 CH_4:C_3H_8 fuel mixture (a) without and (b) with 10% steam dilution. Open symbols are linear extrapolation to zero strain rate and closed symbols are measurements from Bunsen flame technique (estimated to correct for steam dilution level).

Table 6.4. Markstein length for ϕ = 0.8, 60:40 CH_4:C_3H_8 mixtures with and without steam dilution. Values based on linear fit to strained flame speed results for 5 atm pressure and 650 K preheat.

	Markstein length (μm)		
	Experiment	**San Diego**	**NUI**
No dilution	– 2 ± 56	– 58	– 58
10% H_2O	– 319 ± 35	– 68	– 75

Figure 6.19 presents the strained flame speed measurements for a ϕ = 1.2 methane/propane mixture at 5 atm and 650 K preheat, with varying steam dilution level.

The measurements show that the Markstein length for the mixture decreases (becomes more negative) with steam dilution (see Table 6.5). Furthermore, comparisons with the prediction from chemical kinetics mechanism show that the NUI mechanism is in slightly better agreement with the measurements as compared to the San Diego mechanism. In comparison, at atmospheric pressure, the San Diego mechanism predictions were in better agreement with the experiments. Furthermore at high pressure, both the mechanisms predict strain sensitivities that are much larger than the measured value and show a smaller change with the steam dilution level. A possible reason for these differences could be the high uncertainty in the measured Markstein length. For example for 10% steam dilution (Figure 6.19b), the measured Markstein length would agree better with the predicted values if the strain rate range for the linear fit is limited to 300–700 s^{-1}, whereas for 14.4% steam dilution case (Figure 6.19c) there is higher uncertainty because the number of measurements available is low, due to insufficient seeding density.

Table 6.5. Markstein length for ϕ = 1.2, 60:40 CH_4:C_3H_8 mixtures with and without steam dilution. Values based on linear fit to strained flame speed results for 5 atm pressure and 650 K preheat.

	Markstein length (μm)		
	Experiment	**San Diego**	**NUI**
No dilution	– 39±71	– 63	– 55
10% H_2O	– 189±15	– 97	– 79
14.4% H_2O	– 265±57	– 98	– 74

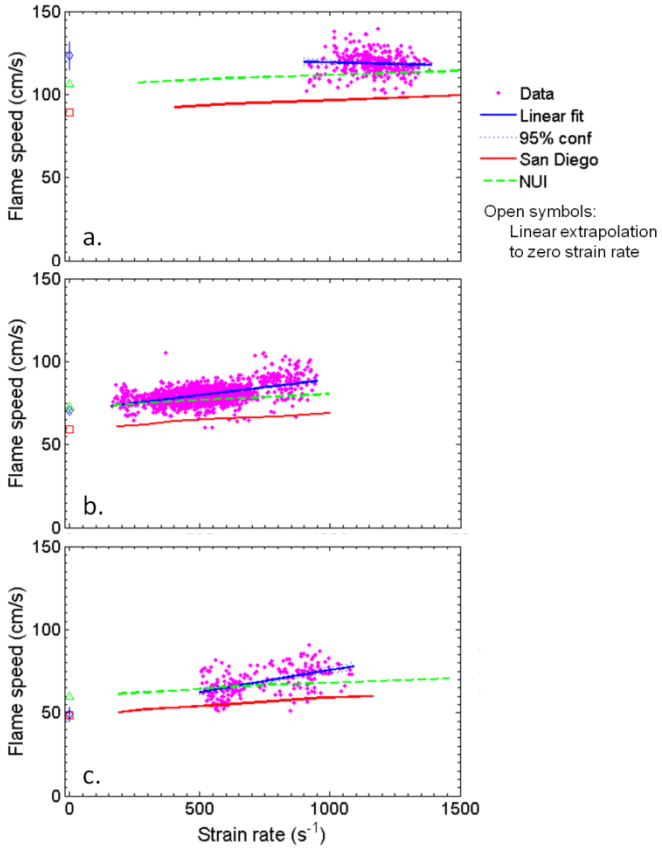

Figure 6.19. High pressure (5 atm) strained laminar flame speed of rich (ϕ = 1.2) 60:40 CH_4:C_3H_8 fuel mixture (a) without, (b) with 10% and (c) with 14.4% steam dilution. The extent of linear fit (blue curve) indicates the range of strain rate where the measurements were performed. Open symbols are linear extrapolation to zero strain rate and closed symbols are measurements from Bunsen flame technique (estimated to correct for steam dilution level).

6.3.3 Relationship between strain sensitivity and measured flame speed

Section 5.3 explored the relationship between flame height and the difference between the predicted and measured flame speeds. While no clear correlation was found, flame height is a global parameter that influences the degree of stretch (due to both the curvature and strain) experienced by the Bunsen flame. It does not, however, address the stretch sensitivity of the flame. To examine whether there is any correlation between strain sensitivity and the observed differences in flame speeds for the binary mixtures, the

normalized difference between the predicted and measured flame speed is plotted against the Markstein number[ii] for select fuel mixtures in Figure 6.20.[jj]

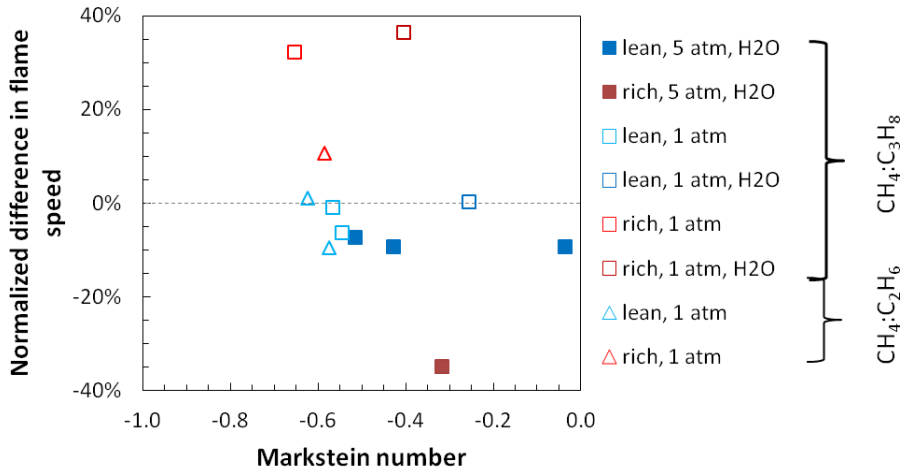

Figure 6.20. Difference between the predicted and measured flame speed (normalized by measured flame speed) as a function of Markstein number for a mixture. Results are for 60:40 CH_4:C_3H_8 (square) and 60:40 CH_4:C_2H_6 (triangle) mixtures at 650 K. 1 and 5 atm pressure result are represented by closed and open symbols respectively. Lean and stoichiometric mixtures are in blue and rich mixtures in red. Darker shades represent steam dilution, whereas lighter shades are without steam dilution. Flame speed predictions are from San Diego mechanism.

The results do not show a clear correlation between the strain sensitivity of the mixture and the difference in the flame speed; for the same strain sensitivity, lean and rich mixtures show significantly different flame speed differences. For rich mixtures, the difference in flame speed does appear to decrease as the Markstein number increases (toward zero for these negative Markstein number mixtures). However this could also be

[ii] Markstein number is defined as $\mathrm{Ma} = l/\delta_L^0$, where l is the Markstein length and δ_L^0 is the flame thickness determined, based on the maximum temperature gradient in an unstretched flame (PREMIX calculations), as follows,

$$\delta_L^0 = \frac{T_{\max} - T_u}{(dT/dx)_{\max}}$$

where $T_{\max}$ is the maximum temperature in the flame (generally equal to the adiabatic flame temperature) and T_u is the reactant temperature.

[jj] The stretch sensitivity (Markstein length) of a reactant mixture is a function of the geometry of the flame [90]. As such one can expect the stretch sensitivities calculated from Bunsen, stagnation flame or outwardly propagating spherical flame geometries to be different. The Markstein length used here is determined from the opposed flow stagnation flame geometry (as modeled by Chemkin's OPPDIF reactor). While the Bunsen flame stretch sensitivity is not expected to be uniform over the flame surface, no tool for calculating that flame configuration was available.

attributed to the change in pressure between the low Markstein number data point (at 5 atm) and the other rich points (at 1 atm). Since the number of measurements is limited, it is not possible to conclusively say if there is any correlation between the difference in the flame speed and strain sensitivity for rich mixtures.

6.3.4 Summary

This section has presented the effect of steam dilution on binary mixtures of methane/ethane and methane/propane. As expected, increasing the amount of ethane or propane in the fuel mixture increases the flame speed of the mixture. The flame speed decreases in a slightly non-linear fashion with steam dilution level for the different fuel mixtures considered. Furthermore, the methane/propane mixtures show a similar quasi-linear dependence of the flame speed to the change in the flame temperature as found for pure propane with m' ~ 6–7.3. This suggests that it is possible to parameterize the results to predict the change in flame speed with dilution for pure fuels and binary mixtures.

For atmospheric pressure, the Bunsen flame technique provides a faithful measurement of flame speeds at the lean and stoichiometric conditions studied, and the results are in agreement with predictions from the chemical kinetics mechanisms. However at rich conditions, the technique generally produces significantly lower flame speeds than those predicted by the mechanisms, especially for methane/propane mixtures. Such a difference is not observed in the stagnation flame speed measurements. This indicates needed improvements in the Bunsen flame technique; preliminary comparisons do not show any clear correlation between the stretch sensitivity and differences in the measured flame speeds. Furthermore, significant difference is observed between the

flame speed predictions from different mechanisms, indicating a possibility of needed improvements in the mechanisms at rich conditions.

At high pressure, the measurements for methane/ethane mixtures show a significant change (15–25%) in flame speed with amount of ethane. There is also significant difference between the measured and predicted flame speeds at lean equivalence ratios, whereas rich mixtures show good agreement. However unlike the atmospheric pressure results, the mechanisms now show a higher difference (> 20%) in flame speed for lean conditions and have better agreement with the measurements at rich conditions. Thus there is a need for possible improvement in the mechanisms while accounting for effect of pressure for methane/ethane mixtures. On the other hand, high pressure flame speeds for the methane/propane fuel still show good agreement for lean and stoichiometric mixtures but have significant differences for rich mixtures. However the mechanism predictions show good agreement with the strain flame speed measurements. These results for the atmospheric and high pressure cases indicate a need for improving the understanding of the Bunsen flame technique at these conditions. Furthermore the measurements for lean 80:20 CH_4:C_3H_8 mixtures with steam dilution exhibit a significantly higher flame speed than expected. The reason for this is not fully understood, even though most of the experimental sources of uncertainty have been accounted for.

6.4 Mixing rules

As discussed in Section 2.2, different mixing rules are used to estimate the flame speed of fuel mixture. This section explores the performance of some of these mixing rules under high preheat and steam dilution conditions. Since measurements were not

performed for pure fuels at desired conditions, the results presented in this section are based on predictions from the San Diego mechanism. The mixing rules tested are derived based on:

1. mole fraction weighting;
2. mass fraction weighting; and
3. adiabatic flame temperature weighting.

$$S_{L,m} = \sum_i x_i S_{L,i} \tag{1a}$$

$$\frac{1}{S_{L,m}} = \sum_i \frac{x_i}{S_{L,i}} \tag{1b}$$

$$S_{L,m} = \sum_i y_i S_{L,i} \tag{2a}$$

$$\frac{1}{S_{L,m}} = \sum_i \frac{y_i}{S_{L,i}} \tag{2b}$$

$$\ln S_{L,m} = \frac{\sum_i x_i n_i T_{\mathrm{ad},i} \ln S_{L,i}}{\sum_i x_i n_i T_{\mathrm{ad},i}} = \frac{\sum_i x_i n_i T_{\mathrm{ad},i} \ln S_{L,i}}{n_m T_{\mathrm{ad},m}} \tag{3}$$

Figure 6.21 compares the performance of these mixing rules viz. expressions 1–3, for an 80:20 CH_4:C_2H_6 mixture with air at atmospheric pressure and 650 K preheat temperature over a range of equivalence ratios. The plot presents a normalized difference of the estimated flame speed from the actual flame speed of the mixture. The results show that all the mixing rules provide a reasonable estimate of the flame speed. However they all tend to under-estimate the flame speed of the mixture.

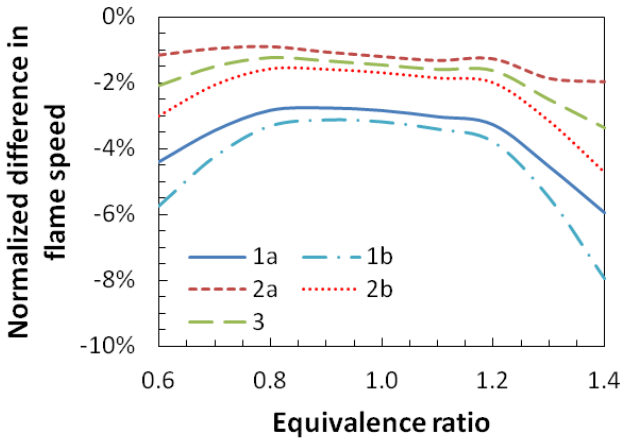

Figure 6.21. Normalized difference in flame speed estimated using different mixing rules and the actual flame speed of 80:20 CH_4:C_2H_6 mixture with air. Calculations performed using San Diego mechanism at atmospheric pressure and 650 K preheat temperature. The numbers in the legend refer to the expressions presented in the text.

It is worth nothing that the approaches based on reciprocal of flame speed (viz. expression 1b and 2b) always provide a lower estimate of the mixture flame speed compared to their counterparts (viz. expressions 1a and 2a respectively). This is because these expressions provide a higher weight to the component with lower flame speed. However from the measurements presented in this thesis, it is evident that addition of propane or ethane to methane will shifts the flame speed of the mixture significantly towards the higher flame speed component viz. propane or ethane. As such combining the reciprocals of flame speed will not produce a good estimate of the mixture flame speed and hence is not considered further.

Figure 6.22 presents difference in actual and estimated flame speed, at 10 atm, for a 60:40 CH_4:C_3H_8 mixture at 300 K and 650 K. For methane/propane mixtures, the adiabatic flame temperature based mixing rule provides a better estimate of the flame speed compared to the mass fraction based mixing rule, while the latter tends to be better for methane/ethane mixtures. Furthermore, an increase in preheat temperature does not have any systematic effect on the accuracy of the flame speed estimate.

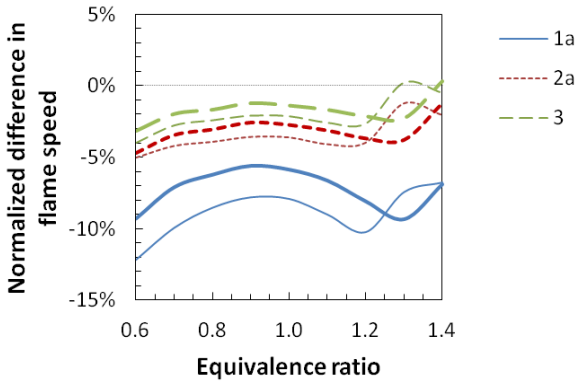

Figure 6.22. Normalized difference in flame speed estimated using different mixing rules and the actual flame speed of 60:40 CH_4:C_3H_8 mixture with air. Calculations performed using San Diego mechanism at 10 atm pressure and 300 K (thin lines) and 650 K (thick lines). The numbers in the legend refer to the expressions presented in the text.

Figure 6.23 presents the difference in flame speed for methane/ethane mixtures with steam dilution at 1 and 10 atm. There is no clear systematic trend with change in pressure. However, compared to undiluted cases, the mass fraction weighted flame speed estimates are higher than the actual flame speed for some of the equivalence ratios. In general, the flame speed estimates from the mass fraction and adiabatic temperature weighted mixing rules tend to be within ±5% of the actual flame speed over most of the tested range of fuel mixtures, equivalence ratios, preheat temperatures and pressures.

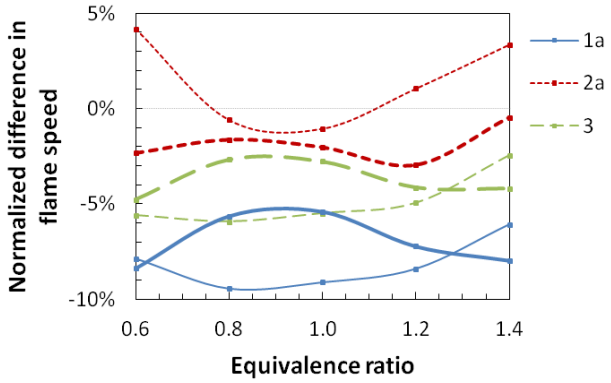

Figure 6.23. Performance of different mixing rules for 60:40 CH_4:C_2H_6 mixture with steam dilution (15%) at 650 K. Calculations are for atmospheric (thin lines) and 10 atm (thick lines) pressure.

Finally, Figure 6.24 shows the difference in the estimated and actual flame speeds as a function of amount of methane in the fuel mixture. Once again, the mass- and temperature-weighted estimates are quite close to the actual mixture values. The flame speed estimates are asymmetric (about the 50% level) with respect to the mole fraction of methane but more symmetric as a function of the methane mass fraction. This could simply be a coincidence for the given fuel mixture. It is known that the flame speed changes marginally between higher-order alkanes (> C_3) because the adiabatic flame temperature change between these alkane is small [9]. Also for estimates of flame speed for mixtures of methane and a higher order alkane, based on mass fraction weighting, the flame speed will be weighted more towards the flame speed of the higher order alkane. However because the flame speed does not change significantly between higher order alkanes, the estimate can be skewed for higher order alkane.

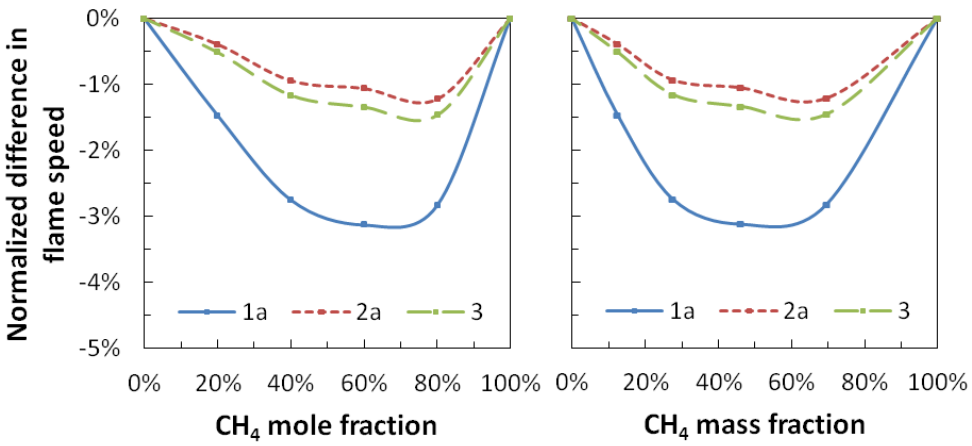

Figure 6.24. Normalized difference in flame speed estimated using different mixing rules and the actual flame speed of stoichiometric CH_4:C_2H_6 mixture with air as a function of amount of methane in the fuel. Calculations performed using San Diego mechanism at atmospheric pressure and 650 K preheat temperature. The numbers in the legend refer to the expressions presented in the text.

To summarize, all the different mixing rules tests mixing rule tested provide a reasonable estimate of the actual flame speed of a binary fuel mixture. However in general, the mass fraction mixing rule provides a better estimate for the methane/ethane

mixtures, while the adiabatic temperature based rule works best for methane/propane. In general, the flame speed estimates are only a few percent lower than the actual flame speed. However, this is not the case under all conditions, as seen here for steam dilution. Furthermore, increasing the pressure and preheat temperature appears to have no systematic effect on the accuracy of the flame speed estimate.

CHAPTER 7

CONCLUSIONS

7.1 Summary and conclusions

This thesis investigated laminar flame speeds of pure and binary mixtures of C_1–C_3 alkanes over a range of conditions relevant to gas turbine conditions. To perform the flame speed measurements two techniques viz. a modified Bunsen flame approach (for unstretched flame speed measurements) and a bluff-body stabilized stagnation flame approach (for flame speed strain sensitivity measurements) were implemented. Various leading chemical kinetics mechanisms and a 1-d laminar flame simulation were also used to predict flame speeds under these conditions. This chapter summarizes the key results and provides suggestions for further study. The key goals of this work can be divided into three areas:

1. Flame speed measurement techniques
    a. Extend the modified Bunsen flame measurement approach to measure flame speeds of hydrocarbon fuels and to improve understanding of the uncertainties associated with such measurements.
    b. Implement a bluff-body stabilized stagnation flame approach with high resolution PIV imaging for measuring strain sensitivity.
2. Flame speed database
    a. Develop an unstretched and stretched flame speed database for C_1–C_3 alkanes at high preheat and dilution.

b. Understand the effect of binary fuel mixtures and vitiation on the flame speed of the mixture.

3. Mechanism comparison
    a. Investigate the performance of leading chemical kinetics mechanisms for predicting flame speed at relevant conditions and identify possible regions of improvements.

7.1.1 Measurement techniques validation

7.1.1.1 Modified Bunsen flame approach

The modified Bunsen flame approach was previously used by Natarajan [55] to successfully measure flame speeds of syngas fuel mixtures. In this work, the technique has been validated for flame speed measurement of hydrocarbon fuels over a range of conditions. The validation results show that the technique is suitable for measuring unstretched flame speed for a number of pure alkane fuels (methane/ethane/propane), with different diluents (nitrogen, steam and helium), at lean and rich conditions (ϕ = 0.6–1.3), and at various pressures (1–10 atm) and reactant temperatures (300–650 K). The flame speeds measured using this approach are generally within ±10% of stretch-corrected results from other widely accepted techniques viz. stagnation and spherical flame configurations. The results also show that measurements are reproducible and insensitive to the burner diameter (6–16.6 mm). However, a significant decrease in the non-dimensional flame height (h/D < 1.3) introduces a systematic error, a higher than actual flame speed. To conclude: *the reaction-zone area based approach using a Bunsen flame configuration is suitable for determining the unstretched flame speed of*

hydrocarbon fuels, within ±10%, over a wide range of conditions. The technique is suitable for high temperature and pressure measurements (with negligible effect of fuel degradation due to low residence time) and reasonably fast to perform measurements over many conditions. However as detailed in Section 7.1.2, discrepancies were observed in the Bunsen measurements at certain conditions, such as rich mixtures with low O_2 content in the oxidizer.

7.1.1.2 Stagnation flame approach

The stagnation flame configuration has been widely used for flame speed and strain sensitivity measurements. The current implementation of the bluff-body stabilized stagnation flame with PIV for velocity measurement, as opposed to the more common opposed jet flame configuration with LDV measurements, has been shown to be suitable for accurate flame speed and strain rate measurements, with demonstrated errors of less than 5%. Furthermore the setup also allows for acquiring instantaneous flame speed and strain rate sweeps with high accuracy and precision (less than 1% difference for 95% confidence interval).

7.1.2 Laminar flame speed results

Laminar flame speed measurements were performed over a range of conditions using the Bunsen and stagnation flame techniques. Table 7.1 provides an overview of the conditions where the flame speed measurements were performed. A complete flame speed database of the measurements, performed during this work, along with relevant experimental conditions is provided on the Georgia Tech's Smartech repository. Except for the validation tests (primarily at low preheat temperature), most of the flame speed

measurements presented here are the first reported at the conditions listed in the table, i.e., combinations of high preheat, dilution, fuel composition and elevated pressure. Thus these measurements represent a unique database at conditions relevant in gas turbine combustor. The measurements are useful for evaluating the performance of chemical kinetics mechanisms for C_1-C_3 alkanes and also for understanding the uncertainties in the Bunsen flame technique for measuring flame speed. The subsequent sections discuss some of the key observations from the measurements, including the validation of various chemical kinetics mechanisms and their implication on improving the understanding of the Bunsen flame technique.

Table 7.1. Overview of the range of conditions where flame speed measurements were performed. Each symbol corresponds to a variation in equivalence ratio or strain rate (tick mark) and dilution level (asterisk). The color of the symbols correspond to the room temperature (blue) and high temperature (red).

Technique:		Bunsen (based on reaction zone area)							Stagnation		
Diluent:		N_2			He	CO_2	H_2O		N_2	H_2O	
Pressure (atm):		1	5	5	10	1	1	5	1	1	5
CH_4		✓			✓		*		✓		
C_2H_6		✓	✓						✓		
C_3H_8		✓*				✓*	✓				
CH_4:C_2H_6	80:20				✓		✓*	✓	✓		
	60:40	✓		✓	✓		✓*	✓			
CH_4:C_3H_8	80:20			✓			✓*	✓*			
	60:40			✓			✓*	✓*		✓*	✓*

7.1.2.1 Pure fuels and vitiation

Measurements of flame speed were performed for propane–air mixtures with N_2 (0–28.5%), CO_2 (0–10%) and H_2O (15.5%) dilution at high preheat (650 K). The O_2 mole

faction in the oxidizer varied from 15–21%. As expected, the measured flame speed decreases with addition of the diluents. Furthermore for equal amounts of diluent, the flame speed is most affected by CO_2 addition, followed by H_2O and N_2.

The simulation data shows that the flame speed decrease with increasing dilution, for propane–air mixtures, is nearly linear with N_2, slightly non-linear with H_2O and significantly non-linear with CO_2 addition (with a slower decrease in flame speed at higher dilution levels). This is because, unlike N_2, both H_2O and CO_2 are chemically active and thus affect the flame speed through a decrease in both the flame temperature and the radical pool concentration, and also because for the same dilution level the change in the flame temperature is highest for CO_2 addition followed by H_2O and N_2. Furthermore the relative decrease in the flame speed, for a given diluent, is similar over a range of equivalence ratios (0.7–1.3).

The simulations also show that the log of normalized flame speed ($\ln(S_L/S_L^0)$) is roughly linear with the fractional change in adiabatic flame temperature ($\Delta T_{\mathrm{ad}}/T_{\mathrm{ad}}^0$). The negative slope of these curves, m', is between 4.8–7.7, increasing for dilution with N_2 (4.8–5.5) to H_2O (5.7–6.6) to CO_2 (6.8–7.7) for propane flames. The linear trend is also observed for methane-propane fuel mixtures with steam dilution with roughly the same range of sensitivity values as for pure propane (m' ~ 5.9–6.9). *These findings suggest that it is possible to develop simple correlations for the variation in flame speed with dilution that is valid for a large range of equivalence ratios and fuel mixtures.*

Based on the simulations, the chemical effect of CO_2 is responsible for almost 30% of the decrease in the flame speed from the undiluted condition (the remaining 70% decrease is due to the thermal effect). The chemical effect of H_2O accounts for up to a

10% decrease in the flame speed, while the chemical effect for N_2 is negligible (< 1%). The direct chemical effect of dilution is most significant near stoichiometric conditions due to the high flame temperature and hence higher radical concentration at these conditions. How the third body efficiency of the diluent is accounted for is also important in defining the chemical effect of the diluent.

Measurements were also performed at constant adiabatic flame temperature at different equivalence ratios, as they are helpful in isolating the chemical kinetics effect from the flame temperature effect on the flame speed and also because such measurements can be of practical use in real combustors where temperature is an important design consideration. Measurements were performed for methane–air mixtures with H_2O dilution and propane–air mixtures with N_2 and CO_2 dilution. These measurements show that the minimum flame speed location is close to the stoichiometric condition. On either side of stoichiometric condition, the flame speed increases due to increase in O_2 and fuel concentration. However for sufficiently rich conditions (ϕ >1.2), the flame speed starts decreasing due to the decrease in the H radical concentration, which is consumed by fuel breakup and recombination reactions.

7.1.2.2 Binary fuel mixtures

Flame speed measurements of binary fuel mixtures of methane/ethane and methane/propane show that changing the amount of higher alkane from 20% to 40% (mole fraction in fuel mixture) results in a marginal increase in the flame speed (< 5%). However for high pressure methane/ethane flames with steam dilution the results show a much higher (15–25%) change in flame speed with increase in ethane mole fraction.

Simulation results for atmospheric pressure indicate that addition of higher alkane (viz. ethane and propane) to methane significantly shifts the flame speed towards that of the higher alkane. Further increase in mole fraction of higher alkane increase the flame speed marginally. Similar results are observed at higher pressure for methane/propane mixture. However for methane/ethane mixtures, the fractional increase in flame speed is lower at high pressures (5 and 10 atm) than at atmospheric pressure.

Steam dilution measurements, for the binary fuel mixtures at 1 and 5 atm and up to 30% H_2O mole fraction in the oxidizer, show a similar behavior for the relative change in flame speed as the pure fuel results. For example, the relative impact of H_2O addition is similar for different equivalence ratios. In addition, the same behavior is observed for different fuel mixture compositions. The measurements confirm the expected trends of decrease in flame speed with increase in steam dilution or decrease in fraction of higher alkane in the fuel mixture. Also like the pure fuel results, the decrease in normalized flame speed can be related to the normalized decrease in the flame temperature with $m' \approx$ 6–7.3. Strained flame speed measurements, for methane/propane mixtures with steam dilution at 5 atm pressure, show that steam dilution results in a slight increase in the strain sensitivity of the mixture, whereas for atmospheric pressure, the strain sensitivity decreases. In comparing the differences between the measured and predicted (unstretched) flame speeds, no clear correlation was observed.

Predictions from chemical kinetics mechanisms were used to empirically investigate the performance of different mixing rules in estimating the flame speed of binary fuel mixtures from the properties of individual components. In general, all the mixing rules considered provided a reasonable estimate (generally within 10%) of the

flame speed of the mixture. More specifically for methane/ethane mixtures, mass fraction based mixing rule provided better estimate of the mixture flame speed, whereas for methane/propane mixtures, adiabatic flame temperature based mixing rule performed better. The results from these two mixing rules are generally within ±5% of the actual flame speed. While the estimated flame speed from the mixing rule tends to be lower than actual value for most conditions tested, this is not always the case as shown for steam dilution condition. Furthermore the accuracy of the mixing rules does not have any systematic dependence on the pressure or preheat temperature conditions. The accuracy of these simple mixing rules, in estimating the flame speed of a fuel mixture, is comparable to uncertainties in the flame speed simulations. In addition, the wide range of applicability of these rules, suggests that they can be useful for estimating flame speed of fuel mixtures for practical use, without having to run the full chemical kinetics mechanisms at all conditions.

7.1.3 Evaluation of chemical mechanisms

Comparison of the experimental measurements and predictions from leading chemical kinetics mechanisms are useful in validating the mechanisms, as well as providing information on the accuracy of the current measurements. Comparisons of unstretched flame speed predictions with validation test results show that mechanism results are generally within ±30% of the measured values with systematic trend in the differences between the mechanism predictions and actual measurements, over the conditions tested.

7.1.3.1 Pure fuels and vitiation

Comparisons for propane/air mixture at vitiated conditions show a systematic difference between the measured and predicted flame speeds. For lean and stoichiometric mixtures, the flame speed predictions are usually within ±10% of the measured value. However for rich mixtures, the mechanisms significantly over-predict (> 20%) the flame speed for N_2 and CO_2 dilution. The trends are similar for both San Diego and NUI mechanism predictions, although the NUI mechanism predictions tend to show higher difference. These observed differences suggest that the mechanisms tend to under-predict the change in flame speed with increase in dilution level (and corresponding decrease in O_2 concentration). Furthermore the differences in measured and predicted flame speed values do not show any systematic dependence on the flame height (for $h/D > 1.3$), indicating that above the observed differences in flame speed, if due to the stretch effect on Bunsen flame, are not limited to geometry of the flame.

7.1.3.2 Binary fuel mixtures

Comparisons for binary fuel mixtures show that the flame speed predictions are generally within ±20%, of the measured flame speed, over a wide range of equivalence ratios (0.7–1.3), pressure (1–10 atm) and fuel mixtures. The mechanisms predictions, at 1 and 5 atm, tend to be lower for lean and stoichiometric mixtures and high for rich mixtures. For 10 atm, the results are generally higher for both lean and rich mixtures.

7.1.3.2.1 Steam dilution

Atmospheric pressure steam dilution results for all fuel mixtures studied, show that mechanisms accurately predict the flame speed of lean and stoichiometric mixtures

(within 5–15%) but tend to over-predict (> 30%) the flame speed for rich mixtures. This discrepancy for rich mixtures can be attributed to a systematic error in the Bunsen flame speed measurements at these conditions, as confirmed by the stagnation flame speed measurements.

In addition, the flame speed predictions at high pressure (5 atm) for methane/propane mixture show a similar trend, except that for the rich 60:40 CH_4:C_3H_8 mixture the mechanisms under-predict the flame speed. The strained flame speed measurements, which show better agreement with the mechanism predictions, again suggest that this could be due to uncertainty in the Bunsen flame speed approach. The mechanisms under-predict (by 20–60%) the flame speed of lean and stoichiometric methane/ethane mixtures at high pressure, but produce reasonable agreement (better than 20%) for rich mixtures.

To conclude, *the mechanisms predictions are generally within ±20% of the measured flame speeds for lean and stoichiometric mixtures but show significant differences for rich mixtures (where even the predictions from the different mechanisms differ significantly).* The agreement between the strained flame speed measurements and predictions, especially at rich conditions, suggest a better understanding is required of the Bunsen flame approach at these conditions (as it measures a lower than expected flame speed). Interestingly the differences between the two mechanisms also tend to be higher at the same conditions where there are significant differences from the Bunsen flame measurements.

7.2 Suggestions for future work

7.2.1 Modified Bunsen flame approach

The current measurements show that the modified Bunsen flame approach based on reaction zone area measurement is suitable for measuring unstretched flame speed of hydrocarbon fuels, especially from lean to slightly rich (ϕ = 1.1) conditions. However due to the observed discrepancies in the measured flame speed, there is a need for better understanding the stretch effects on Bunsen flame, especially at moderately rich (ϕ = 1.2–1.6) conditions. Some of the specific conditions where inconsistencies are observed in measured flame speed were:

1. Flame speed measurements for rich methane/oxygen/helium flames at 10 atm were significantly lower than those reported using spherical flame approach.
2. Strained flame speed measurements indicate that for rich (ϕ = 1.2) 60:40 CH_4:C_3H_8 mixtures the Bunsen flame technique results in a significantly lower unstretched flame speed values.
3. The flame speed measured, at 5 atm pressure with steam dilution, for lean 80:20 CH_4:C_3H_8 mixture is significantly higher than the corresponding value for stoichiometric 80:20 mixture or lean 60:40 mixture, even after having accounted for possible experimental uncertainties. The reason for these differences is not fully understood.
4. Significant difference (~20%) in flame speed was observed for rich (ϕ = 1.2) 80:20 CH_4:C_3H_8 mixture at similar steam dilution level with change in flowrate (~40%) of the reactants. The Bunsen flames at these conditions were visibly similar and acceptable for performing measurement. Furthermore such

a high difference in the flame speed with change in flowrate is generally not observed at other conditions.

5. Flame speed measurements for propane–air mixtures with dilution show a systematic trend with high difference from mechanism predictions for rich mixtures (~1.2–1.6) and low O_2 content (< 17% mole fraction of the oxidizer). While these differences could be due to the uncertainties in the predicted values, the disagreement of Bunsen flame results with stagnation flame measurements (for rich methane/propane), suggest that it would be helpful to further investigate the Bunsen flame results at these conditions.

If these discrepancies for (methane/propane flames) are due to the failure of the assumption that these Bunsen flames are weakly affected by stretch effects except very close to the tip and the base, then it has to be due to combined effect of conditions that make these flames different. This is because the Bunsen approach was shown to be accurate for rich mixtures of pure methane and propane flames, based on comparisons with other stretch corrected techniques. Essentially these effects are not limited to the geometry of the flame but are influenced by other conditions such as fuel, pressure and preheat. Furthermore as discussed in Section 5.3, there *appears to be no correlation between the flame height and difference between predicted and measured flame speeds*. Also Section 6.3.3 shows that *for lean mixtures the difference in the flame speed does not show any clear correlation with the strain sensitivity of the mixture*. It should be noted that the strain sensitivity of the mixture was calculated for a positively stretched, stagnation flame geometry. However the Bunsen flame is affected by both the strain and curvature effects and has an overall negative stretch. This suggests that further study, for

example with a 2D axisymmetric modeling of the Bunsen flame, may be required to conclusively show that the difference in flame speed is un-correlated to the stretch effect (due to strain and curvature).

The validation data presented in Chapter 4 had a limited equivalence ratio range (ϕ = 0.6–1.3), based on the available results from other techniques. However most of the differences in the predicted and measured flame speeds were observed at richer equivalence ratios. Furthermore, the Markstein numbers were negative for the cases where comparisons were made with other techniques. Thus it would be useful to validate the Bunsen flame measurement approach over a wider range of equivalence ratio where a change in the sign of Markstein number is observed.

The results presented here try to account for unsteadiness in the flame surface by measuring the RMS in the flame area fluctuations. However this may not be sufficient to fully account for the stretch effect due to the movement of the flame surface. Measuring the fluctuations in the flame surface by either measuring the local movement in the flame edge location at a given height from the burner exit or by measuring the movement of the flame tip might be a better estimate of the unsteadiness in the flame surface. Although any flame surface movement parallel to the line of sight would still be lost. Ideally it is advisable to have a steady flame surface by reducing any fluctuations that may be introduced due to factors such flowrate oscillation and non-uniformity, and poor flame anchoring.

Another avenue to explore is the effect of equivalence ratio of the pilot flame on anchoring the main flame and final flame speed result. For most of the tests reported here, the pilot equivalence ratio was slightly lean (~0.9–1.0). However it is expected that

increasing the pilot equivalence ratio to rich (~1.1) may improve the stability and the flowrate at which the main flame (specifically for lean mixtures) can be anchored. A more systematic study can also be performed to account for the effect of flame lift-off distance on the measured flame speed.

7.2.2 Stagnation flame approach

The accuracy of the current stagnation flame approach implementation is limited due to the strain rate range over where the measurements could be performed. At the lower end, the limitation is due to insufficient seeding density, whereas at the higher end, a change in flame shape (from a flame anchored in the stagnating flow to one anchored in the shear layer) restricts the measurements. The seeding density can be increased by improvements in the seeder design, using a larger diameter burner (currently 9 mm)[kk] or by increasing the separation distance between the nozzle and the stagnation plane[ll], which may necessitate a need for larger diameter bluff-body to ensure that the flowfield around the stagnation streamline is not altered significantly. The change in flame shape can be influenced by changing shape of the bluff-body or by adjusting the nozzle and stagnation plane separation distance.

In addition to the strain rate range, the run time was limited, especially at high pressure and hence higher seeding density, due to the seed particles sticking to the stagnation plug. This was more pronounced when the plug was at high temperature. A possible suggestion is to try changing the material of the stagnation plug (currently

[kk] Increasing the burner diameter results in an increased flowrate through the seeder which can improve the seeding density.

[ll] Increased separation distance between the nozzle and stagnation plug decreases the strain rate experienced by the flame for the same flow velocity. This is equivalent to increasing the flow velocity for the same strain rate, thereby increasing the amount of seeding the flow can pick.

stainless steel) and/or the seeding particle (currently alumina). A plug made from material with low thermal conductivity (such as ceramic) may be helpful in extending the run time of the experiments. For seeding, alumina particles are known to coagulate which may be the reason for particle buildup on the stagnation plug. Other particles for high temperature applications such as titanium dioxide and silicon carbide may be worth investigating.

7.2.3 Chemical kinetics mechanism

The flame speed predictions from the tested San Diego and NUI mechanisms, in general, are good agreement with the measurements for lean mixtures. However significant differences (> 20%; higher than expected uncertainties in the measurements) with measured flame speed suggest possible avenues for improving the flame speed predictions. More specifically, both the mechanisms (viz. San Diego and NUI) over-predict the flame speed for moderately rich propane–air mixtures with N_2 and CO_2 dilution. Furthermore the mechanisms under-predict the effect of dilution on flame speed for these mixtures. The mechanisms also predict a higher change in flame speed with increase in mole fraction of higher alkane in binary fuels mixtures. For methane/ethane mixture, at 5 atm and ~26% steam dilution, the mechanisms significantly over-predict (up to 40–60% higher) the flame speed for lean and stoichiometric mixtures.

APPENDIX A

FLOWMETER CALIBRATION

The rotameters used for the current experiments were calibrated using either a wet drum-type flow meter (Ritter TG-50) for high flowrates (2–100 slpm) or a bubble flow meter (Sensidyne Gilibrator-2) for low flowrates (0.1–2 slpm). Both the flow calibration systems measure the volumetric displacement (at room conditions) due to a constant flowrate and the corresponding time duration to determine the flowrate.

The drum-type flow meter measures the gas volume by measuring the rotation of a drum over fixed time duration. To reduce the uncertainty in the measured flowrate it is necessary to measure the flowrate over long time durations. In general, each measurement was timed for ~4–5 min. During this time reading were also recorded at intermediate time intervals to check if the flowrate is converging. This also confirmed that the flowrate was steady over the measurement duration. At high flowrates instead of making measurements over long time duration, the measurements were made for fixed volumetric displacement (typically 5–10 revolutions of the drum, which correspond to a volume of ~250–500 liter).

In case of the bubble flow meter, the displacement volume is fixed and the readout provides a direct flowrate reading based on the time taken for the bubble to traverse two fixed locations. To reduce the uncertainty in the measurements, the flowrate reading was averaged over 6–8 values. At high flowrates, it was observed that the bubble would start deforming i.e. it would progressively become more convex instead of staying

flat. Since this can introduce systematic error in measured flowrate, this calibration system was limited to flowrate less than 2 lpm even though it was rated for higher flowrate. One possible reason for this could be the soap solution used for forming bubbles was different than the one recommended. Instead the drum-type flow meter was used to measure the higher flowrates.

The Matheson FM-1050 series rotameter tubes consist of two floats (one made of glass and other steel). Calibrations were performed at multiple float positions; ~5–8 positions for each float, depending on the observed linearity in the flowrate vs. float position plot. The results were then fitted with a third-order polynomial to help interpolate to desired float position or flowrate value. An example calibration case is presented in Figure A.1.

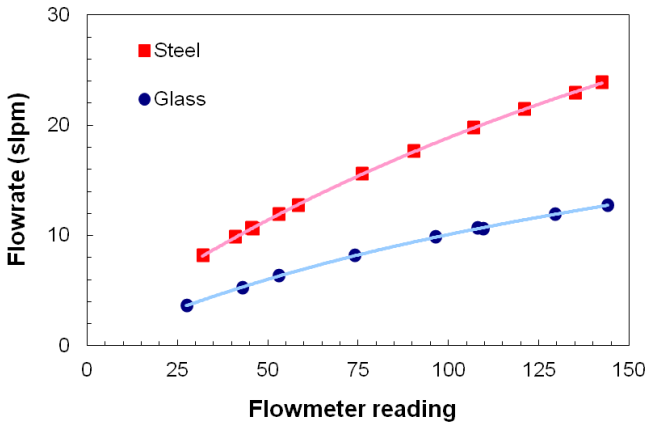

Figure A.1. Flow calibration readings for oxygen at 230 psig pressure in the rotameter tube. The symbols are measured flowrate values and the curves are for third-order polynomial fit.

REFERENCES

1. Lefebvre, A. H., Ballal, D. R., "Gas Turbine Combustion: Alternative Fuels and Emissions," CRC Press, 2010.

2. Lieuwen, T. C., Yang, V., "Combustion Instabilities in Gas Turbine Engines," Progress in Astronautics and Aeronautics, 2005.

3. US EIA (US Energy and Information Administration), "Annual Energy Outlook 2013 with Projections to 2040," DOE/EIA-0383(2013), April 2013.

4. Hammer, G., Lübcke, T., Kettner, R., Pillarella, M. R., Recknagel, B., Commichau, A., Neumann, Hans-J., Paczynska-Lahme, B., "Natural Gas," Wiley Critical Content - Petroleum Technology, Volume 1-2, 2007.

5. Ginter, D., Simchick, C., Schlatter, J., "Durability of Catalytic Combustion Systems, Appendix VI: Variability in Natural Gas Fuel Composition and its Effects on the Performance of Catalytic Combustion Systems," Contractor Report for California Energy Commission, Contract No. 500-97-033, November 2001.

6. "Trent 60 Uprated to 64MW by Series of Water Injection Mods," GTW Handbook, 2010, pp. 12-14.

7. Lovett, J. A., Brogan, T. P., Philippona, D. S., Keil B. V. and Thompson T. V., "Development Needs for Advanced Afterburner Designs," 40th AIAA Joint Propulsion Conference, AIAA 2004-4192, July 2004.

8. Hughes, K. J., Turányi, T., Clague, A. R., Pilling, M. J., "Development and Testing of a Comprehensive Chemical Mechanism for the Oxidation of Methane," International Journal of Chemical Kinetics, Vol. 33, 2001, 513–538.

9. Law, C. K., "Combustion Physics," Cambridge University Press, 2006.

10. Glassman, I., "Combustion," Academic Press, 1996.

11. Lewis, B., von Elbe, G., "Theory of Flame Propagation," Chemical Reviews, Vol. 21 (2), 1937, pp 347–358.

12. Andersen, J. W., Fein, R. S., "Measurements of Normal Burning Velocities and Flame Temperatures of Bunsen Flames," The Journal of Chemical Physics, Vol. 17 (12), 1937, pp. 1268–1273.

13. Smith, F. A., "Problems of Stationary Flames," Chemical Reviews, Vol. 21 (3), 1937, pp 389–412.

14. Linnett, J. W., “Methods of Measuring Burning Velocities,” Fourth Symposium International on Combustion, Williams & Wilkins, Baltimore, 1953, pp. 20–35.

15. Andrews, G. E., Bradley, D., “Determination of Burning Velocities: A Critical Review,” Combustion and Flame, Vol. 18, 1972, pp. 133–153.

16. Rallis C. J., Garforth A. M., “The Determination of Laminar Burning Velocity,” Progress in Energy and Combustion Science, Vol. 6, 1980, pp. 303–329.

17. Van Maaren, A., Thung, D.S., De Goey, L.P.H., “Measurement of Flame Temperature and Adiabatic Burning Velocity of Methane/Air Mixtures,” Combustion Science and Technology, Vol. 96 (4), 1994, pp. 327–344.

18. Vagelopoulos, C. M., Egolfopoulos, F. N., Law, C. K., “Further Considerations on the Determination of Laminar Flame Speeds with the Counterflow Twin-Flame Technique,” Symposium (International) on Combustion, Vol. 25 (1), 1994, pp. 1341–1347.

19. Hassan, M. I., Aung, K. T., Faeth, G. M. "Measured and Predicted Properties of Laminar Premixed Methane/Air Flames at Various Pressures", Combustion and Flame, Vol. 115, 1998, pp. 539–550.

20. Gu, X. J., Haq, M. Z., Lawes, M., Woolley, R., “Laminar burning velocity and Markstein lengths of methane–air mixtures,” Combustion and Flame, Vol. 121 (1–2), April 2000, pp. 41–58.

21. Rozenchan, G., Zhu, D. L., Law, C. K., Tse, S. D., “Outward Propagation, Burning Velocities and Chemical Effects of Methane Flames up to 60 atm,” Proceedings of the Combustion Institute, Vol. 29, 2002, pp. 1461-1469.

22. Smith, G. P., Golden, D. M., Frenklach, M., Moriarty, N. W., Eiteneer, B., Goldenberg, M., Bowman, C. T., Hanson, R. K., Song, S., Gardiner, W. C. Jr., Lissianski, V. V., Qin, Z., http://www.me.berkeley.edu/gri_mech/, accessed: 2014-03-28.

23. Dong, Y., Vagelopoulos, C. M., Spedding, G. R., Egolfopoulos, F. N., “Measurements of Laminar Flame Speeds through Digital Particle Image Velocimetry: Mixtures of Methane and Ethane with Hydrogen, Oxygen, Nitrogen, and Helium,” Proceedings of the Combustion Institute, Vol. 29, 2002, pp. 1419–1426.

24. Zhu, D.L., Egolfopoulos, F. N., Law, C. K., “Experimental and Numerical Determination of Laminar Flame Speeds of Methane/(Ar, N_2, CO_2)–Air Mixtures as Function of Stoichiometry, Pressure and Flame Temperature,” Symposium (International) on Combustion, Vol. 22, 1988, pp. 1537-1545.

25. Ogami Y., Kobayashi H., “Laminar Burning Velocity for CH_4/air Premixed Flames at High Pressure and High Temperature for Various Equivalence Ratios,” 5th Asia-Pacific Conference on Combustion, Adelaide, Australia, July 2005.

26. Mazas, A. N., Lacoste, D. A., Schuller, T., “Experimental and Numerical Investigation on the Laminar Flame Speed of CH_4/O_2 Mixtures Diluted with CO_2 and H_2O,”

Proceedings of ASME Turbo Expo 2010: Power for Land, Sea and Air, GT2010-22512, Glasgow, UK, June 2010.

27. Galmiche, B., Halter, F., Foucher, F., Dagaut, P., "Effects of Dilution on Laminar Burning Velocity of Premixed Methane/Air Flames," Energy & Fuels, Vol. 25 (3), 2011, pp. 948–954.

28. Boushaki, T., Dhué, Y., Selle, L., Ferret, B., Poinsot, T., "Effects of Hydrogen and Steam Addition on Laminar Burning Velocity of Methane–Air Premixed Flame: Experimental and Numerical Analysis," International Journal of Hydrogen Energy, Vol. 37 (11), June 2012, pp. 9412–9422.

29. Jomaas, G., Zheng, X. L., Zhu, D. L., Law, C. K., "Experimental Determination of Counterflow Ignition Temperatures and Laminar Flame Speeds of C_2–C_3 Hydrocarbons at Atmospheric and Elevated Pressures," Proceedings of the Combustion Institute, Vol. 30, 2005, pp. 193–200.

30. Qin, Z., Lissianski, V. V., Yang, H., Gardiner, W. C., Davis, S. G., Wang, H., "Combustion Chemistry of Propane: A Case Study of Detailed Reaction Mechanism Optimization," Proceedings of the Combustion Institute, Vol. 28 (2), 2000, pp. 1663–1669.

31. Konnov, A. A., Dyakov, I. V., De Ruyck, J., "Measurement of Adiabatic Burning Velocity in Ethane–Oxygen–Nitrogen and in Ethane–Oxygen–Argon Mixtures," Experimental Thermal and Fluid Science, Vol. 27 (4), 2003, pp. 379–384.

32. Zhao, Z., Kazakov, A., Li, J., Dryer, F. L., "The Initial Temperature and N_2 Dilution Effect on the Laminar Flame Speed of Propane/Air," Combustion, Science and Technology, Vol. 176, 2004, pp. 1705–1723.

33. Yu, G., Law, C. K., Wu, C. K., "Laminar Flame Speeds of Hydrocarbon + Air Mixtures with Hydrogen Addition," Combustion and Flame, Vol. 63 (3), 1986, pp. 339–347.

34. Park, O., Veloo, P. S., Liu, N., Egolfopoulos, F. N., "Combustion Characteristics of Alternative Gaseous Fuels," Proceedings of the Combustion Institute, Vol. 33 (1), 2011, pp. 887–894.

35. Kishore, R. V., Duhan, N., Ravi, M. R., Anjan, R., "Measurement of Adiabatic Burning Velocity in Natural Gas-like Mixtures," Experimental Thermal and Fluid Science, Vol. 33 (1), 2008, pp. 10-16.

36. Bourque G., Healy D., Curran H., Zinner C., Kalitan D., de Vries J., Aul C. and Petersen E., "Ignition and Flame Speed Kinetics of Two Natural Gas Blends with High Levels of Heavier Hydrocarbons," Journal of Engineering for Gas Turbines and Power, Vol. 132, (021504) 2009, 11 pages.

37. Bourque, G., Healy, D., Curran, H. J., Zinner, C., Kalitan, D., de Vries, J., Aul, C., and Petersen, E., "Ignition and Flame Speed Kinetics of Two Natural Gas Blends with High

Levels of Heavier Hydrocarbons, Proceedings of ASME Turbo Expo, 3:1051–1066 2008. http://c3.nuigalway.ie/naturalgas2.html, accessed: 2014-03-28.

38. Hirasawa, T., Sung, C. J., Joshi, A., Yang, Z., Wang, H., Law, C. K., "Determination of Laminar Flame Speeds Using Digital Particle Image Velocimetry: Binary Fuel Blends of Ethylene, n-Butane, and Toluene," Proceedings of the Combustion Institute, Vol. 29 (2), 2002, pp. 1427–1434.

39. Ji, C., Egolfopoulos, F. N., "Flame Propagation of Mixtures of Air with Binary Liquid Fuel Mixtures," Proceedings of the Combustion Institute, Vol. 33 (1), 2011, pp. 955–961.

40. Sileghem, L., Vancoillie, J., Demuynck, J., Galle, J., Verhelst, S., "Alternative Fuels for Spark-Ignition Engines: Mixing Rules for the Laminar Burning Velocity of Gasoline–Alcohol Blends," Energy & Fuels, Vol. 26 (8), 2012, pp. 4721–4727.

41. Tang, C. L., Huang, Z. H., Law, C. K., "Determination, Correlation, and Mechanistic Interpretation of Effects of Hydrogen Addition on Laminar Flame Speeds of Hydrocarbon–Air Mixtures," Proceeding of the Combustion Institute, Vol. 33 (1), 2011, pp. 921–928.

42. Wu, F., Kelley, A. P., Tang, C., Zhu, D., Law, C. K., "Measurement and Correlation of Laminar Flame Speeds of CO and C_2 Hydrocarbons with Hydrogen Addition at Atmospheric and Elevated Pressures," International Journal of Hydrogen Energy, Vol. 36 (20), 2011, pp. 13171−13180.

43. Powling, J., "A New Burner Method for the Determination of Low Burning Velocities and Limits of Inflammability," Fuel Vol. 28 (2), 1949, pp. 25–28.

44. Botha, J. P., Spalding, D. B., "The Laminar Flame Speed of Propane/Air Mixtures with Heat Extraction from the Flame," Proceedings of the Royal Society of London, Vol. 225, 1954, pp. 71–96.

45. Bosschaart, K. J., de Goey, L. P. H., "Detailed Analysis of the Heat Flux Method for Measuring Burning Velocities," Combustion and Flame, Vol. 132 (1–2), 2003, pp. 170–180.

46. Lewis, B., Von Elbe, G., "Combustion, Flames, and Explosions of Gases," Academic Press, 3rd edition, 1987.

47. Dowdy, D. R., Smith, D. R., Taylor, S. C., Williams, A. "The Use of Expanding Spherical Flames to Determine Burning Velocities and Stretch Effects in Hydrogen–Air Mixtures," Proceedings of the Combustion Institute, Vol. 23, 1990, pp. 325–332.

48. Bouvet, N., Chauveau, C., Gökalp, I., Halter, F., "Experimental Studies of the Fundamental Flame Speeds of Syngas (H2/CO)/Air Mixtures," Proceedings of the Combustion Institute, Vol. 33 (1), 2011, pp. 913–920.

49. Moghaddas, A., Eisazadeh-Far, K., Metghalchi, H., "Laminar Burning Speed Measurement of Premixed n-Decane/Air Mixtures Using Spherically Expanding Flames

at High Temperatures and Pressures," Combustion and Flame, Vol. 159 (4), 2012, pp. 1437–1443.

50. Tse, S. D., Zhu, D. L., Law, C. K., "Morphology and Burning Rates of Expanding Spherical Flames in H_2/O_2/Inert Mixtures up to 60 atmospheres," Proceedings of the Combustion Institute, Vol. 28 (2), 2000, pp. 1793–1800.

51. Lowry, W., de Vries, J., Krejci, M., Petersen, E., Serinyel, Z., Metcalfe, W., Curran, H., Bourque, G., "Laminar Flame Speed Measurements and Modeling of Pure Alkanes and Alkane Blends at Elevated Pressures," Proceedings of ASME Turbo Expo 2010: Power for Land, Sea and Air, GT2010-23050, Glasgow, UK, June 2010.

52. Wu, C. K., Law, C. K., "On the Determination of Laminar Flame Speeds from Stretched Flames," Symposium (International) on Combustion, Vol. 20 (1), 1985, pp. 1941–1949.

53. Gibbs, G. J., Calcote, H. F., "Effect of Molecular Structure on Burning Velocity," Journal of Chemical and Engineering Data, Vol. 4 (3), 1959, pp. 226–237.

54. Mazas, A. N., Fiorina, B., Lacoste, D. A., Schuller, T., "Effects of Water Vapor Addition on the Laminar Burning Velocity of Oxygen-Enriched Methane Flames," Combustion and Flame, Vol. 158 (12), 2011, pp. 2428–2440.

55. Natarajan, J., "Experimental and Numerical Investigation of Laminar Flame Speeds of $H_2/CO/CO_2/N_2$ Mixtures," Dissertation, Georgia Institute of Technology, 2008, http://hdl.handle.net/1853/22685 (Accessed: 2014 April 24)

56. Singer, J. M., "Burning-velocity Measurements on Slot Burners; Comparison with Cylindrical Burner Determinations," Symposium (International) on Combustion, Vol. 4 (1), 1953, pp. 352–358.

57. Choi, C. W., Puri, I. K., "Contribution of Curvature to Flame-Stretch Effects on Premixed Flames," Combustion and Flame, Vol. 126 (3), 2001, pp. 1640–1654.

58. Natarajan, J., Lieuwen, T., Seitzman, J., "Laminar Flame Speeds of H_2/CO Mixtures: Effect of CO_2 Dilution, Preheat Temperature and Pressure," Combustion and Flame, Vol. 151 (1-2), 2007, pp. 104–119.

59. Sun, C. J., Sung, C. J., He, L., Law, C. K., "Dynamics of Weakly Stretched Flames: Quantitative Description and Extraction of Global Flame Parameters," Combustion and Flame, Vol. 118 (1–2), 1999, pp. 108–128.

60. Yamaoka, I., Tsuji, H., "Determination of Burning Velocity Using Counterflow Flames," Symposium (International) on Combustion, Vol. 20 (1), 1985, pp. 1883–1892.

61. Egolfopoulos, F. N., Zhang, H., Zhang, Z., "Wall Effects on the Propagation and Extinction of Steady, Strained, Laminar Premixed Flames," Combustion and Flame, Vol. 109 (1–2), 1997, pp. 237–252.

62. Tien, J. H., Matalon, M., "On the Burning Velocity of Stretched flames," Combustion and Flame, Vol. 84 (3–4), 1991, pp. 238–248.

63. Sung. C. J., Liu, J. B., Law, C. K., "Structural Response of Counterflow Diffusion Flames to Strain Rate Variations," Combustion and Flame, Vol. 102 (4), 1995, pp. 481–492,

64. Wang, Y. L., Holley, A. T., Ji, C., Egolfopoulos, F. N., Tsotsis, T. T., Curran, H. J., "Propagation and Extinction of Premixed Dimethyl-Ether/Air Flames," Proceedings of the Combustion Institute, Vol. 32 (1), 2009, pp. 1035–1042.

65. Di Sarli, V., Di Benedetto, A., "Laminar Burning Velocity of Hydrogen–Methane/Air Premixed Flames," International Journal of Hydrogen Energy, Vol. 32 (5), 2007, pp. 637−646.

66. Law, C. K., Sung, C. J., "Structure, Aerodynamics, and Geometry of Premixed Flamelets," Progress in Energy and Combustion Science, Vol. 26 (4–6), 2000, pp. 459–505.

67. Keane, R. D., Adrian, R. J., "Theory of Cross-Correlation Analysis of PIV Images," Applied Scientific Research, Vol. 49 (3), 1992, pp 191–215.

68. LaVision, "DaVis 7.0 FlowMaster manual".

69. NIST/SEMATECH e-Handbook of Statistical Methods, http://www.itl.nist.gov/div898/handbook/pmd/section8/pmd812.htm (Accessed: 2014 April 24).

70. Bergthorson, J. M., "Experiments and modeling of impinging jets and premixed hydrocarbon stagnation flames," Dissertation, California Institute of Technology, 2005, http://resolver.caltech.edu/CaltechETD:etd-05242005-165713 (Accessed: 2014 April 24).

71. Metghalchi, M., Keck, J. C., "Laminar Burning Velocity of Propane–Air Mixtures at High Temperature and Pressure," Combustion and Flame, Vol. 38, 1980, pp.143–154.

72. Konnov, A. A., "The Effect of Temperature on the Adiabatic Laminar Burning Velocities of CH_4–Air and H_2–Air Flames," Fuel, Vol. 89 (9), 2010, pp. 2211–2216.

73. Turns, S. R., "An Introduction to Combustion: Concepts and Applications," McGraw-Hill, 2000.

74. Sung, C. J., Law, C. K., Axelbaum, R. L., "Thermophoretic Effects on Seeding Particles in LDV Measurements of Flames," Combustion Science and Technology, Vol. 99 (1-3), 1994, pp. 119–132.

75. "Chemkin", Reaction Design, http://reactiondesign.com/products/chemkin/ (Accessed: 2014 April 24).

76. Kee, R. J., Grcar, J. F., Smooke, M. D., Miller, J. A., Meeks, E., "PREMIX: A FORTRAN Program for Modeling Steady Laminar One-Dimensional Premixed Flames," Reaction Design report, 1998.

77. Lutz, A. E., Kee, R. J., Grcar, J. F., Rupley, F. M., "OPPDIF: A FORTRAN Program for Computing Opposed-Flow Diffusion Flames," Sandia National Laboratories Report SAND96-8243, 1997.

78. Grcar, J. F., "The Twopnt Program for Boundary Value Problems," Sandia National Laboratories Report SAND91-8230, 1992.

79. Smith, G. P., Golden, D. M., Frenklach, M., Moriarty, N. W., Eiteneer, B., Goldenberg, M., Bowman, C. T., Hanson, R. K., Song, S., Gardiner Jr., W. C., Lissianski, V. V., Qin, Z., "GRI-Mech 3.0", http://www.me.berkeley.edu/gri_mech/ (Accessed: 2014 April 24).

80. "Chemical-Kinetic Mechanisms for Combustion Applications", San Diego Mechanism web page, Mechanical and Aerospace Engineering (Combustion Research), University of California at San Diego, http://combustion.ucsd.edu (Accessed: 2014 April 24).

81. Wang, H., You, X., Joshi, A. V., Davis, S. G., Laskin, A., Egolfopoulos, F., Law, C. K., "USC Mech Version II: High-Temperature Combustion Reaction Model of H_2/CO/C_1-C_4 Compounds", http://ignis.usc.edu/Mechanisms/USC-Mech II/USC_Mech II.htm (Accessed: 2014 April 24).

82. Natarajan, J., Nandula, S., Lieuwen, T., Seitzman, J. M., "Laminar Flame Speeds of Synthetic Gas Fuel Mixtures," Proceedings of the ASME/IGTI Turbo Expo 2005, GT 2005-68917, Reno, NV June 6-9, 2005.

83. Egolfopoulos, F. N., Zhu, D. L., Law, C. K., "Experimental and Numerical Determination of Laminar Flame Speeds: Mixtures of C_2-Hydrocarbons with Oxygen and Nitrogen," Symposium (International) on Combustion, Vol. 23 (1), 1991, pp. 471–478.

84. Babkin, V. S., V'yun, A. V., "Effect of Water Vapor on the Normal Burning Velocity of a Methane-Air Mixture at High Pressures," Combustion, Explosion and Shock Waves, Vol. 7 (3), 1971, pp. 339–341.

85. Li, J., Zhao, Z., Kazakov, A., Chaos, M., Dryer, F. L., Scire, J. J., "A Comprehensive Kinetic Mechanism for CO, CH_2O, CH_3OH Combustion," International Journal of Chemical Kinetics, Vol. 39 (3), 2007, pp. 109–136.

86. Turanyi, T., Zalotai, L., Dobe, S., Berces, T., "Effect of the Uncertainty of Kinetic and Thermodynamic Data on Methane Flame Simulation Results," Physical Chemistry Chemical Physics, Vol. 4 (12), 2002, pp. 2568–2578.

87. Law, C. K., Zhu, D. L., Yu, G., "Propagation and Extinction of Stretched Premixed Flames," Symposium (International) on Combustion, Vol. 21 (1), 1988, pp. 1419–1426.

88 Ranzi, E., Frassoldati, A., Grana, R., Cuoci, A., Faravelli, T., Kelley, A. P., Law, C. K., "Hierarchical and Comparative Kinetic Modeling of Laminar Flame Speeds of

Hydrocarbon and Oxygenated Fuels," Progress in Energy and Combustion Science, Vol. 38 (4), 2012, pp. 468–501.

89. Kochar, Y., Seitzman, J., Lieuwen, T., Metcalfe, W., Burke, S., Curran, H., Krejci, M., Lowry, W., Petersen, E., Bourque, G., "Laminar Flame Speed Measurements and Modeling of Alkane Blends at Elevated Pressures With Various Diluents," Proceedings of the ASME/IGTI Turbo Expo 2011, GT 2011-45122, Vancouver, Canada June 6-10, 2011.

90. Amato A., Day, M. S., Cheng, R. K., Bell, J. B., Lieuwen, T. C., "Leading Edge Statistics of Turbulent, Lean, H_2–Air Flames," to be presented at the 35th International Symposium on Combustion, San Francisco, CA, August 2014.

VITA

YASH N. KOCHAR

Yash Kochar was born in Ajmer, Rajasthan to Dr. Nirdosh Kumar Kochar and Dr. Neeta Kochar and is married to Komal Khabya. He completed his schooling in Nagpur, Maharashtra along with his sister Vasudha. He received his B. Tech. degree in Aerospace engineering from the Indian Institute of Technology, Madras in 2004. He received M. S. degree in Aerospace engineering from Georgia Institute of Technology, Atlanta in 2011 while pursuing his doctoral degree. Besides his research he enjoys outdoor activities, computer programming, reading books and stories and solving mechanical puzzles.